UNIVERSITÀ
DEGLI STUDI
FIRENZE

**DOTTORATO DI RICERCA IN**
**FISICA E ASTRONOMIA**

CICLO XXIX

COORDINATORE Prof. Massimo Gurioli

# *Hybrid scheme for magnetic-based quantum devices*

Settore Scientifico Disciplinare: FIS/03


**Dottorando**
Dott. Davide Nuzzi

**Tutor**
Prof. Alessandro Cuccoli

**Coordinatore**
Prof. Massimo Gurioli


Anni 2013/2016

# Contents

# List of Publications

Part of the research described in the present thesis (in particular the content of chapter 3 and chapter 4) has been presented in the following journal papers and conference proceedings. The content of chapter 5, which is not published yet, is the subject of the paper, "to be submitted", reported the last reference.

- Cuccoli, A., Nuzzi, D., Vaia, R. and Verrucchi, P. (2015) "Getting through to a qubit by magnetic solitons", *New Journal of Physics*, **17**(8):083053.
- Cuccoli, A., Nuzzi, D., Vaia, R. and Verrucchi, P., (2016) "Remote manipulation of individual qubits by magnetic solitons", *Journal of Magnetism and Magnetic Materials*, **400**:149-153. Proceedings of the 20th International Conference on Magnetism (Barcelona) 5-10 July 2015
- Cuccoli, A., Nuzzi, D., Vaia, R. and Verrucchi, P., (2014) "Using solitons for manupulating qubits" *International Journal of Quantum Information*, **12**(02):1461013
- Cuccoli, A., Nuzzi, D., Vaia, R. and Verrucchi, P., (2014) "Quantum gates controlled by spin chain soliton excitations", *Journal of Applied Physics* , **115**(17)
- Nuzzi, D., Cuccoli, A., Vaia, R. and Verrucchi, P., (2017) "Entanglment generation via semi-classical channels", *to be submitted.*

# Introduction and thesis outline

The realization of a quantum computer, although having been considered for long time almost as science fiction, looks now more concrete, thanks to the huge effort that has been made by the scientific community working on quantum technologies in the last decades. In fact, many proposals, for different physical architecture of quantum computing machines, have been put forward [1–7] and some of them have also been realized, at least on a small scale, i.e. for a limited number of qubits [8, 9]. Moreover, a quantum annealer, i.e. a quantum device able to simulate (and thus solve) optimization problems [10, 11], has been already commercialized, by the *D-Wave* company. These astonishing progresses make the major issues about the realization of a quantum computer look like "engineering problems", whose solution is not far to be found.

The most considerable open problems concerning the realization of a quantum computer are the *sensitivity*, the *addressability*, and the *scalability*: the *sensitivity* of *quantum devices* (i.e. any device which exploits the quantum features of its constituents to realize some operation) to external disturbances relates to the fact that systems designated to accomplish quantum operations are typically delicate and must be carefully protected to let them to properly work; the *addressability* of any single qubit of a *qubit registers* is fundamental since any application requires the possibility of reaching and controlling qubits singularly; finally, the *scalability* of the proposed architectures consists in how to scale to larger qubit registers, for making useful calculation conceivable, and also to evidence the power of quantum computing with respect to classical one.

These problems may have opposite solutions, since a good scalability could, e.g., be achieved embedding the qubits in solid state matrices, where, however, it may become very complicated to control each of them separately, and to screen their interactions with the environment, thus making very hard to assure qubit addressability and an adequate protection. Conversely, well separated qubits realized by "trapped-" atoms [6, 12] or ions [13, 14], can be singularly addressed, and assuring a certain level of protection is less difficult; however, due to the resources needed, large scalability is not easily achievable for these

realizations.

Another aspect related to the realization of generic quantum devices is connected to the way we ultimately interface with them: due to our perceptions, we live in a "classical world", meaning that our way of communicating and understanding our surroundings is intrinsically classical. Thus, any quantum device will have to interface, at least at some stage, with our classical experience of the world: control and measuring apparatuses, having to be set or read by a human operator, are the obvious examples of what we are referring to. The effort, in this case, is keeping our classical disturbances as far as possible from the action taking place at the heart of the quantum device.

Sometimes, however, this feature can be turned into an advantage, if one is able to find the proper "interface" (i.e. something able to put in touch two unrelated systems) between classical and quantum world. In fact, classical systems may posses robustness features which can be, in the suitable conditions, exploited for the realization of novel quantum devices where the sensitivity problem is much alleviated.

An example of the interface we have in mind is provided by the field of *quantum optics* where the so called *coherent states* of light are employed to realize quantum applications [15, 16]. These states are often referred to as *classical states*, since their behaviour is well described by the classical Maxwell Equations, but regardless their name, they are to all respects quantum states describing a system of photons. They represent a convenient interface because they allow for quantum application to be realized, being also readily obtained using commonly available instruments such as lasers. We refer to such objects with the adjective *semi-classical* that will describe, in our acceptation, systems whose nature is intimately quantum, but whose features and behaviour is well framed within a classical description.

Any scheme, application or device, where a semi-classical system interacts with some pure quantum object (e.g. a qubit) for realizing a quantum operation, will be referred to as *hybrid*.

Summarizing, we want to push forward the above idea studying the possibility of exploiting the robustness features of some non-linear classical systems in order to realize quantum devices where the sensitivity problem is alleviated; thus, we will focus on spin systems, since magnetic qubit realizations (as, e.g., N-V centres in diamond [17–21] and quantum dots [22, 23]) are the most diffuse in solid state proposals, where the scalability promises to make them the most suitable candidates for the realization of a large-scale quantum computer.

In this thesis we propose a *hybrid* scheme for accomplishing the most basic actions related with the realization of a magnetic-based quantum device, i.e. the control of a qubit state and entanglement generation. In particular we will develop it, focusing on magnetic

one-dimensional systems, i.e. spin chains, as channels connecting one or more qubits to some external control apparatus.

This choice follows from the observation that classical spin chains are non-linear systems which enumerate *solitons* among the dynamical configurations which are solution of their equation of motion [24–29].

In fact, solitons are those particular solutions of the equations of motion of non-linear systems which are celebrated for their impressive properties of robustness against scattering and external disturbances, space-time localization and shape-invariant evolution. These properties make them suitable candidates for practical purposes.

Although solitons characterize only non-linear classical systems, there are both theoretical and experimental evidences that they continue characterizing also real one-dimensional magnetic systems [30–34]; moreover, the comparison between theoretical results and experiments shows that a semi-classical (or just classical, plus a renormalization of the spin magnitude) treatment accounts correctly for the behaviour of these materials even for spin systems with $S = 1$ [35–39].

We hereafter consider systems made by one-dimensional discrete lattices hosting, at each lattice site, one *classical* spin vector field (*classical spin chain*) or a *large-S* spin, i.e. a quantum spin characterized by a $S$-value large enough for the spin to be well described by a semi-classical behaviour (*large-S spin chain*).

In view of these consideration a classical, or large-$S$, spin chain (with its solitons) can play the role, in our scheme, of the robust partner while the role of the fragile quantum system is played by the qubit, which is the agent of the relevant quantum operations in our hybrid quantum device.

In order to pursue our goal, we first introduce a method for generating solitons on discrete, classical Heisenberg chains by applying a time-dependent magnetic field to one of the chain extremities. The method has been numerically checked, revealing the effective possibility of obtaining soliton-like dynamical configurations running along the spin chain, which resemble the known analytical soliton solutions of the continuous chain, if their typical width is large with respect to the chain lattice spacing. The robustness of the generated solitons has been also tested with respect to thermal noise present in the system [40, 41].

We then propose a set-up where the generated soliton acts as a magnetic signal that travels along the chain and eventually reaches a qubit and changes its quantum state. Since any unitary action on a single qubit can be represented in terms of a Zeeman interaction lasting for a precise time interval, qubit state control [22] is usually assumed to be obtained by applying suitable sequences of external magnetic fields. Indeed, for this particular application, the spin chain need not to be quantum and the suitable magnetic field is provided by the moving deformation of the uniform chain configuration which is represented by the

magnetic soliton travelling along the chain. Numerical results confirm that solitons are indeed suitable for this task, giving the possibility to remotely control the qubit state by an appropriate choice of soliton shape and qubit-chain coupling [40–43].

We finally address the problem of entanglement generation between distant qubits by introducing a model where two qubits, distant and non-interacting, are each coupled with one spin-$S$ belonging to a large-$S$ Heisenberg chain, whose dynamics is assumed to be characterized by the presence of solitons. The aim of this study is to verify if, by properly choosing the state of the spin chain, the evolution of such a robust semi-classical system can bring the two qubits from a separable initial state to a non-separable state after a certain amount of time, i.e., if a semi-classical channel can generate entanglement between the two qubits.

At variance with the previous application, the spin chain must here be considered, and consequently treated, as a quantum system in order to allow for entanglement generation and transfer. Since accounting for the exact evolution of a large-$S$ spin chain is out of reach, even numerically, a suitable approximation is needed to solve its dynamics: this leads us to introduce a particular set of chain states built as product of single-spin coherent states, which are in one-to-one correspondence with the configurations of the classical spin chain, and are thus referred to as the *semi-classical states* of the chain. Being able to solve the evolution of the coherent state products, allow us to complete the hybrid scheme for entanglement generation: in fact, it is shown that, choosing the chain initial state as a semi-classical state corresponding to a soliton configuration, the correlations, generated between one qubit and the corresponding spin-$S$, are efficiently transferred along the chain up to the other qubit, finally leaving the two qubits in an entangled state [44].

The thesis is structured as follows:

**Chapter 1**, is devoted to introduce basic concepts about Quantum Mechanics for the building of the subsequent chapters; in particular, *spin coherent states*, as well as the *generalized coherent states*, are introduced and their fundamental properties outlined, being of central importance in the development of our hybrid scheme.

**Chapter 2**, aims to discuss the general robustness features of non-linear classical systems and in particular of the solutions of their equations of motion, known as *solitons*. Some example of solitons are presented along with their exemplifying features. The last section is devoted to introduce the classical Heisenberg spin chain and its specific soliton solution which will be largely used in the subsequent chapters.

In **Chapter 3**, we model our proposal for achieving soliton generation in a discrete, classical Heisenberg spin chain by the application of a specific time-dependent magnetic field. The numerical methods used for solving the chain dynamics are also presented in detail. Finally, results about soliton generation are presented and discussed for the different

cases considered: an "ideal" situation, in order to verify the effective functioning of the injecting scheme; a "noisy" situation, for testing the strength both of the injection scheme and of the generated dynamical shapes; a more realistic situation where a finite penetration of the injecting field along the chain is considered.

**Chapter 4** is devoted to show how classical Heisenberg solitons can be used to address and manipulate the state of a single qubit. A specific scheme is proposed where the spin chain represents a sort of transmission line and a soliton running on it a specific magnetic signal. The moving deformation of the uniform chain configuration, caused by the soliton travelling along the chain, provides an effective magnetic field for an external magnetic qubit interacting with a finite portion of the spin chain. Different kinds of qubit-chain interactions are considered. The results about qubit state dynamics, together with a thorough characterization of the qubit final state as a function of the relevant parameters, are then presented with respect to the different interactions considered.

In **Chapter 5** a scheme for obtaining entanglement between distant and non-interacting qubits using a large-$S$ Heisenberg chain as a semi-classical channel is introduced: the spin chain is exactly represented through the basis provided by the tensor product of single-spin coherent states, whose evolution is obtained by an approximation which is shown to represent a large-$S$ limit of the exact dynamics. The dynamics of a system made by the spin chain and two qubits, each interacting with a different spin-$S$ of the chain, is studied, starting from a factorized state of the whole system, where the chain initial state is chosen as the semi-classical state corresponding to a solitonic classical configuration. Analytical and numerical results confirming the possibility of generating entanglement between the two qubits are finally reported; in the final section, a discussion of the approximations considered is also given.

The **Concluding remarks and future perspectives** chapter contains the "highlights" of the results presented in the previous chapters, along with a discussion about their possible applications and future developments.

Finally, in the **Appendices**, the explicit calculations, for the fundamental formula of the numerical algorithm used to integrate the equations of motion of the classical chain, and for the construction of the generalized coherent states for the spin chain in the $S \to \infty$ limit, are, respectively, shown.

# Chapter 1

# Basic concepts in a quantum world

This chapter provides the essential tools employed in this thesis. The level of the discussion on each topic will be calibrated accordingly to the functional use in the thesis. We will start with a brief review of the basic concepts of quantum mechanics, focussing on those which will be more relevant, from the fundamental ways of representing isolated and composite systems, and quantifying their quantum correlations, to a survey about how to describe the evolution of quantum systems. Finally, we will make a step forward to our "classical reality" discussing the concept of classical limit. At this stage we will also introduce the quantum states whose dynamical behaviour is closest to that of classical systems and will allow us to establish a connection between the quantum evolution and the Equations of Motion (EoM) of the classical counterpart of the system under consideration.

## 1.1 Founding blocks of quantum mechanics

The route to build some quantum machine is studded by "quantum stuff", i.e. words preceded by the prefix *quantum*, such as, e.g., quantum register, quantum protocol, quantum gate, quantum channel, etc. Each of them relies its meaning and working on some basic elements which we refer to as "founding blocks" of quantum mechanics. Those blocks are used in this thesis and are the central topics of this section.

### 1.1.1 The qubit

The simplest non trivial quantum system is described by a two-dimensional Hilbert space: such system is called *qubit*. The name qubit is given in relation to the field of quantum information theory where it represents the analogue of the fundamental element of classical information, i.e. the *bit*. The bit is a Boolean variable assuming two values $\{0, 1\}$: it can be realized, e.g., by a macroscopic object whose states are defined by one or more continuous parameters; within the range of variability of those parameters, two well distinct region are

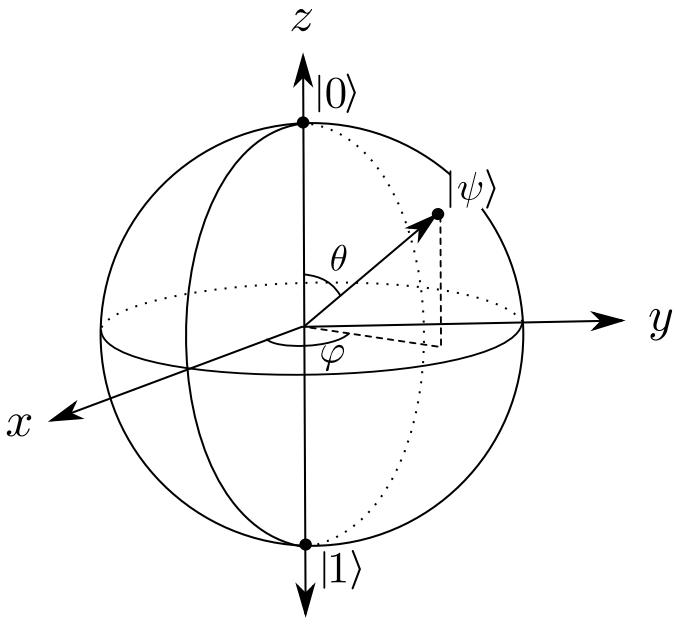


**Figure 1.1:** Qubit state ($|\psi\rangle$) on the Bloch's sphere.

chosen in order to represent the two possible states. Analogously, its quantum counterpart, the qubit, is described by a vector space of dimension two, meaning that its basis is formed by two orthogonal, normalized, vectors $\{|0\rangle, |1\rangle\}$, embodying the analogue of the classical boolean values, and often called *computational basis*. Thus, a qubit can be realized by any physical system described by two-dimensional Hilbert space as for example an atomic two-level system or, even more naturally, by a spin-1/2 object. If a system is *isolated*, i.e. its not interacting with anything else, or *closed*, i.e. it is the only system to be considered even if interactions with external effective fields are also present, its state is described by a *ket* in its Hilbert space and it is said to be a *pure* state. The pure qubit state is represented by the linear superposition

$$|\psi\rangle \;=\; \alpha\,|0\rangle \;+\; \beta\,|1\rangle \tag{1.1}$$

where $\alpha, \beta \in \mathbb{C}$ are such that $|\alpha|^2 + |\beta|^2 = 1$. The above equation can be rewritten as

$$|\psi\rangle \;=\; \cos\frac{\vartheta}{2}\,|0\rangle \;+\; e^{i\varphi}\sin\frac{\vartheta}{2}\,|1\rangle\;, \tag{1.2}$$

where $\vartheta \in [0, \pi]$ and $\varphi \in [0, 2\pi]$ parametrize the surface of the unit sphere in three-dimensional space, often referred to as the *Bloch's sphere*. Any qubit state can thus be represented by a point on the Bloch's sphere, as in figure 1.1, and the unit vector $(\sin\vartheta\cos\varphi, \sin\vartheta\sin\varphi, \cos\vartheta)$ identifies the *Bloch's vector* of the state. This geometrical representation is useful since it allows us to easily visualize all the *operations* on a single-qubit state. An *operation* on a qubit state is defined as the effect of a unitary operator on the

qubit state itself. The general unitary operation can be written as

$$R_l(\theta) \,=\, e^{-\frac{i\theta\hat{l}\cdot\vec{\sigma}}{2}} \,=\, I\cos\frac{\theta}{2} - i\left(\hat{l}\cdot\vec{\sigma}\right)\sin\frac{\theta}{2}\,, \tag{1.3}$$

i.e. an SU(2) rotation where $\hat{l}$ is the direction of the rotation axis and $\boldsymbol{\sigma} = (\sigma^x, \sigma^y, \sigma^z)$ is the vector of the Pauli matrices

$$\sigma^x \,=\, \begin{pmatrix} 0 & 1 \\ 1 & 0 \end{pmatrix}\,; \quad \sigma^y \,=\, \begin{pmatrix} 0 & -i \\ i & 0 \end{pmatrix}\,; \quad \sigma^z \,=\, \begin{pmatrix} 1 & 0 \\ 0 & -1 \end{pmatrix}\,, \tag{1.4}$$

satisfying the $\mathbf{su}(2)$ algebra commutation relations

$$\sigma^\mu\sigma^\nu \,=\, \delta^{\mu\nu}\mathbb{1} + i\sum_\xi \varepsilon^{\mu\nu\xi}\sigma^\xi\,, \tag{1.5}$$

where $\delta^{\mu\nu}$ is the Kronecker delta and $\varepsilon^{\mu\nu\xi}$ is the three-dimensional Levi-Civita symbol. The components of the Bloch's vector are given by $\langle\boldsymbol{\sigma}\rangle \equiv \langle\psi|\boldsymbol{\sigma}|\psi\rangle$. With the notation $\langle\mathcal{O}\rangle \equiv \langle\psi|\,\mathcal{O}\,|\psi\rangle$, we define the the *expectation value* of an observable $\hat{\mathcal{O}}$ on the pure state $|\psi\rangle$. Equation (1.3) entails that any single-qubit operation can be represented as a rotation on the Bloch's sphere.

### 1.1.2 Composite Systems: the reduced density matrix

Given two systems $A$ and $B$ described, respectively, by the Hilbert spaces $\mathscr{H}_{_A}$ and $\mathscr{H}_{_B}$, the pure state $|\psi\rangle$ of the composite system constituted by both $A$ and $B$ belongs to the Hilbert space $\mathscr{H}_{_A}\otimes\mathscr{H}_{_B}$, i.e. the tensor product of the two Hilbert spaces. Then, if $\mathscr{A} = \{|\alpha\rangle\}$ and $\mathscr{B} = \{\,|\beta\rangle\}$ are bases, respectively, for $\mathscr{H}_{_A}$ and $\mathscr{H}_{_B}$, then the set of states $\{|\alpha\rangle\otimes|\beta\rangle \;|\; |\alpha\rangle\,(|\beta\rangle) \in \mathscr{A}\,(\mathscr{B})\,\}$ forms a basis of $\mathscr{H}_{_A}\otimes\mathscr{H}_{_B}$. The linear superposition

$$|\psi\rangle \,=\, \sum_{\alpha,\beta} x_{\alpha\beta}\,|\alpha\rangle\otimes|\beta\rangle \tag{1.6}$$

is the general state describing the system $(A, B)$ with $|\alpha\rangle\,|\beta\rangle \equiv |\alpha\rangle\otimes|\beta\rangle$ and $x_{\alpha\beta}\in\mathbb{C}$. As it can be seen from the above equation, not all the states can be written in the form $|\psi\rangle = |\psi_A\rangle\otimes|\psi_B\rangle$. When such a situation occurs (i.e. when $|\psi\rangle \neq |\psi_A\rangle\otimes|\psi_B\rangle$) we say that the state $|\psi\rangle$ is *non-separable*, this meaning that the states of the two subsystems $A$ and $B$ are not vectors belonging to $\mathscr{H}_{_A}(\mathscr{H}_{_B})$. Anyway it is still possible to give a description of any subsystem in terms of the so called *reduced density matrix*, which is obtained by a partial trace operation on the projector defined by the (pure) state $|\psi\rangle\in\mathscr{H}_{_{A\otimes B}}$,

$$\rho_{A(B)} \,=\, \mathrm{Tr}_{B(A)}\,|\psi\rangle\,\langle\psi|\;. \tag{1.7}$$

The density matrix operator is a hermitean, trace 1 (guaranteed by the normalization of the original state $|\psi\rangle$) and semi-definite positive operator reproducing the expectation values of the local observables [1]: take $\mathcal{O}_A$, an observable in the space $\mathscr{H}_A$ then it is easy to see that

$$\langle \mathcal{O}_A \rangle \equiv \mathrm{Tr}_A \left( \rho_A \mathcal{O}_A \right) = \langle \psi | \, \mathcal{O}_A \otimes \mathbb{1}_B \, | \psi \rangle \ , \tag{1.8}$$

where $\mathcal{O}_A \otimes \mathbb{1}_B$ is the natural extension of $\mathcal{O}_A$ on the whole system space. Of course the density matrix picture is also valid when the original state is separable, in fact, in this case the reduced density operator of one of the subsystems is just the projector on the direction defined by the well definite subsystem states, i.e. if

$$|\psi\rangle = |\psi_A\rangle \otimes |\psi_B\rangle \ , \tag{1.9}$$

then from the definition (1.7)

$$\rho_{A(B)} = |\psi_{A(B)}\rangle \langle \psi_{A(B)}| \ . \tag{1.10}$$

Starting with a reduced density operator, there is a simple quantity that allows us to distinguish if it is a projector as above (the original state is separable), or if it is not (non-separable state); this quantity is the trace of the square of the density matrix, $\mathrm{Tr}(\rho^2) \leq 1$, which is equal to one if and only if $\rho$ is a projector. We have, in fact, that if $\rho$ is equal to a projector $\mathcal{P}$ then, being $\mathcal{P}^2 = \mathcal{P}$, we have $\mathrm{Tr}\, \rho^2 = \mathrm{Tr}\, \rho = 1$; otherwise let us start from the condition $\mathrm{Tr}\, \rho^2 = 1$: this implies that, being $\rho$ hermitean,

$$\sum_i \lambda_i^2 = 1 = \sum_i \lambda_i \, , \tag{1.11}$$

where the $\lambda_i$ are the eigenvalues of the density matrix and in the last step we exploited the fact that $\mathrm{Tr}\, \rho = 1$ by definition. Since $0 \leq \lambda_i \leq 1 \forall i$ the conditions (1.11) can be satisfied only if one $\lambda_i = 1$ for one single $i$ while all the others are equal to zero, i.e. $\rho$ is a projector.

If the subsystem we are interested in is a qubit we can still represent its state in terms of the Bloch vector introduced in the previous section: exploiting the fact that the Pauli matrices plus the identity on the two dimensional space form a basis of the $2 \times 2$ matrix space on the field $\mathbb{C}$, we can write $\rho$ as

$$\rho = \frac{1}{2} \left( \mathbb{1}_2 + \boldsymbol{n} \cdot \boldsymbol{\sigma} \right) \ , \tag{1.12}$$

[1] The space of density operators is the space of all semi-posistive, hermitean, trace-one operators acting on $\mathscr{H}$, with the Hilbert-Schmidt inner product:

$$(\rho, \rho')_{\mathrm{HS}} \equiv \mathrm{Tr}(\rho^\dagger \rho')$$

with $\rho^\dagger$ indicating the conjugate transpose of $\rho$.

where $\boldsymbol{n}$ is the Bloch vector, and $\boldsymbol{\sigma}$ is the Pauli-matrix vector. In the previous section we also defined the Bloch's vector as a unit vector, and this leads us to define the Bloch's sphere as the locus of all pure qubit states. In the general case, from equations (1.11) and (1.7), we find the following condition

$$\mathrm{Tr}(\rho^2) = \frac{1}{2}\left(1 + |\boldsymbol{n}|^2\right) \leq 1 \qquad \Longrightarrow \qquad |\boldsymbol{n}|^2 \leq 1\,, \tag{1.13}$$

where the equality is found only if the state described by $\rho$ is a projector in the qubit Hilbert space. The above condition implies that, in general, qubit states are included within the *Bloch's ball* rather than staying only on its surface.

In the next section we will focus on non-separable states. Non-separability testifies the presence of quantum correlations between the two subsystems. These correlations are generically called *entanglement* and the study of their classification and of their properties is of crucial importance in the different fields of quantum physics.

## 1.2 Entanglement

The term "entanglement" indicates the presence of non-local correlations between the outcomes of measurements realized on different subsystems and, as we already noted, it is related to the non separability of the whole system state, which makes entanglement a property of the quantum state with no counterpart in classical physics [2]. Entanglement is not an observable, i.e. its value is not related to the expectation value of some hermitean operator. Nevertheless it can be quantified and also indirectly measured [46–50]. Besides being interesting for deepening our knowledge of quantum physics, quantum correlations are those features that make, at least in principle, quantum computing more efficient than classical computation. For this reason, the research activity on these topics has been and still is very intense, resulting in a rich specific literature. Different proposals for new definitions to better quantify or classify quantum correlations continue to appear. Since a thorough review of such a vast research field is beyond the scope of this section, we here limit our discussion to the entanglement definitions [3] used in the followings.

### Entanglement of Formation

The most celebrated measure of entanglement is the *entanglement of formation* or, sometimes, simply *entanglement*. The name "Entanglement of formation" comes from its original

[2] It has been shown that some dynamical classical phases (Berry phases) can emerge in the classical limit process as remnant of the entanglement present in the original state of the quantum system [45].

[3] We are here referring to measures of bipartite entanglement, i.e. quantities that quantifies how much two subsystem of a given (bi-)partition are correlated. We clarify here that any entanglement measure has sense only in relation to a specific system partition (different partitions give different values of entanglement on the same state).

operative definition where it was related to the quantification of the information (in terms of entangled qubit-pairs) that must be exchanged between two parties in order to construct a copy of a state [51].

If we consider the whole system to be in a pure state, the *entanglement of formation* is also called,*entropy of entanglement*, since its formal definition depends on another quantity, which is also very renowned in quantum information theory, the so called *Von Neumann Entropy*. Von Neumann Entropy, $\mathcal{S}$, is defined as

$$\mathcal{S}(\rho) \;=\; -\operatorname{Tr}\rho\log\rho\,, \tag{1.14}$$

where the logarithm is intended to be in base 2 (henceforth log will be assumed always base 2, except when differently specified [4]), and we have assumed $0\log_{\mathrm{d}}0 \equiv 0$, as it is usually done, e.g. for the Shannon Entropy. The Von Neumann entropy, though being well defined for any density operator, directly quantifies the entanglement only of the pure states of bipartite systems [5]. In fact, taking a pure state $|\psi\rangle$ and a partition $AB$ of the system, the entanglement between the two subsystems, $A$ and $B$, is given by the entropy of entanglement which is, by definition, equal to the Von Neumann entropy as reported below:

$$\mathcal{E}_{AB}(|\psi\rangle) \;\equiv\; \mathcal{S}(\rho_A) \;=\; -\operatorname{Tr}\rho_A\log\rho_A\,, \tag{1.15}$$

where $\rho_A$ is the reduced density matrix [6] for the subsystem $A$ as described in equation (1.7) and the trace is intended over the degrees of freedom of the subsystem $A$. The basic properties of $\mathcal{S}(\rho)$ are:

i)- The entropy is non-negative and it is equal to zero if and only if the state is pure (i.e. a projector)

ii)- In a d-dimensional Hilbert space the entropy is at most $\log \mathrm{d}$. The maximum value is found if and only if the system is in a *completely mixed state*, i.e. $\rho = \mathbb{1}/\mathrm{d}$

iii)- If a composite system is in a pure state, then $\mathcal{S}(\rho_A) = \mathcal{S}(\rho_B)$.

Property i) follows from the definition and, together with the cyclic invariance of the trace operation, assures that $\mathcal{S}$ is invariant under local unitary transformations and that $\mathcal{S} = 0$ for separable states. The second property sets a limit on the value of the entanglement

[4] The choice of the logarithm base is customary since, any different choice only differs for a multiplying constant. This choice sets equal to one the maximum value for the Von Neumann entropy of a qubit, in analogy with the classical binary entropy. For a d-dimensional system the maximum value is $\log_2 \mathrm{d}$ (see equation (1.18)), testifying the fact that more degrees of freedom correspond to more possibilities for setting correlations.

[5] The generalization for mixed state is discussed later in this section.

[6] The choice of evaluating the entropy on $\rho_A$ instead of $\rho_B$ is irrelevant since, as we will show in the following, $\mathcal{S}(\rho_A) = \mathcal{S}(\rho_B)$ if one starts from a pure state of the whole system.

evaluated on the state of d-dimensional Hilbert space; its proof needs the introduction of the following quantity, the *quantum relative entropy*. Given two density matrices $\rho$ and $\sigma$ the relative entropy of $\rho$ with respect $\sigma$ is defined by

$$\mathcal{S}(\rho\,\|\,\sigma) \equiv \mathrm{Tr}(\rho\log\rho) - \mathrm{Tr}(\rho\log\sigma)\,. \tag{1.16}$$

The relative entropy is subject to the so called *Klein's inequality*,

$$\mathcal{S}(\rho\,\|\,\sigma) \geq 0\,, \tag{1.17}$$

i.e. it is non-negative and is equal to zero if and only if $\rho = \sigma$. The proof of the Klein's inequality can be found, e.g., in [52]. The proof of property ii) is a straightforward consequence of Klein's inequality: in fact, evaluating the relative entropy of any density matrix $\rho$ with $\mathbb{1}/\mathrm{d}$ we find

$$\mathcal{S}(\rho\,\|\,\mathbb{1}/\mathrm{d}) = -\mathcal{S}(\rho) + \log\mathrm{d} \geq 0 \quad\Longrightarrow\quad \mathcal{S}(\rho) \leq \log\mathrm{d} \tag{1.18}$$

Finally the third property follows from the *Schmidt decomposition theorem* which states:

*If $|\psi\rangle$ is a vector in a tensor product space $\mathscr{H}_A \otimes \mathscr{H}_B$, then there exists an orthonormal basis $\{|\varphi_l^A\rangle\}$ for $\mathscr{H}_A$ and an orthonormal basis $\{|\varphi_m^B\rangle\}$ for $\mathscr{H}_B$, and non negative real numbers $\{p_i\}$ such that*

$$|\psi\rangle = \sum_i \sqrt{p_i}\,|\varphi_i^A\rangle \otimes |\varphi_i^B\rangle\,. \tag{1.19}$$

The coefficients $\sqrt{p_i}$ are called *Schmidt coefficients*, and their number is, of course, smaller than or equal to the smallest between the dimensions of $\mathscr{H}_A$ and $\mathscr{H}_B$. It is important to stress that the two Schmidt bases and the relative coefficients are not general but depend on the specific state $|\psi\rangle$ considered. Thanks to this theorem, we can rewrite the projector of any pure state as

$$|\psi\rangle\langle\psi| = \left(\sum_i \sqrt{p_i}\,|\varphi_i^A\rangle \otimes |\varphi_i^B\rangle\right)\left(\sum_i \sqrt{p_j}\,\langle\varphi_j^A| \otimes \langle\varphi_j^B|\right)\,; \tag{1.20}$$

this particular form makes very easy to compute the partial trace over each subsystem, in fact

$$\begin{aligned}\rho_A = \mathrm{Tr}_B\,|\psi\rangle\langle\psi| &= \sum_{i,j} \sqrt{p_i p_j}\,|\varphi_i^A\rangle\langle\varphi_j^A|\,\langle\varphi_j^B|\varphi_i^B\rangle \\ &= \sum_i p_i\,|\varphi_i^A\rangle\langle\varphi_i^A|\,.\end{aligned} \tag{1.21}$$

For the other subsystem we analogously obtain

$$\rho_{_B} \,=\, \mathrm{Tr}_{_A}\,|\psi\rangle\langle\psi| \,=\, \sum_i p_i\,|\varphi_i^{B}\rangle\langle\varphi_i^{B}|\,. \tag{1.22}$$

The last two expressions tell us that both $\rho_{_A}$ and $\rho_{_B}$ have the same eigenvalues, meaning that $\mathcal{S}(\rho_{_A}) = \mathcal{S}(\rho_{_B})$, since the Von Neumann entropy is completely determined by the density matrix spectrum. Due to the connection between $\mathcal{S}$ and $\mathcal{E}$ we can extend the property we have just demonstrated also to the entropy of entanglement of pure states: $\mathcal{E}_{_{AB}}(|\psi\rangle)$ is invariant under local unitary transformations; $\mathcal{E}_{_{AB}}(|\psi\rangle) = 0$ iff $\rho_{_{A(B)}}$ is a projector (i.e. $\psi \,=\, |\psi_{_A}\rangle \otimes |\psi_{_B}\rangle$); $0 \,\leq\, \mathcal{E}_{_{AB}} \,\leq\, \log \mathrm{d}$ and $\mathcal{E}_{_{AB}} \,=\, \log \mathrm{d}$ iff $\rho_{_{A(B)}} \,=\, \mathbb{1}/\mathrm{d}$ is the completely mixed state. We want to note also that, as a consequence of the Schmidt decomposition, $\mathcal{S}(\rho_{_A}) = \mathcal{S}(\rho_{_B}) \leq \log m$, where $m = \min(\{\dim \mathscr{H}_{_A}, \dim \mathscr{H}_{_B}\})$.

If the state we want to describe is not a pure state $|\psi\rangle$ but rather a density operator $\rho$ the Von Neumann entropy is no more adequate for correctly quantifying entanglement. Suppose the system is in a mixed state $\rho$; we can represent it as follows

$$\rho \,=\, \sum_i p_i\,|\psi_i\rangle\langle\psi_i| \quad \text{with} \quad p_i \in \mathbb{R},\;\; \sum_i p_i \,=\, 1\,, \tag{1.23}$$

for some set $\{p_i, |\psi_i\rangle\}$, which is said *to realize* the state $\rho$. We note that the set of coefficients and states realizing $\rho$ is not unique, but, conversely, infinite in number, since the states $|\psi_i\rangle$ are not required to be orthogonal [7], nor in a number equal to $\dim \mathscr{H}$. Thus, in this case, the former entanglement definition must be generalized to the following one [51]

$$\mathcal{E}_{_{AB}}(\rho) \,=\, \min_{\{p_i,|\psi_i\rangle\}} \sum_i p_i \mathcal{E}_{_{AB}}(|\psi_i\rangle)\,, \tag{1.24}$$

where the minimization process is over all the sets $\{p_i, |\psi_i\rangle\}$ realizing $\rho$, and $\mathcal{E}_{_{AB}}(|\psi_i\rangle)$ is the entanglement entropy of the pure state $|\psi_i\rangle$ according to definition (1.15).

The objective difficulty in evaluating the minimization over the infinite number of sets realizing each mixed state, makes the definition (1.24) quite difficult for the practical use.

However there is a specific case in which the minimization can be carried out and an explicit expression can be given as function of $\rho$: this particular case is met when the system is made up of two qubits. In this case the entanglement of formation of a generic two-qubit state $\rho$ reads as follows [53, 54]

$$\mathcal{E}(\rho) \,=\, \mathcal{F}(\mathcal{C}(\rho))\,, \tag{1.25}$$

[7] Requiring the orthogonality the set $\{p_i, |\psi_i\rangle\}$ is the unique spectral decomposition of $\rho$.

where

$$\mathcal{F}(\mathcal{C}) \,=\, h\left(\frac{1+\sqrt{1-\mathcal{C}^2}}{2}\right) , \tag{1.26}$$

with $h = -x\log_2 x - (1-x)\log_2(1-x)$ the binary entropy, and $\mathcal{C}$ is the so called *Concurrence*, a function that varies between 0 and 1, defined as follows.

**Concurrence**

The concurrence of a generic two-qubit state $\hat{\rho}$, is defined as

$$\mathcal{C}(\hat{\rho}) \,\equiv\, \max\left(0, \lambda_1 - \lambda_2 - \lambda_3 - \lambda_4\right) , \tag{1.27}$$

where $\{\lambda_1,\, \lambda_2,\, \lambda_3,\, \lambda_4\}$ are the eigenvalues (in decreasing order) of the hermitian matrix

$$R \,=\, \sqrt{\sqrt{\hat{\rho}}\,\tilde{\rho}\,\sqrt{\hat{\rho}}} \tag{1.28}$$

with

$$\tilde{\rho} \,=\, \left(\sigma^y \otimes \sigma^y\right)\, \hat{\rho}^*\, \left(\sigma^y \otimes \sigma^y\right) , \tag{1.29}$$

where $\sigma^y$ is the corresponding Pauli matrix. Since the function $\mathcal{F}(\mathcal{C})$ is a monotonic function of its argument ranging from 0 to 1, the *Concurrence* $\mathcal{C}$, accounts properly for the entanglement of a generic (pure or generally mixed) two-qubit state.

## 1.3 Evolution of quantum systems

Any closed quantum system, which is described by a pure state $|\psi\rangle$ in its Hilbert space $\mathscr{H}$, evolves according to the Schrödinger equation

$$i\hbar\frac{d}{dt}\,|\psi\rangle = \mathcal{H}(t)\,|\psi\rangle \ , \tag{1.30}$$

where $\mathcal{H}$ is the system Hamiltonian which can be, in general, time-dependent. The Schrödinger equation is a linear equation preserving the norm, $\langle\psi|\psi\rangle$, of vectors in $\mathscr{H}$: this implies that its solutions can be expressed through a unitary operator $\mathcal{U}$. Thus the evolution of a state $|\psi\rangle$ in the time interval $[t_0, t]$ is given by the following expression

$$|\psi(t)\rangle \,=\, \mathcal{U}(t,t_0)\,|\psi_0\rangle \,=\, T\left\{\exp\left[-\frac{i}{\hbar}\int_{t_0}^{t} dt'\,\mathcal{H}(t')\right]\right\}|\psi_0\rangle \ , \tag{1.31}$$

where, $|\psi_0\rangle = |\psi(t=t_0)\rangle$, is the initial state at $t = t_0$ and $T$ represents the time-ordering operator. If the Hamiltonian does not depend on time, the evolution operator assumes the

simple form

$$\mathcal{U}(t,t_0) \;=\; e^{-i\frac{\mathcal{H}}{\hbar}(t-t_0)}\,. \tag{1.32}$$

The evolution operators satisfy the following relations

$$\mathcal{U}(t_0,t_0)=\mathbb{1}\,;\quad \mathcal{U}(t,t_0)=\mathcal{U}(t,t_1)\mathcal{U}(t_1,t_0)\,;\quad \mathcal{U}^{-1}(t_0,t)=\mathcal{U}(t,t_0)=\mathcal{U}^{\dagger}(t_0,t)\,. \tag{1.33}$$

In the case of the time-independent Hamiltonian the dependence on $t$ and $t_0$ reduces to a dependence on their difference $s=t-t_0$ and the set of the evolution operators $\mathcal{U}(s)$ is a *one-parameter group*.

If we consider now a density operator $\rho$, at $t=t_0$, equation (1.31) gives us the recipe for its evolution which will be simply given by

$$\rho(t,t_0)=\mathcal{U}(t,t_0)\,\rho\,\mathcal{U}^{\dagger}(t,t_0)\,. \tag{1.34}$$

Of course this is still the case of a density operator representing a closed system.

Suppose now the system is divided into two subsystems A and B and that we are interested in the evolution of only one of them, say A. If we start with the density operator of the whole system as an initial state, equation (1.34) can still be used in order get the evolution of the overall system, eventually obtaining the evolved reduced operator $\rho_{\mathrm{A}}(t,t_0)$ through a partial trace on subsystem B. But what can we say about the map, between density operators spaces,

$$\mathcal{M}_{(t,t_0)}\,:\,\rho_{\mathrm{A}}(t_0)\;\longrightarrow\;\rho_{\mathrm{A}}(t,t_0) \tag{1.35}$$

connecting the initial ($\rho_{\mathrm{A}}$) reduced density operator to the evolved one ($\rho_{\mathrm{A}}(t,t_0)$)? A map $\mathcal{M}$ like that described in the former equation is called a *dynamical map*; the problem with such kind of map is that it in general depends not only on the global evolution operator $\mathcal{U}(t,t_0)$ and on the properties of the subsystem B, but also on the initial state of the subsystem A itself. In fact, it can be demonstrated that any time-evolution of a reduced state $\rho_{\mathrm{A}}\equiv\rho_{\mathrm{A}}(t_0)$ can be written as

$$\rho_{\mathrm{A}}(t,t_0)\;\equiv\mathcal{M}_{(t,t_0)}(\rho_{\mathrm{A}})\;=\;\sum_a K_a(t,t_0;\rho_{\mathrm{A}})\,\rho_{\mathrm{A}}\,K_a^{\dagger}(t,t_0;\rho_{\mathrm{A}})\,, \tag{1.36}$$

where the $K_a(t,t_0;\rho_{\mathrm{A}})$ are operators [8] which depends on the state $\rho_{\mathrm{A}}$ at time $t_0$. This last expression shows that it is difficult to state something general about the evolution of reduced density operators, in fact, given that some $\rho_{\mathrm{A}}$ evolve from a time $t_0$ to a successive time $t$ according to a dynamical map $\mathcal{M}$, any further evolution can be no more described by the same $\mathcal{M}$, unless $\rho_{\mathrm{A}}(t,t_0)=\rho_{\mathrm{A}}$, because of the explicit dependence on the initial

[8] We note here that this decomposition is not even unique as it is shown in [55, 56].

state.

Although we will not make explicit use of the dynamical map formalism, it is worth spending few more words for introducing two fundamental concepts in the description of the evolution of quantum systems, the *Universal Dynamical Map*, and the *Kraus decomposition*. In fact, a particularly interesting case is obtained when considering a factorized initial state $\rho = \rho_{\rm A} \otimes \rho_{\rm B}$. Under this assumption it is easily found that the decomposition (1.36) becomes

$$\rho_{\rm A}(t,t_0) \equiv \mathcal{M}_{(t,t_0)}(\rho_{\rm A}) = \sum_a K_a(t,t_0)\,\rho_{\rm A}\,K_a^\dagger(t,t_0)\,, \tag{1.37}$$

i.e., the dependence on the initial state disappear. We have in fact

$$\begin{aligned}
\rho_{\rm A}(t,t_0) &= \mathrm{Tr}_B\left\{\mathcal{U}(t,t_0)\,\rho_{\rm A}\otimes\rho_{\rm B}\,\mathcal{U}^\dagger(t,t_0)\right\} \\
&= \sum_i \lambda_i\,\mathrm{Tr}_B\left\{\mathcal{U}(t,t_0)\,\rho_{\rm A}\otimes|\psi_i\rangle\langle\psi_i|\,\mathcal{U}^\dagger(t,t_0)\right\} \\
&= \sum_{i,j}\lambda_i\,\langle\psi_j|\,\mathcal{U}(t,t_0)\,|\psi_i\rangle\;\rho_{\rm A}\;\langle\psi_i|\,\mathcal{U}^\dagger(t,t_0)\,|\psi_j\rangle \\
&= \sum_a K_a(t,t_0)\,\rho_{\rm A}\,K_a^\dagger(t,t_0)\,,
\end{aligned} \tag{1.38}$$

where in the second line we used the spectral decomposition of $\rho_{\rm B}$ and we finally defined the multi-index $a \equiv (i,j)$ and $K_{ij}(t,t_0) \equiv \sqrt{\lambda_i}\,\langle\psi_j|\,\mathcal{U}(t,t_0)\,|\psi_i\rangle$. In this case the map $\mathcal{M}_{t,t_0}$ such that $\mathcal{M}_{t,t_0}(\rho_{\rm A}) = \rho_{\rm A}(t,t_0)$ is called *Universal Dynamical Map* (UDM). The operators $K_a(t,t_0)$ do also fulfil the following relation

$$\sum_a K_a^\dagger(t,t_0)K_a(t,t_0) \;=\; \mathbb{1}\,, \tag{1.39}$$

since the evolution of the whole system is unitary and thus $\mathrm{Tr}_A\,\rho_{\rm A} \;=\; \mathrm{Tr}_A\,\rho_{\rm A}(t,t_0)$ for whatever initial state. The main features of UDM are the following

*i)* A Dynamical map is a UDM iff it is induced by a larger system with initial condition $\rho_{\rm A}\otimes\rho_{\rm B}$ with $\rho_{\rm B}$ fixed for any $\rho_{\rm A}$.

*ii)* UDM are *linear*, *completely-positive* and *trace-preserving* maps.

*iii)* If a UDM is invertible, its inverse is a UDM; this happens iff the UDM is unitary.

Complete-positiveness comes from the observation that, if there is another subsystem C, which is not interacting with A and B, i.e. the global evolution reads $\mathcal{U}_{\rm AB}\otimes\mathcal{U}_{\rm C}$ with $\mathcal{U}_{\rm C}$ unitary, then, for whatever initial state in the form $\rho_{\rm AC}\otimes\rho_{\rm B}$ where $\rho_{\rm AC}$ is any state (factorized or not) of AC, the evolution of the subsystem AC can be written

$$\rho_{\rm AC}(t,t_0) = (\mathcal{M}_{t,t_0}\otimes\mathcal{U}_{\rm C}(t,t_0))\rho_{\rm AC}(t_0) \tag{1.40}$$

with $\mathcal{M}_{t,t_0}$ the same UDM as if the subsystem C were not present. We have then that, for any unitary $\mathcal{U}(t,t_0)$ in any dimension, the map,

$$\mathcal{M}_{t,t_0} \otimes \mathcal{U}(t,t_0) = [\mathcal{M}_{t,t_0} \otimes \mathbb{1}]\,[\mathbb{1} \otimes \mathcal{U}(t,t_0)]\ , \tag{1.41}$$

is also a UDM. A linear map fulfilling the above condition is said to be *completely positive* [57]. The operators $K_a(t,t_0)$ are called *Kraus operators*, while expression (1.37) is called *Kraus decomposition* after the name of Karl Kraus who proved that any completely-positive linear map can be written as in (1.37). As for the other properties listed in *ii)* the linearity is evident from the definition (1.37), and the trace-preserving property arises from the unitarity of the overall evolution.

Finally we want to point out that UDM do not share the composition relations (1.33) of the unitary evolutions. Let us consider, for example, the evolution of the density operator $\rho_{\mathrm{A}}$ from time $t_0$ to some time $t$ and say that it is described by some UDM, $\mathcal{M}_{(t_0,t)}$. Consider then the evolution from $t_0$ to some $t_1$ such that $t_0 < t_1 < t$: this will be obtained through a UDM, $\mathcal{M}_{(t_0,t_1)}$, since the global evolution and the global initial state are the same as before. Now if we consider the evolution from $t_1$ to $t$, starting from the state $\rho_{\mathrm{A}}(t_1,t_0) = \mathcal{M}_{(t_0,t_1)}\rho_{\mathrm{A}}$, this is no more given by a UDM, unless the global evolution is trivially factorized [9]. Thus the evolution of the subsystem A from $t_0$ to $t$ cannot be written as the composition of two UDM, even though it is described by a UDM itself, i.e.

$$\mathcal{M}_{(t_0,t)} = \mathcal{M}_{(t_0,t_1)}\mathcal{M}'_{(t_1,t)}\,, \tag{1.42}$$

where $\mathcal{M}'_{(t_1,t)}$ cannot be a UDM even if both $\mathcal{M}_{(t_0,t)}$ and $\mathcal{M}_{(t_0,t_1)}$ are so.

As a last remark, we note that any *quantum operation*, i.e. any unitary action on a qubit-register, can be thought of as the evolution of a system for a specific time-interval.

## 1.4 A ticket to Classical-Land

Hybrid schemes are situations where a system is made by a (semi-)classical robust partner interacting with purely quantum objects. Such a situation is peculiar since two different levels of *quanticity* are present within the same system. Usual semi-classical techniques, such as perturbative methods, involve the system as whole flattening the quanticity difference which is fundamental and must be preserved in hybrid schemes.

A new approach have to be introduced and this section is devoted to show how the usual classical-limit reveal us which are the best tools to deal with hybrid schemes. Aim of the present thesis is to exploit some classical features of non-linear systems in order to

[9] The global state $\rho(t_1,t_0) = \mathcal{U}(t_1,t_0)\rho(t_0)$ is in general different from $\rho_{\mathrm{A}}(t_1,t_0) \otimes \rho_{\mathrm{B}}(t_1,t_0)$ unless $\mathcal{U}(t_1,t_0) = \mathcal{U}_{\mathrm{A}}(t_1,t_0) \otimes \mathcal{U}_{\mathrm{B}}(t_1,t_0)$, i.e. the subsystems A and B are not interacting.

achieve quantum operations such as entanglement generation. This goal requires to put into contact two worlds that appear completely separated: the classical world with its phase space, variables and the related equations of motion, and the quantum world with its Hilbert spaces, state vectors and operators. The typical approach for relating the quantum picture to the classical picture of the same system, is to cross from the completely quantum side toward the completely classical one thanks to the so called *classical limit*. In a hybrid scheme, considering the robust partner as classical, can be good for applications which do not require to preserve any of its specifically quantum features: this is the case, for example, of the application we will describe in chapter 4, where the manipulation of a qubit state only requires some magnetic field which can be effectively produced through the dynamics of a classical system [42, 43]. The situation is different when some of the quantum characteristics must be kept, e.g. when trying to establish quantum correlations between different parts of the system: in these cases considering the robust partner as classical doesn't work, since this would erase the quantum structures which are fundamental for accomplishing the required tasks. We thus have to move somehow "in between" the classical and the quantum pictures. Nevertheless it is worth discussing the classical limit because the knowledge of how a system on quantum edge "crosses the river" toward the classical one may let us collect precious hints on how to treat the situations in which we are interested in.

The expression "classical limit" stands for the mathematical limit process, applied on quantum theories, which is obtained assuming that the number of particles (degrees of freedom) goes to infinity $N \to \infty$ or, formally, the fundamental quantum constant, $\hbar$, goes to zero. This limit demands that the uncertainty-bounds on physical observables vanish on physical states, i.e. that $\langle AB \rangle = \langle A \rangle \langle B \rangle + \mathcal{O}(\hbar)$, so that quantum fluctuations become irrelevant in the classical limit. It turns out that there is a particularly convenient framework to treat this problem in general, which is provided by a class of states named *Coherent states*. Within this framework, Lieb showed [58], for example, that in the classical limit [10] $S \to \infty$ the free energy of a quantum spin system becomes equivalent to the classical one. The same conclusion has been successively extended also to all systems with a compact *dynamical group* [11] and to a non-compact group with a square-integrable Hilbert space [59–61].

In consideration of the cited results, it appears now that coherent states may provide a suitable tool for the kind of applications we are trying to develop. We here give an introduction to these particular states trying to highlight the major features that will be the most useful in the successive chapters.

[10] For spin system the classical limit is obtained sending the spin modulus $S$ to infinity $S \to \infty$ while the constant $\hbar \to 0$ keeping the product, $\hbar S$, finite. This kind of classical limit can be related to the usual $N \to \infty$ by noting that large $S$ can be obtained by selecting the highest $S$-value sector of the total angular momentum in a system of $N$ spin with $S = 1/2$.

[11] The precise definition of dynamical group will be given in section 1.4.3.

### 1.4.1 Field Coherent States

The most celebrated coherent states are the *Field Coherent States* (FCS) often called *Glauber's coherent states* after the name of Glauber [62, 63] that, almost at the same time with Sudarshan [64] and Klauder [65, 66] , first built these states in the modern fashion [12] and first used the term *coherent states* [62, 63] The FCS, $|\alpha\rangle$, indicated by the label $\alpha \in \mathbb{C}$, are defined by the application of a *displacement operator* to the vacuum state of the harmonic oscillator $|0\rangle$ as follows

$$|\alpha\rangle \equiv e^{-|\alpha|^2/2} e^{\alpha a^\dagger} |0\rangle \ , \tag{1.43}$$

where $a$ and $a^\dagger$ are the usual creation and annihilation operators of the harmonic oscillator, obeying the commutation relation $[a, a^\dagger] = \mathbb{1}$.

The general Baker-Campbell-Hausdorff formula for decoupling exponential operators reads

$$e^{\hat{A}} e^{\hat{B}} = \exp\left(\hat{A} + \hat{B} + \frac{1}{2}[\hat{A}, \hat{B}] + \frac{1}{12}([\hat{A}, [\hat{A}, \hat{B}]] - [\hat{B}, [\hat{A}, \hat{B}]]) + \dots\right) , \tag{1.44}$$

where $\hat{A}$ and $\hat{B}$ are two non-commuting operators and the dots stand for an infinite series of increasing order nested commutators. When A and B are $a$ and $a^\dagger$, respectively, the above relation reads

$$e^{(\alpha^\star a + \alpha a^\dagger)} = e^{-|\alpha|^2/2} e^{\alpha^\star a} e^{\alpha a^\dagger} , \tag{1.45}$$

and it is easy to prove that the FCS $|\alpha\rangle$, as defined in 1.43, is the normalized eigenstate of the annihilation operator $a$ with eigenvalue $\alpha$, i.e. $a\,|\alpha\rangle = \alpha\,|\alpha\rangle$. Although normalized, the FCS are non-orthogonal and thus form an overcomplete set of states. In fact, the overlap between two FCS is

$$\langle \alpha | \alpha' \rangle = e^{-\frac{1}{2}(|\alpha|^2 + |\alpha'|^2 - 2\alpha^\star \alpha')} ; \tag{1.46}$$

while the resolution of unity reads

$$\int \frac{d^2\alpha}{\pi} \, |\alpha\rangle\langle\alpha| = \mathbb{1} . \tag{1.47}$$

Moreover defining the "uncertainty" of an observable $\hat{\mathcal{O}}$ on a certain state $|\psi\rangle$ as

$$\Delta\hat{\mathcal{O}} = \sqrt{\langle \hat{\mathcal{O}}^2 \rangle - \langle \hat{\mathcal{O}} \rangle^2} , \tag{1.48}$$

[12] Well before the modern definition of Glauber, the FCS were introduced in a seminal paper by Schrödinger [67], looking for wave-function whose mean behaviour resemble that of the classical harmonic oscillator.

we find that FCS satisfy the minimum uncertainty relation

$$\Delta\hat{X}\Delta\hat{P} = \frac{\hbar}{2}\,, \tag{1.49}$$

for whatever value of the parameter $\alpha \in \mathbb{C}$, where $\hat{X}$ and $\hat{P}$ are the position and momentum operators

$$\hat{X} = \sqrt{\frac{\hbar}{2m\omega}}(a + a^\dagger)\,, \qquad \hat{P} = \frac{1}{i}\sqrt{\frac{m\hbar\omega}{2}}(a - a^\dagger)\,, \tag{1.50}$$

with $\omega$ is the angular frequency of the oscillator and $m$ its mass.

An important property of the FCS is related to their evolution. Consider, for example, the unperturbed oscillator Hamiltonian $\hbar\omega(\hat{N} + 1/2)$ with $\hat{N} \equiv a^\dagger a$ the *number* operator. Writing the evolution for the coherent state $|\alpha\rangle$ gives the following result

$$\begin{aligned} |\alpha(t)\rangle &= e^{-i\omega(\hat{N}+1/2)t}\,|\alpha\rangle \\ &= e^{-|\alpha|^2/2}e^{-i\omega t/2}\sum_n \frac{\left(\alpha e^{-i\omega t}\right)^n}{\sqrt{n!}}\,|n\rangle \\ &= e^{-i\omega t/2}\,|e^{-i\omega t}\alpha\rangle\ . \end{aligned} \tag{1.51}$$

The above equation states that if you let a FCS evolve according to the unperturbed harmonic oscillator Hamiltonian you will always end up with a FCS (except for an oscillating phase factor), whose parameter is a function of time. In particular we see that, being the FCS parameter related to the expectation values of position and momentum as follows:

$$\langle\alpha|\,\hat{X}\,|\alpha\rangle = \sqrt{\frac{2\hbar}{m\omega}}\,\mathrm{Re}(\alpha) \qquad \langle\alpha|\,\hat{P}\,|\alpha\rangle = \sqrt{2m\hbar\omega}\,\mathrm{Im}(\alpha), \tag{1.52}$$

there is a strict correspondence between $\alpha$, the FCS parameter, and the "classical" phase space, $x$ and $p$, obtained by associating the classical variables with the expectation values of the corresponding quantum operators. Moreover, writing $\alpha = |\alpha|e^{i\phi}$ we find

$$\begin{aligned} x(t) &\equiv \langle\alpha(t)|\,\hat{X}\,|\alpha(t)\rangle = \sqrt{\frac{2\hbar}{m\omega}}\,|\alpha|\,\cos(\omega t + \phi) \\ p(t) &\equiv \langle\alpha(t)|\,\hat{P}\,|\alpha(t)\rangle = \sqrt{2m\hbar\omega}\,|\alpha|\,\sin(\omega t + \phi)\,. \end{aligned} \tag{1.53}$$

This means that the variables $x(t)$ and $p(t)$ evolve as the position and momentum of a classical harmonic oscillator. Something similar to equation (1.51) can be demonstrated also if the Hamiltonian contains time-dependent terms in the form

$$\hbar\omega a^\dagger a + \lambda(t)a + \lambda^\star(t)a^\dagger\,, \tag{1.54}$$

where $\lambda(t)$ is a complex valued continuous function of time $t$. Considering general time-

dependent coefficients makes the proof less straightforward than that of equation 1.51 since the evolution operator involves a time-ordered exponential (see equation (1.31)), however the result is analogous being the evolved coherent state still a coherent state where the parameter at general time is given by the corresponding quantity evolved according to the classical EoM. It turns out that this is a general property of coherent states that can be summarized by the sentence "once a coherent state always a coherent state", if the system is initially in a coherent state it will be, at any later(previous) time in a coherent state; moreover, the link between the initial state and that at a general time is provided by the Hamilton EoM of the corresponding classical system.

### 1.4.2 Single-Spin Coherent States

We now introduce a set of coherent states, that will be of central importance to build the approximation for solving the evolution of a spin chain, in chapter 5. This set is that of the so called *Single-Spin Coherent States* (SSCS), often named *Atomic coherent states* [68], or *spin coherent states* [69]. We here define them in analogy to the FCS, following reference [69].

Taken a system made by a single spin-$S$ with Hilbert space $\mathscr{H}_{\boldsymbol{S}}$, and chosen a quantization axis $\hat{z}$, the SSCS with parameter $\tau \in \mathbb{C}$ is defined as follows

$$\begin{aligned} |\tau\rangle \;&\equiv\; \frac{1}{(1+|\tau|^2)^S}\; e^{\tau^\star \hat{S}^-}\,|0\rangle \\ &=\; \left(\cos\frac{\theta}{2}\right)^{2S} \exp\left(\tan\frac{\theta}{2} e^{i\phi}\hat{S}^-\right)|S\rangle\;, \end{aligned} \tag{1.55}$$

where $|S\rangle \equiv |m=+S\rangle$ is the extremal eigenvector of $\hat{S}^z$, $\hat{S}^\pm = \hat{S}^x \pm i\hat{S}^y$ the spin raising/lowering operators, and the prefactor assures the normalization. In the last term of equation (1.55), we set

$$\tau = e^{-i\phi}\tan(\theta/2) \tag{1.56}$$

where $\theta \in [0,\pi]$ and $\phi \in [0,2\pi]$, represent polar angle-variables such that $\hat{S}^z$ is the spin component along the polar axis $\theta = 0$. The introduction of these angle variables allows us to establish a direct connection between each SSCS and a vector of fixed modulus, i.e. a classical spin. In fact, an important property of SSCS is that the expectation values of the spin-component operators are equal to the components of a vector of modulus $S$ oriented along the direction identified by $(\theta,\phi)$, i.e.

$$\langle\tau|\hat{\boldsymbol{S}}|\tau\rangle \;=\; S(\sin\theta\cos\phi, \sin\theta\sin\phi, \cos\theta)\,, \tag{1.57}$$

where $\tau$ is given in (1.56). Having set this correspondence it is convenient to label the SSCS directly with the angles $(\theta,\phi)$ rather than with the complex parameter $\tau$, so, with reference

to equations (1.55) and (1.56), we henceforth set $\Omega \equiv (\theta, \phi)$ and $|\Omega\rangle \equiv |\tau\rangle$.

Expressing the SSCS with respect to the basis of the $S^z$-eigenvectors, $\{|m\rangle \mid m = -S, -S+1, ..., S-1, S\}$, which are also called the *Dicke states*, one finds

$$|\Omega\rangle = \sum_{m=-S}^{S} \langle m|\Omega\rangle \, |m\rangle \, , \tag{1.58}$$

where the overlaps between the $\hat{S}^z$-eigenvectors $|m\rangle$ and the coherent states $|\Omega\rangle$ read

$$\langle m|\Omega\rangle \; = \; \left(\cos\frac{\theta}{2}\right)^{2S} \sqrt{\frac{2S!}{(S-m)!(S+m)!}} \left(\tan\frac{\theta}{2}\right)^{(S-m)} e^{i(S-m)\phi} \, . \tag{1.59}$$

Analogously to the FCS, the SSCS form a non-orthogonal and over-complete set of states in $\mathscr{H}_{\boldsymbol{S}}$; in fact, the overlap between two different SSCS is

$$\langle \Omega'|\Omega\rangle \; = \; \left[\cos\frac{\theta}{2}\cos\frac{\theta'}{2} \, + \, \sin\frac{\theta}{2}\sin\frac{\theta'}{2} e^{i(\phi-\phi')}\right]^{2S} \, , \tag{1.60}$$

which implies

$$|\langle \Omega'|\Omega\rangle|^2 \; = \; \left(\frac{1+\hat{\Omega}\cdot\hat{\Omega}'}{2}\right)^{2S} \; = \; \left[\cos\left(\frac{\widehat{\Omega\Omega'}}{2}\right)\right]^{4S} \, , \tag{1.61}$$

i.e. the modulus of the overlap depends on the angle $\widehat{\Omega\Omega'}$ between the directions identified by the angles $\Omega$ and $\Omega'$. It is important to note that the overlap tends to a Dirac delta of the angles when the spin-modulus $S$ tends to infinity. Finally, the (over)completeness relation reads

$$\frac{2S+1}{4\pi} \int d\Omega \; |\Omega\rangle \, \langle\Omega| = \mathbb{1}_S \, , \tag{1.62}$$

where $d\Omega = d(\cos\theta)d\phi$. In analogy with the FCS we can also show that, using the definition (1.55), the SSCS satisfy the minimum uncertainty relation, which, for a spin system reads

$$\Delta S^x \Delta S^y \geq \frac{\hbar}{2} \, |\langle S^z\rangle| \, , \tag{1.63}$$

where the uncertainties $\Delta S^\alpha$ ($\alpha = x, y, z$) are given in equation (1.48). If the uncertainties on spin operators are evaluated on a SSCS $|\Omega\rangle$ the equality holds in the above relation. As in the case of FCS, if the dynamics of the spin is described by a Hamiltonian linear in spin operators, a SSCS will always remain a SSCS during its evolution, this is no more true, e.g. if the Hamiltonian contains a quadratic spin term. This is a property of coherent states in general and stems from the particular way (useful) coherent states are built, i.e. starting from the Hamiltonian which defines the dynamical properties of the system [13].

[13] As shown in section 1.4.3, the group of transformations, fundamental in the construction of the generalized coherent states, is determined by Hamiltonian structure, hence the name *dynamical group*.

### 1.4.3 Generalized Coherent State

Coherent states for the Harmonic oscillator, and those for the spin operators, seem to put in contact the Hilbert space of the quantum system with the phase space of some classical counterpart. Moreover, under some assumptions, also the dynamical features relate the evolution of coherent states with the classical equations (Hamilton equations) ruling the evolution of the above classical counterpart on in its phase space.

These are perfect properties for what concerns our objectives: in fact, allowing us to set specific relations between quantum and classical dynamics, they give us the possibility, in principle, of keeping some of the properties of classical non-linear dynamics down to the quantum level, and to exploit them for our purposes. It is not obvious, however, that these generalizations be straightforward and to what extent they can be significant, relatively to the specific application. This is because, although a coherent state can be related to a point in the phase space of the corresponding classical system, it is still a quantum state, i.e. a vector in a Hilbert space, and not a classical configuration.

It is clear that we must find the specific coherent states that suite correctly the system of our interest (which can be different from a single spin or a harmonic oscillator), making the generalization of the concept of coherent states to different systems a necessary prerequisite for our analysis. Gilmore and Perelomov [70–72], independently, indicated a method for constructing coherent states for any system, setting the inputs of such construction-technique. The coherent states obtained with this construction go under the name of *Generalized Coherent States* (GCS). We will now sketch the general construction for building GCS following Gilmore's method as can be found in Ref. [73] and, as an example, we will briefly recover the FCS and SSCS within this new general frame.

First of all, let us identify what are the inputs needed for the construction of GCS. The basic mathematical ingredients are: 1) a group $G$ with its generators algebra $\boldsymbol{g}$; 2) A Hilbert space $\mathscr{H}$ which contains a unitary irreducible representation of $G$; 3) An arbitrary normalized state, which will be the *reference state*, belonging to $\mathscr{H}$ [14].

These are general ingredients which appear to be purely mathematical, making the GCS concept quite abstract. However this is not true: in fact, from a physical point of view, it is easy to fulfil the above general requirements. Consider a specific quantum system, with its Hilbert space, and its Hamiltonian operator defining the dynamical properties. This

[14] Taking only the mathematical objects 1),2),3), the construction of the GCS is not unique and, in particular, it is necessary to better specify some of them in order to obtain a useful set of states. A detailed discussion about which are the possible additional requests to 1),2),3) and which are the consequences of each choice can be found e.g. in ref. [71–73]. However such discussion is not reported here since it is beyond the scope of the present work.

Hamiltonian will most often be of the form

$$\mathcal{H} = \sum_i (a_i T_i + h.c.)\,, \tag{1.64}$$

where the $a_i \in \mathbb{C}$ are numbers (possibly time-dependent) and $T_i$ are linear operators (*h.c.* represent the hermitean conjugate of the preceding term). These operators will obey some commutation relations and may constitute a subset of some Lie algebra. If this is the case, one can choose this Lie algebra, and the corresponding group to be the $\boldsymbol{g}$ and $G$ of the above input 1), respectively. The group so defined is then called the *dynamical group* of the system. Input 2) is usually given, without extra specifications, simply by the Hilbert space of the system. For what concerns the point 3) we can choose any normalized vector in the system Hilbert space (i.e. any physical state of the system); of course it will be more useful if the reference state is chosen among those states which have some dynamical relevance as, e.g., the Hamiltonian eigenstates.

According to the above reasoning, we see that a set of GCS can be built basically for any well-posed physical problem. In fact, although the three input are all present, the actual computation is often cumbersome and may lead to complicated results of difficult interpretation and little utility. It may happen (as it is the case for the spin chain we will consider in chapter 5) that operators $T_i$ are not a subset of an infinite dimensional Lie algebra, which makes the explicit construction of the spin-chain coherent states not possible.

Let us now go more in detail and show how the general constructing method works in the two cases already discussed. In the case of the FCS it is straightforward to refer to the harmonic oscillator Hamiltonian, $\mathcal{H}_{\text{HO}} = \hbar\omega(a^\dagger a + 1/2)$ or an Hamiltonian in the form (1.54). The three operators $\hat{n}$, $a$, $a^\dagger$ together with the identity $\mathbb{1}$ span a Lie algebra which is often referred to as $\boldsymbol{h}_4$, corresponding to the so called Heisenberg-Weyl group, $H_4$. As reference state one chooses $|0\rangle$, the state such that $a\,|0\rangle = 0$. The construction of the GCS proceed as follows:

- First, identify the *stability subgroup*. i.e., the subgroup of $H_4$ which leaves the reference state unchanged (except for a phase factor). In this case the stability subgroup is U(1)⊗U(1) generated by $\hat{n}$ and $\mathbb{1}$, i.e. by the operators $h$ of the form

$$h = e^{\delta\hat{n} + \eta\mathbb{1}} \tag{1.65}$$

- Second, the *coset space* with respect to the stability subgroup provides the operators for constructing the coherent states. The coset space is the quotient space between the dynamical group and the stability subgroup whose elements, $D$, provide a unique

decomposition of any element $g \in G$ of the form $g = Dh$, with $h$ belonging to the stability subgroup. In this example the coset space is $H_4/\mathrm{U}(1)\otimes\mathrm{U}(1)$ and its generic element reads

$$D(\alpha) = e^{\alpha a^\dagger - \alpha^\star a}\,, \tag{1.66}$$

where $\alpha \in \mathbb{C}$.

- Third, build the coherent state by applying the coset elements to the reference state. The coherent state, for the $H_4$ group, labelled by the complex number $\alpha$ is thus

$$|\alpha\rangle \equiv D(\alpha)\,|0\rangle = e^{\alpha a^\dagger - \alpha^\star a}\,|0\rangle\ . \tag{1.67}$$

Taking into account the BCH formula (1.45), it can be easily seen that the above definition is the same as that given in (1.43).

In the case of the SSCS one considers the spin operators which span the $\boldsymbol{su}(2)$ algebra, obeying the commutation relations

$$[S^z, S^\pm] \,=\, \pm\hbar S^\pm\,; \qquad [S^+, S^-] \,=\, 2\hbar S^z\,. \tag{1.68}$$

The dynamical group is thus SU(2) and the corresponding Hilbert space has dimension d$= 2S+1$ and is spanned by the Dicke states, $\{|m\rangle \mid m = -S, -S+1, ..., S-1, S\}$. The reference state is chosen to be one of the extremal state $|\pm S\rangle$: we here choose the one with the plus sign, i.e. such that $S^z\,|S\rangle \,=\, +S\,|S\rangle$. With these choices it is evident that the stability subgroup is the U(1) whose elements $h$ are generated by $S^z$ as follows

$$h = e^{i\delta S^z} \quad\Longrightarrow\quad h\,|S\rangle = e^{i\delta S}\,|S\rangle\ , \tag{1.69}$$

i.e. the rotations around the direction identified by $\hat{z}$. Consequently we obtain the coset with respect to the stability subgroup, SU(2)/U(1), whose elements are

$$D(\zeta) \,=\, e^{\zeta^\star S^- - \zeta S^+}\,, \tag{1.70}$$

where $\zeta$ is a complex parameter. The elements $D(\zeta)$ of SU(2)/U(1) are such that each element $g$ of SU(2) can be written as $g = D(\zeta)h$ for some $\zeta \in \mathbb{C}$.

Since the geometry of the coset SU(2)/U(1) is still a two-dimensional sphere, we set $\zeta = e^{-i\phi}\theta/2$ with $0 \le \theta \le \pi$ and $0 \le \phi \le 2\pi$. Finally, the SU(2) coherent states will be given by

$$D(\zeta)\,|S\rangle = e^{\zeta^\star S^- - \zeta S^+}\,|S\rangle\ . \tag{1.71}$$

The above definition may look different from the one given in equation (1.55) but, taking

into account the following disentangling formula (which is one of the BCH formula for SU(2) Lie group) [71, 73]

$$\exp(\zeta^\star S^- - \zeta S^+) = \exp(\tau^\star S^-)\, \exp[-\ln(1+\tau^\star\tau)S^z]\, \exp(-\tau S^+)\,, \tag{1.72}$$

where $\tau = e^{-i\phi}\tan\theta/2$, the equality between the two definitions is immediately demonstrated (remember that $S^+ |S\rangle = 0$ and $S^z |S\rangle = S |S\rangle$).

The advantage of this method for building the GCS, besides its generality, relies on the possibility of deriving the coherent states properties within the formal framework of (Lie-)Group theory. Even in these two simple cases, where all the properties listed in the respective sections can be derived by the definitions (1.43) and (1.55), the GCS construction technique allows one to derive other important features such as the geometrical structures of the parameter-space, e.g. its symplectic structure, giving also the possibility to set precise relations between this parameter-space and the phase-space of the physical system one is describing.

Finally, we specify a general feature related to the GCS dynamics, which has been already anticipated at the end of section 1.4.1, in the particular case of the FCS and SSCS. It can be generally demonstrated that the integral solution (1.31) of the time-dependent Schrödinger equation can be explicitly calculated if the system Hamiltonian is of the form (1.64) and the initial state is one of the corresponding GCS. The consequent general solution of the Schrödinger equation reveals one of the most interesting properties of GCS: a GCS always evolve into another GCS (that's why $G$ is called "dynamical group") and the relation between the initial state and the evolved one, i.e. by the parameter $\zeta(t_0)$ labelling the initial and $\zeta(t)$ is provided by classical-like EoM [73–75]. This property thus establishes a strict connection between the quantum and the classical evolution, by stating that it is possible to describe the classical and the quantum evolution through the same classical EoM, provided the suitable set of GCS.

# Chapter 2

# Robustness in non-linear classical systems

As it has already been noted in the introduction, classical systems do possess remarkable robustness features which we would like to exploit for practical purposes, not only in their original classical framework, but rather for accomplishing tasks that explicitly require quantum properties to be taken into account and that are thus usually achieved through purely quantum devices. What are these alleged features of non-linear classical systems? Why are they useful? What does it mean robust? And why these systems must be non-linear? These are all the questions we will try to answer throughout the following sections. The remaining of the chapter will be instead devoted to introduce the Heisenberg spin chain, as the specific prototype of non-linear classical system which we will refer to in the rest of this thesis as the medium for conveying classical signals, or for generating entanglement between distant qubits.

Speaking about the features of classical systems we are referring to the typical behaviour characterizing the systems themselves in relation to their Hamiltonians, Equations of Motion (EoM) and, more specifically, their solutions. Consider for example the wave-EoM for the function $f(x,t)$ in 1 spatial- + 1 time-dimensions,

$$\Box f(x,t) \equiv \left(\frac{1}{c^2}\frac{\partial^2}{\partial t^2} - \frac{\partial^2}{\partial x^2}\right) f(x,t) = 0\,; \tag{2.1}$$

this is linear and dispersion-less (i.e. its dispersion relation $\omega = ck$, implies that phase velocity, $v_{\rm ph} \equiv \omega/k = c$, do not depend on the wave vector $k$) partial differential equation whose solutions are spanned by the complete set provided by plane waves in the form $\exp[i(kx \pm \omega t)]$. Any well behaved function of the form $f(x \pm ct)$ is a solution of eq. (2.1)

and can be written as a linear superposition in the form

$$f(x,t) = f(x \pm ct) = \int dk\, f_k\, e^{i(kx \pm \omega t)}\,. \tag{2.2}$$

We can thus build a localized wave packet travelling at velocity $c$ without distortion in shape, since any component $k$ travels at the same velocity $c$. Moreover, let us take two localized solutions $f_1(x-ct)$ and $f_2(x+ct)$, then their sum, $f_3 = f_1(x-ct) + f_2(x+ct)$, is still a solution of (2.1): $f_3$ represents, at a large negative time $t = -\infty$, two wave-packets that are widely separated (i.e. their centroids are much more distant than the typical width of the two packets) and that are travelling undistorted towards each other. At some finite time $t$ they collide, but after the collision they will be asymptotically, i.e. for $t \to \infty$, well separated each retaining its original shape and velocity. Of course the situation here described is valid for an arbitrary number of wave packets and is due to the particularly simple (linearity and non-dispersive) form of equation (2.1). It is, in fact, enough to add a mass term to the former equation to spoil all the features we have just described. Consider, for example, the Klein-Gordon (KG) equation:

$$(\Box + m^2c^2) f(x,t) = 0\,, \tag{2.3}$$

this equation is still linear, i.e. plane waves still span its solutions, but it is also dispersive, as the phase velocity $\omega_k/k$ now depends on $k$, meaning that each component $k$ in a given wave packet of the form (2.2) travels with its own velocity causing the packet to be deformed during its propagation. Of course typical EoM are more complicated than these: they can be defined for fields on more than 1+1 dimensions or for vector field rather than scalar fields; they can also contain both dispersive and non-linear terms or even terms for describing the interaction with different kind of fields. Setting aside the complication arising from the vectorial/scalar nature of the field and those arising from the dimension of the subspace or from the interaction with different fields, and focussing our attention on dispersion and non-linearity, it may happen that the contributions of these different terms to the solution of the corresponding EoM have opposite effects, i.e. if one term tends to spread the localized solutions the other one may tend to localize them. We are now going to give an example. Consider first the following equation:

$$\frac{\partial f}{\partial t} + f\frac{\partial f}{\partial x} = 0\,, \tag{2.4}$$

which is called Burgers-Hopf (BH) equation. Due to the second term in the left-hand side, the above equation is non-linear although it looks similar in form to the simple linear and dispersionless equation $\partial f/\partial t + v\partial f/\partial x = 0$, where $v$ is some real constant, which admits solution $f(x-vt)$ with velocity $v$. As the coefficient of the space-derivative term in the

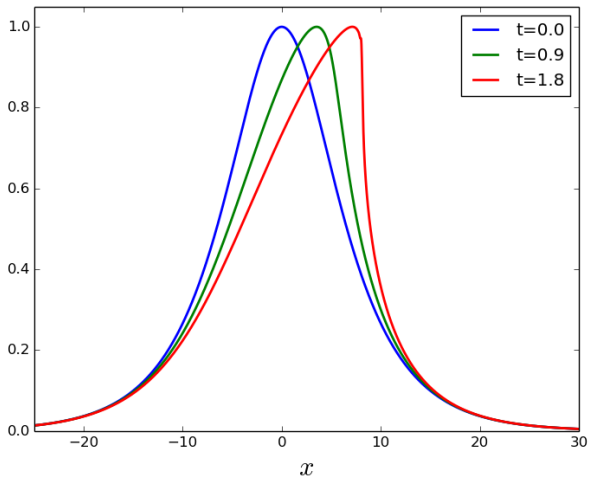


**Figure 2.1:** Evolution of the localized shape $\mathrm{sech}(x/a)$ with $a = 5$ (blue line), according to BH equation of Eq. (2.4) for two subsequent times $t = 0.9$ (green line), $t = 1.8$ (red line). As time runs the right part of sech steepens due to the non-linear term as described in the text.

linear equation sets the velocity of the solution, we may expect that something similar also happens with the BH equation, but this time, since the coefficient is proportional to the field itself (it is, in fact, the non-linear term in the BH equation), the velocity of a solution will depend on the local values of the solution itself, i.e. points where $f$ assumes high values will have high velocities while points where $f$ has low values will also have low velocities. This behaviour tends to shrink the localized solution favouring the formation of *shock-waves*, i.e. discontinuous solutions with a vertical slope in the field time-variation, as it is shown in figure 2.1 where some snapshots of the exact evolution of a localized profile according to the BH equation are shown. Consider now the equation:

$$\frac{\partial f}{\partial t} + \frac{\partial^3 f}{\partial x^3} = 0\,. \tag{2.5}$$

The equation above is linear in the field $f$, but dispersive with a dispersion relation $\omega = -q^3$ implying that the phase velocity $v_{\mathrm{ph}} = \omega/q$ depends on wave-number $q$. Due to the fact that each Fourier component of a given function travels with a different velocity, even a narrow pulse-shaped configuration will broaden during the evolution. Finally consider the following equation

$$\frac{\partial f}{\partial t} + af\frac{\partial f}{\partial x} + b\frac{\partial^3 f}{\partial x^3} = 0\,, \tag{2.6}$$

where $a$ and $b$ are real coefficients. This equation contains both the non-linear and the dispersive terms of the previous ones. Since the effects of the two terms are somehow opposite, with the non-linear term favouring localization around a vertical discontinuity, and with the dispersive term tending to broaden the shape, it may happen that these


**Figure 2.2:** Some example of solitons in nature. **Upper left panel**: KdV soliton in the Union canal near the Heriot-Watt University, 12 July 1995. (Photo from *Nature* **376**, p. 373, 1995) **Upper right panel**: a *frozen kink*, which was naturally created by snow fallen on an horizontal bar. (Credit: Thierry Cretegny 2001, from reference [76]) **Lower left panel**: *Morning Glory Clouds*, are spectacular cloud formations related to a low-level atmospheric soliton, which are typically observed between in the gulf of Carpentaria, Australia. (Credit: Mick Petroff, August 2009) **Lower right panel**: a solitary wave on shore of Maui beach. (Credit: R. Odom, University of Washington)

"trends" compensate each other and give rise to localized solutions that behave like the localized wave packets for equation (2.1), i.e. they are shape-invariant, travelling with constant velocity and they also emerge unchanged after collision with other such solutions. It turns out that such solutions indeed exist and may also result very stable with respect to small perturbations of the solution itself: a famous example is provided by equation 2.6 with $a = 6$ and $b = 1$: the resulting equation is the so called Korteweg-de Vries equation whose solutions will be studied in the next section. All these very special solutions of non-linear dispersive systems generically go under the name of *solitons* and, in virtue of their peculiar features, they deserved an intensive and broad study in the most diverse branches of physics as, for example, hydrodynamics, optics, solid state physics, magnetic systems, particle physicsetc. Some example of solitons that can be found in nature are shown in figure 2.2. In the next section we will give our definition of soliton and will discuss two of the most celebrated equations that count solitons among their solutions.

## 2.1 Solitons

In virtue of its widespread diffusion in the most different fields of physics, the term "soliton" is used in the recent literature with quite diverse meanings. Setting aside optical solitons, the term can indicate specific configurations of low-dimensional many-body systems, ranging from domain walls, to bound states of magnons, or strongly localized modifications of otherwise uniform configurations. Also the difference between solitons, kinks, and solitary waves is not always clear, these terms being used interchangeably or not, depending on the authors. Further whirl is made by considering discrete lattices and/or quantum systems.

Let us hence start by introducing the mathematical definition by means of which solitons were introduced in the analysis of non-linear hydrodynamical phenomena, and that we also adopt in this thesis. For the sake of clarity, we consider a one-component function $f(x,t)$ obeying a given partial differential equation: if a solution $F(x,t)$ of such equation exists, such that $F(x,t) = F(x-vt)$ with $v$ finite and constant, and $F(x,0)$ is exponentially small outside a finite $x$-interval, this solution is a "soliton". Physics can come into play in different ways, for instance by identifying $f(x,t)$ with a scalar classical field, and the differential equation as its equation of motion: the soliton then represents a finite-size modification of the lowest-energy field configuration (i.e. a "localized excitation") that moves with constant profile and finite velocity. As it has been shown, an equation of motion can admit solitonic solutions if it contains both dispersive and non-linear terms: in fact, it is a precise balance between dispersion and localization that allows this type of solutions to exist. As a consequence, solitons are characterized by what is sometimes called a "self-reinforcing" character, from which relevant physical properties follow, such as robustness against scattering and stability with respect to local and global perturbations, as, for example, those due to lattice imperfections and thermal fluctuations, respectively. This kind of precise balance, however, emerges only in a very limited number of physically meaningful equations of motion, so that few types of solitons have deserved extensive study. In order to highlight some relevant features of solitons, let us now briefly describe two of the most celebrated ones, i.e. the Korteweg-de Vries (KdV) soliton (after the names of the two mathematicians who developed the theory underlying the origin of the "wave of translation" originally observed in 1834 by John Scott Russel in a shallow canal), and the sine-Gordon (SG) one (after the similarity of its equation of motion with that of the Klein-Gordon field) [76, 77].

A KdV soliton is a solution

$$F_v^{\mathrm{KdV}}(x,t) = \frac{v}{2}\,\mathrm{sech}^2\left[\frac{\sqrt{v}}{2}(x-vt)\right] \tag{2.7}$$

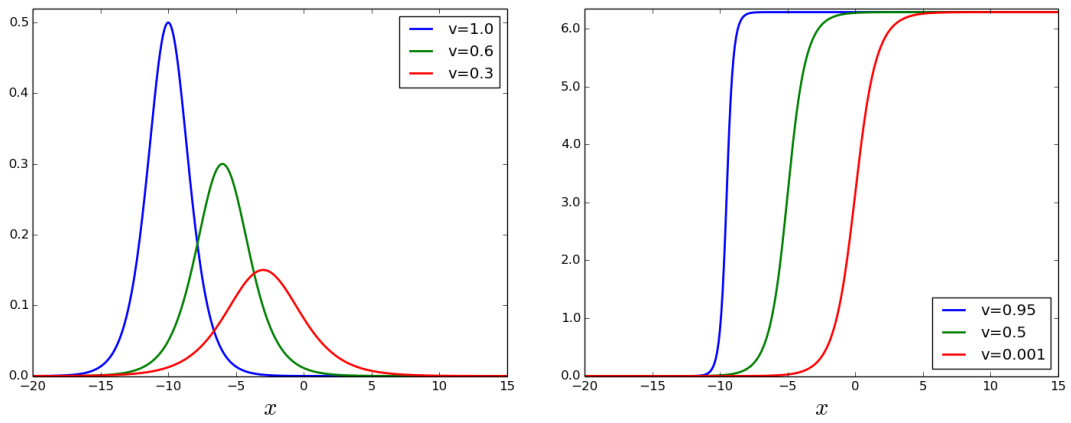


**Figure 2.3:** Left panel: KdV soliton profiles at $t = -10$ for $v$=1 (blue), $v$=0.6 (green), $v$=0.3 (red). Right panel: SG soliton profiles at $t = -10$ for $v$=0.95 (blue), $v$=0.5 (green), $v$=0.001 (red).

of the equation

$$\frac{\partial f}{\partial t} + 6f\frac{\partial f}{\partial x} + \frac{\partial^3 f}{\partial x^3} = 0 \ , \tag{2.8}$$

while a SG soliton is a solution

$$F_v^{\mathrm{SG}}(x,t) = 4\arctan\left[\exp\left(\frac{x - vt}{\sqrt{1-v^2}}\right)\right] \tag{2.9}$$

of the equation [1]

$$\frac{\partial^2 f}{\partial t^2} - \frac{\partial^2 f}{\partial x^2} + \sin f = 0 \ . \tag{2.10}$$

Both Eqs.(2.7) and (2.9) indicate a class of constant-profile solutions, labelled by the soliton velocity $v$, which does not appear in their respective differential equation. In other terms, solitons with different velocity are admitted, although they will have different first integrals, amongst which, in particular, the energy. Velocity also sets the soliton profile, as shown in figure 2.3 where the spatial dependence of $F_v^{\mathrm{KdV}}$ and $F_v^{\mathrm{SG}}$ is shown for different values of $v$. As shown in figure 2.4 for the KdV soliton, the two solutions (2.7) and (2.9) share also the property of undergoing scattering processes without changing their shape: the only possible effect of scattering events between solitons are changes in their phases as it is also evident in the picture.

In the previous section we already analysed the effects of the non-linear and the dispersive term in the left-hand side of the KdV equation on a localised solution; the KdV soliton described in equation (2.7) thus represents an example of the precise balance between these terms to which we were referring before. The consequent emerging "self-reinforcing" character is due to the fact that this balance is somehow stable, in the sense that, if the initial configuration of the system is too narrow(broad), then the dispersive(non-linear)

[1] Among the systems whose dynamics is characterized by the SG EoM and the corresponding solitons, there are the spin chains with a strong easy-plane anisotropy.

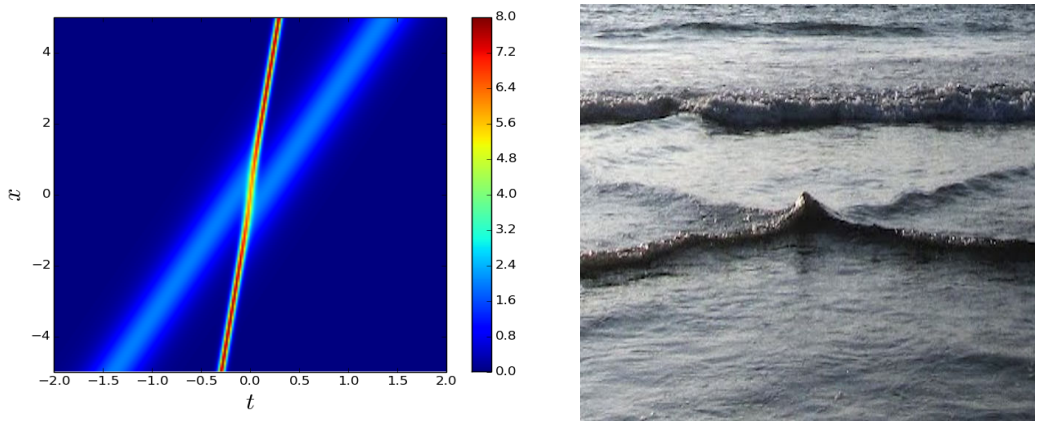


**Figure 2.4:** Example of scattering of two KdV solitons. Left panel: intensity plot obtained by a two-soliton solution; the figure shows the scattering of two solitons, one with $v = 16$ and the other with $v = 4$. It is evident how the two solitons emerge form the scattering completely unmodified but for a shift in their phases. Right panel: an example of scattering of two solitons in the shallow sea water. (Credit: Mark J. Ablowitz, 2009)

term dominates until the balance is restored. The same consideration can be done if some perturbation in the system slightly modifies the equation 2.8. It can happen, however, that this balance is broken leading to the destruction of KdV solitons possibly present in the system. An example is provided by the waves on a shore, i.e., in the framework of hydrodynamical phenomena, by the situation where a wave is propagating in a medium whose depth is decreasing continuously in the direction of the wave propagation. In fact, it can be shown [2] that, if $h$ is the medium depth, the dispersive term is proportional to $h^2$ while the non-linear one to $1/h$: assuming the system depth to be continuously decreasing, let's say $h \to 0$, the dispersive term becomes weaker and weaker than the non-linear term, leading the propagating soliton to steepen its propagation front until it is finally broken. This example shows that situations where solitons can be destroyed are rather extreme: they require perturbations acting systematically in the same direction in order to destroy the balance between dispersion and non-linearities, whereas, typically, the perturbations introduced by imperfections, noise or disorder in the system do not have such a systematic character. Indeed solitons show good robustness features in the real systems where they are observed.

[2] Aiming at describing the time evolution of the shape of the fluid/air interface of a non-viscous fluid in presence of a gravitational field $g$, the KdV equation 2.8 can be rewritten in the following form:

$$\frac{1}{c_0}\frac{\partial \eta}{\partial \tau} + \left(1 + \frac{3}{2h}\eta\right)\frac{\partial \eta}{\partial \xi} + \frac{h^2}{6}\frac{\partial^3 \eta}{\partial \xi^3} = 0\,,$$

where the field $\eta \equiv \eta(x,t)$ represents the height displacement with respect to the medium depth $h$, and $c_0 = \sqrt{gh}$ is the linear wave speed in the long wavelength limit. KdV equation in the form (2.8) is recovered with the following changes:

$$f = \frac{\eta}{h} \qquad t = \frac{c_0}{h}\tau \qquad x = \frac{\xi}{h} - \tau\,.$$

Concerning the SG soliton, we can add something more: this solution is in fact the prototype of the so called *topological solitons*. They represent a class of solitons which, besides having all the typical features of other solitons, have their stability enforced thanks to some special conservation laws which determine the topological structure of the EoM solution space, hence their name. These particular conservation laws happen when the potential energy $V(f)$ is characterised by a discrete number of degenerate absolute minima (say $f_0, f_1, ...$). In fact, assuming we have some EoM derived from a system with a potential energy with this property, any continuous, finite-energy solution (of which solitons are a subset) of these EoM must tend for $x \to \pm\infty$ to one of these minima for any time $t$. Moreover if $F(x,t)$ is one of these solutions such that at some time $t_0$,

$$\lim_{x\to\pm\infty} F(x,t_0) = f_\pm \,, \tag{2.11}$$

where $f_\pm$ must be one of the aforementioned minima, then for each $t$, $F(\pm\infty,t) = f_\pm$, i.e. the solution assumes always the value corresponding to the same minimum ($f_+$ can be different from $f_-$), due to energy conservation. This implies that each finite-energy, non-singular solution $F(x,t)$ can be classified according to the two conserved values $f_\pm$. This defines the specific topology of the solution space which is divided into different sectors labelled by some function of $f_\pm$ which is usually called *topological charge*. Moreover these sectors are disconnected, i.e. a solution belonging to a given sector cannot be continuously deformed into a solution of another sector without violating the energy conservation, an example of continuous deformation being the time-evolution. The SG equation (2.10) can be derived from an Hamiltonian density

$$H_{SG} = \frac{1}{2}\left(\frac{\partial f}{\partial t}\right)^2 + \frac{1}{2}\left(\frac{\partial f}{\partial x}\right)^2 + (1-\cos f)\,, \tag{2.12}$$

where the potential energy $V(f) = 1 - \cos f$ has an infinite, though discrete, numbers of absolute minima for $f_n = 2\pi n$ with $n \in \mathbb{Z}$. The solutions $F(x,t)$ of the SG equation are thus classified by the topological charge $Q$ defined as

$$Q = \frac{1}{2\pi}\left(\lim_{x\to+\infty} F(x,t) - \lim_{x\to-\infty} F(x,t)\right) \in \mathbb{Z}\,. \tag{2.13}$$

For example, the SG soliton of equation (2.9) connects two adjacent minima and has thus a topological charge $Q = +1$. The conservation of the topological charge thus prevents the SG soliton shape to be destroyed: perturbations in an infinitely extended system can, in fact, slow down a moving soliton or even bring it to rest but they cannot destroy it since it would imply a change in the topological charge. This makes topological solitons even more robust than other solitons.

Thanks to the KdV and the SG solitons we were able to outline the main peculiarities relative to the concept of soliton, of course many other solitons do exist but they all share basically the same features of those here described. Solitons are fundamental in the study of the more diverse physical systems, e.g. optical systems, plasmas, superconducting materials, magnetic systems and even in biological molecules such as DNA [78–82].

Finally, in virtue of their specific features of space-time localization, which makes them look like pulse signals, of their stability, and being not affected by dispersion as the usual linear-wave packets, solitons have been and are widely used for the realization of practical applications in different fields among which, for example, electronics, optics, and spintronics. Optical solitons, arising from the so called *non-linear Schrödinger* (NLS) equation for the electromagnetic field in optical fibres, have been indeed used for ultra fast information transport [83–85] . For what concerns the field of spintronics, for example, topological solitons in Ruderman-Kittel-Kasuya-Yoshida (RKKY) multilayer materials or in Ferromagnetic layers, have been shown to be good candidates for storing and moving information in three-dimensional devices or for other applications [86–89].

In this thesis, we will try to use solitons in magnetic one-dimensional systems (spin-chains) as a useful tool for accomplishing the basic operations related with the realization of a quantum computer. Some of these applications, e.g. single-qubit operations, do not necessarily need quantum interaction to be accomplished, this allowing us to directly exploit the classical soliton characteristics. On the other hand, other applications, such as those involving the generation of quantum correlations, require a treatment of the spin chain which must be quantum, at least at an approximate level, and retaining enough of the system quantum features in order to account for entanglement to be generated and possibly transferred. In these cases, effort must spent in developing suitable approximations giving us the possibility of preserving the quantum structures of the spin-chain, but also to keep a connection with its classical description for exploiting the soliton properties. Being that of soliton a classical concept, one may think that quantum spin-chains are no more characterised by this peculiar configurations. Luckily it seems not to be so, since, based on the well established connection between classical vector-field theories and models of interacting spin-$S$ particles on discrete one-dimensional lattices [90], it is expected that soliton-like excitations typify spin chains [24–29]. Moreover, as extensively shown in the literature [30, 33, 35, 91–93] a renormalized classical approach [36–39] is often appropriate for describing the actual behaviour of real compounds with $S > 1/2$ [31, 32, 34], this fostering the idea that some kind of dynamical states with the properties of a classical soliton characterize these systems, although they are intimately quantum in nature.

## 2.2 Heisenberg spin chain

In this section we will introduce the model describing the physical system that, in our scheme, will play the role of the transmission line: the classical discrete isotropic Heisenberg chain.

A classical spin chain is a one-dimensional array of time-dependent vectors $\boldsymbol{S}_l \equiv S\,\boldsymbol{s}_l$, whose magnitude $S$ has the dimension of an action and which obey the following Poisson brackets [3]

$$\{S_l^\alpha, S_j^\beta\} = \delta_{lj} \sum_\gamma \epsilon^{\alpha\beta\gamma} S_l^\gamma \quad \text{or} \quad \{s_l^\alpha, s_j^\beta\} = S^{-1}\,\delta_{lj} \sum_\gamma \epsilon^{\alpha\beta\gamma} s_l^\gamma\,, \tag{2.14}$$

The Heisenberg chain is defined by the Hamiltonian

$$\begin{aligned} \mathcal{H}_{\text{chain}} &= -J \sum_l \boldsymbol{S}_l \cdot \boldsymbol{S}_{l+1} - \gamma H \sum_l S_l^z \\ &= \frac{JS^2}{2} \sum_l (\boldsymbol{s}_l - \boldsymbol{s}_{l+1})^2 + \gamma H S \sum_l (1 - s_l^z) + \text{const}\,, \end{aligned} \tag{2.15}$$

where $J > 0$ is a ferromagnetic nearest-neighbour coupling, $H$ is an external magnetic field whose direction identifies the $z$-axis, and $\gamma$ is the gyromagnetic ratio. Evaluating the Hamilton equations

$$\partial_t \boldsymbol{s}_l \;=\; \{\boldsymbol{s}_l,\, \mathcal{H}_{\text{chain}}\}\,,$$

the following EoM for $\boldsymbol{s}_l$ are obtained

$$\partial_t \boldsymbol{s}_l = \boldsymbol{s}_l \times \left[ JS(\boldsymbol{s}_{l+1} + \boldsymbol{s}_{l-1}) + \gamma \boldsymbol{H} \right]\,, \tag{2.16}$$

where $\boldsymbol{H} = (0, 0, H)$. Provided that the chain is made of a number $N$ of spins, these EoM constitute e set of $3N$ coupled ordinary differential equations which describe the dynamics of the entire chain. Their integration, given the proper boundary conditions, will be the subject of Section 3.

In the next paragraph we will analyse the continuum limit of this model since solitonic analytical solutions, which will be very useful for our purposes, have been found for the corresponding EoM [94, 95] .

[3] The Poisson brackets for two generic functionals $A$ and $B$ of the spin vector fields $\boldsymbol{S}_j$ are the following:

$$\{A, B\} \;=\; \sum_{\alpha,\beta,\gamma,l} \varepsilon^{\alpha\beta\gamma} \frac{\delta A}{\delta S_l^\alpha} \frac{\delta B}{\delta S_l^\beta} S_l^\gamma\,,$$

where $\delta/\delta S_l^\alpha$ indicates the functional derivative with respect to the $\alpha$-component of the vector field $\boldsymbol{S}_l$.

### 2.2.1 Continuum limit

We here introduce the Heisenberg chain model in the limit of continuous support, the mathematical operation that change the spatial dimension of the chain from the discrete set of equidistant, by a distance $d$ (lattice spacing), points to the continuous real axis. This operation is obtained taking the limit of vanishing lattice spacing $d \to 0$ and keeping finite the quantities

$$\mathcal{S} \equiv \frac{S}{d} \quad \text{and} \quad \mathcal{J} \equiv Jd^3 \ . \tag{2.17}$$

We thus define the vector field

$$\boldsymbol{s}(x,t) \equiv \lim_{d \to 0} \boldsymbol{s}_l(t) \,, \quad x \equiv ld \,, \tag{2.18}$$

such that $|\boldsymbol{s}(x,t)| = 1$. The Hamiltonian (2.15) now yields the Hamiltonian density

$$\mathcal{H}(x) = \tfrac{1}{2}\mathcal{J}\mathcal{S}^2 \left[\partial_x \boldsymbol{s}(x,t)\right]^2 + \gamma H \mathcal{S} \left[1 - s^z(x,t)\right] \ . \tag{2.19}$$

From the Hamiltonian density (2.19) we get the following EoM for the vector field $\boldsymbol{s}(x,t)$

$$\partial_t \boldsymbol{s}(x,t) = \boldsymbol{s}(x,t) \times \left[\mathcal{J}\mathcal{S}\ \partial_x^2 \boldsymbol{s}(x,t) + \gamma \boldsymbol{H}\right] \ . \tag{2.20}$$

While analytical soliton-like solutions of Eqs. (2.16) are not known, equations (2.20) have been shown [94] to admit analytical solutions, corresponding to localized excitations, stable under collisions [95], that travel at constant velocity. These solutions will be the subject of the next paragraph.

### 2.2.2 Analytical soliton in the Heisenberg chain

While analysing the problem of the dynamics of the spin vector field $\boldsymbol{s}(x,t)$ and searching for constant profile solutions of equations (2.20), in 1977 Tjon and Wright found the following one-parameter family of solutions which, in the polar representation of the vector field $\boldsymbol{s}(x,t) \equiv (\sin\theta\cos\varphi, \sin\theta\sin\varphi, \cos\theta)$, read

$$\boldsymbol{\Sigma}^{(\beta)}(x,t) : \begin{cases} \theta^{(\beta)}(x,t) = 2\sin^{-1}(\sin\beta\ \operatorname{sech}\xi) \ , \\ \varphi^{(\beta)}(x,t) = \varphi_0 + \cot\beta\,\xi + \tan^{-1}(\tan\beta\ \tanh\xi) \ , \end{cases} \tag{2.21}$$

where

$$\xi \equiv \frac{x - vt}{\lambda_\beta} = \frac{x}{\lambda_\beta} - \frac{t}{\tau_\beta} \ . \tag{2.22}$$

The parameter $\beta$ unambiguously characterizes each $v > 0$ soliton, setting its characteristic

$$amplitude \ : \quad 2\beta = 2\arccos\frac{v}{2\sqrt{\mathcal{J}\mathcal{S}\gamma H}} \ , \tag{2.23}$$

$$length \ : \quad \lambda_\beta = \sqrt{\frac{\mathcal{J}\mathcal{S}}{\gamma H}}\,\frac{1}{\sin\beta} \ , \tag{2.24}$$

$$energy \ : \quad \varepsilon_\beta = 8\mathcal{S}\sqrt{\mathcal{J}\mathcal{S}\gamma H}\,\sin\beta \ , \tag{2.25}$$

$$time \ : \quad \tau_\beta = \frac{1}{\gamma H \sin 2\beta} \ . \tag{2.26}$$

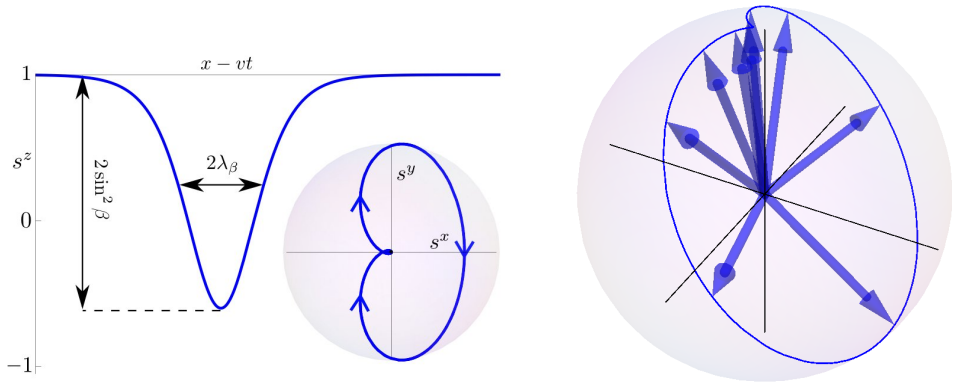


**Figure 2.5:** $\beta$-soliton for $\tan\beta = 2$: left panel, $z$-component of the spins, $s^z = \cos\theta_\beta(\xi)$ and (inset) the corresponding trajectory of the in-plane components $s^x$ and $s^y$; right panel, evolution of the spin vector $\boldsymbol{s}_\beta(\xi)$, reported at constant intervals $\Delta\xi = 0.8$.

A dynamical ($v > 0$) soliton defined by Eqs. (2.21) will be hereafter referred to as "$\beta$-soliton". Notice that Eq. (2.23) sets a maximum value for the velocity, $|v| < 2\sqrt{\mathcal{J}\mathcal{S}\gamma H}$, implying that the second term of the Hamiltonian (2.19) must be finite in order for the model to support dynamical solitons. Once this condition is fulfilled, a $\beta$-soliton can be readily seen as a signal, i.e., a field dynamical configuration with a distinctive trait that can be spotted, for time intervals of the order of $\tau_\beta$, in a spatial region of size $\lambda_\beta$ that moves with constant velocity in the one-dimensional space where the field is defined. An example of $\beta$-soliton is shown in figure 2.5.

Despite the analogies in the EoM, however, there is no analytical counterpart of this solution family in the discrete case, but, as the continuum approximation does make sense whenever the relevant configurations vary slowly on the scale of the lattice spacing, we expect that, for $\lambda_\beta \gg d$, a discrete counterpart of a $\beta$-soliton, $\boldsymbol{\Sigma}_l^{(\beta)}(t)$ defined by Eqs. (2.21) with

$$\xi = l\sqrt{\frac{\gamma H}{JS}}\,\sin\beta - \gamma H t \sin 2\beta \ , \tag{2.27}$$

might still represent an excitation of the model (2.15). In fact, by numerically solving

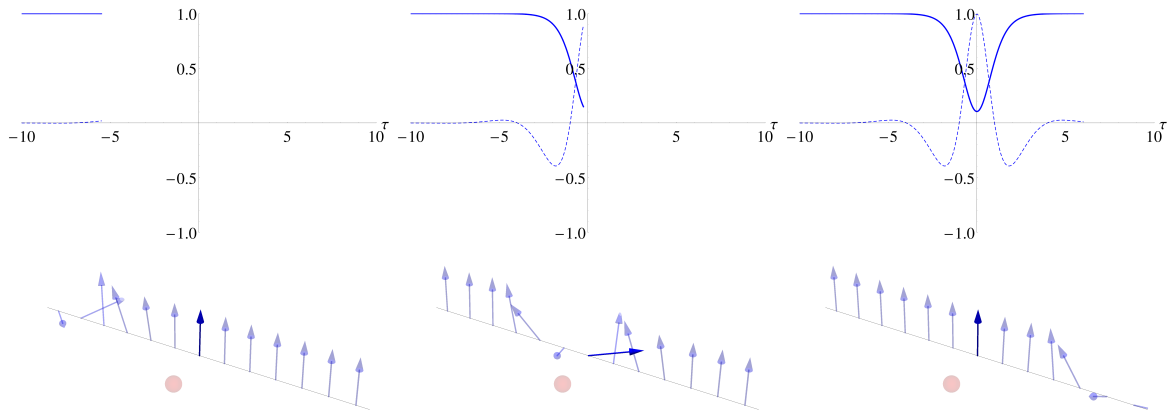


**Figure 2.6:** Time-lapse of a $\beta$-soliton propagating along a classical spin chain; the bold spin represent, $\vec{S}_0$

Eqs. (2.16), we have checked that the Heisenberg spin chain properly supports $\beta$-solitons whenever the Zeeman energy $\gamma HS$ is much smaller than the bond energy $JS^2$, as implied by $\lambda_\beta \gg d$ via Eqs. (2.24) and (2.17). This result fits with the experimental observation, in quasi one-dimensional systems, of magnetic behaviours whose origin can be unequivocally ascribed to the presence of soliton-like excitations [32]. In chapter 4, we will therefore take that the time-dependent chain configuration $\left\{\boldsymbol{s}_l(t) = \boldsymbol{\Sigma}_l^{(\beta)}(t)\right\}$ is a solution of the discrete EoM (2.16), embodying the signal we want to convey, with the respective Heisenberg chain serving as transmission line. The next chapter will be instead devoted to show how to inject soliton in a discrete spin chain initially in a ferromagnetic ordered configuration or some noisy configuration close to the former, through the action of a local time dependent magnetic field.

# Chapter 3

# Soliton generation

In this chapter we will introduce and review our proposal of a method for generating the particular non-linear dynamical configurations, namely the Heisenberg solitons, that we have described at the end of the previous chapter and that we want to exploit, first (see Chap. 4), as some sort of signal for carrying an effective magnetic field and, second (Chap. 5), as the semi-classical state able to transfer the quantum correlations arising from the interaction of the spin chain with some quantum object. After illustrating the idea behind our method, we will introduce the scheme under which we are representing it as well as the numerical techniques we have used to complete the calculations. We will then describe our results classified according to the different cases, i.e., according to the different initial conditions and the specific form of the boundary terms considered.

The division will be as follows: *i) Ideal Dynamics*, test of the generation scheme in the most favourable conditions; *ii) Noisy Dynamics*, check of the robustness of the scheme and of the generated solitons with respect to some noise present in the system; *iii) Penetrating field*, the scheme is tested in a situation where the boundary conditions represent a more physical situation with respect to those of case i).

## 3.1 Our idea at a glance

First of all, let us clarify the meaning of the expression "generating solitons": By achieving the generation of a generic dynamical configuration, and in particular solitons, we mean that, after performing a suitable external action on a target system, the dynamical state of this latter will be given by the space-time configuration we wanted to generate. Thus, taking the attention back on how to generate solitons in the Heisenberg chain, we are now going to explain our idea by specifying what it is meant by the "external action".

Since our last goal will be that of exploiting the generated excitations in order to obtain some non-trivial operations on the states of one or more qubits without disturbing their

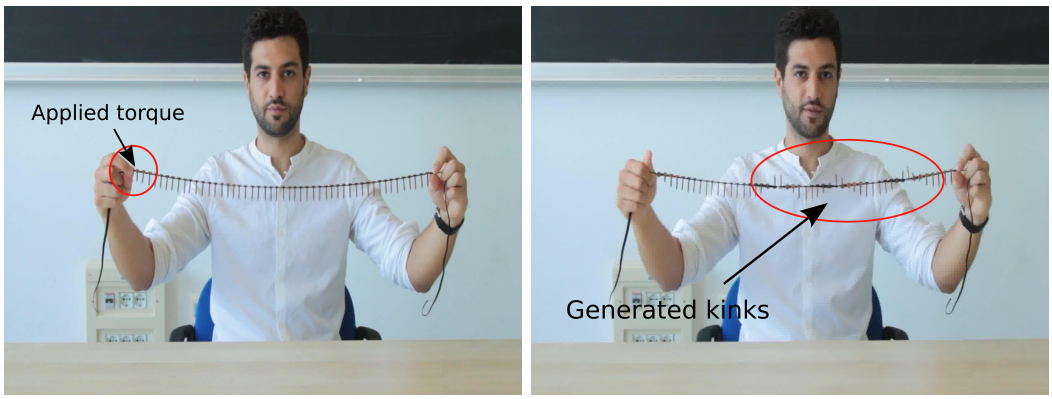


**Figure 3.1:** Pictorial example of the basic idea of the scheme proposed.

neighbourhood, the external action needed to achieve the soliton generation (whatever it is) will have to take place far from the bulk of the system and, in particular, far from the target qubits. For this reason we schematise this action by the application of a forcing term at one of the spin-chain ends. Then, due to the typical magnetic nature of spin interactions, it is natural to represent this forcing term as the interaction of a suitable time-dependent magnetic field with the first spin(s) of the chain.

Before going on, let us give just a pictorial sketch of what we intend to describe in the next paragraphs: referring to figure 3.1, imagine to take an elastic string and pierce it with a number of nails so as to put them at the same distance from each other (as it is shown in the picture); the obtained system is an approximate version of a chain of coupled pendula. Now if we twist the first nail applying a sudden torque to the string extremity, this will result in the injection of one or more moving SG-like kinks depending on the strength of the initial torque. In our specific case, the analogue of the elastic nail chain in the example is given, of course, by the spin chain, while that of the torque is provided by the time-dependent magnetic field acting locally on the first spin(s) of the chain.

Our work will thus consist in integrating the EoM (2.16) of the spin chain imposing particular boundary conditions, which represent an external action on the system; this will allow us to study the dynamics of the system and to show that, as a consequence of the forcing term, soliton-like excitations somehow related with the performed action are generated in and travel along the chain.

In the following subsection we will specify further the particular form of the boundary term we adopted, also discussing the reason of the particular choice.

### 3.1.1 Boundary conditions

In order to find the proper conditions to make one specific soliton $\mathbf{\Sigma}_l^{(\beta)}(t)$ [1] to exist and run through the Heisenberg chain, we first notice the following: Consider a finite (though long at will) chain, with $(2L+1)$ spins sitting on sites labelled from $-L$ to $+L$. Suppose $\boldsymbol{S}_{-L}(t)$ evolved as if a soliton were reaching it travelling from a fictitious, infinitely left-extended chain, $l < -L$: that soliton would continue travelling towards the region $l > -L$, i.e., it would be successfully injected into the chain, at least in the continuum limit [2]. Therefore, enforcing

$$\boldsymbol{s}_{-L}(t) = \mathbf{\Sigma}_{-L}^{(\beta)}(t) \tag{3.1}$$

as a boundary condition should result in the selection of the configuration corresponding to $\mathbf{\Sigma}_l^{(\beta)}(t)$, amongst all those that solve Eqs. (2.16). On the other hand it can be easily seen that Eqs. (2.16) with condition (3.1) enforced are the EoM of a Heisenberg chain with $-L < l \leq L$, and an auxiliary magnetic field

$$\boldsymbol{b}^{(\beta)}(t) = \frac{JS}{\gamma}\mathbf{\Sigma}_{-L}^{(\beta)}(t) \tag{3.2}$$

acting just on $\boldsymbol{s}_{-L+1}$. This suggests that, by applying the magnetic field (3.2) to one end of the transmission line, it should be possible to generate a soliton-like signal, that will then travel through to its target. The consistency of the above description has been checked, for different values of the soliton parameter $\beta$ (i.e. different soliton shapes), studying the model described below.

We considered the system described by the following Hamiltonian

$$\mathcal{H}_{\text{chain}} = \frac{JS^2}{2}\sum_l (\boldsymbol{s}_l - \boldsymbol{s}_{l+1})^2 + \gamma HS\sum_l (1 - s_l^z) + \gamma S\boldsymbol{b}^{(\beta)}(t)\cdot\boldsymbol{s}_{-L+1}\ , \tag{3.3}$$

which is analogous to the Hamiltonian (2.15) plus the term describing the interaction of the spin sitting at $-L+1$ position and the injecting magnetic field given in equation (3.2). The associated Euler-Lagrange EoM analogous to Eqs (2.16) are

$$\partial_t \boldsymbol{s}_l = \boldsymbol{s}_l \times \left[JS(\boldsymbol{s}_{l+1} + \boldsymbol{s}_{l-1}) + \gamma\boldsymbol{H} + \gamma\boldsymbol{b}^{(\beta)}(t)\right]\ ; \tag{3.4}$$

these equations do form a set of coupled, non-linear, ordinary differential equations which will be numerically integrated in time in order to solve the dynamics of the spin chain

[1] The function $\mathbf{\Sigma}_l^{(\beta)}(t)$ refers to the soliton solution of the continuum Heisenberg EoM described in the previous section (equations 2.21).

[2] Although the Heisenberg soliton ($\mathbf{\Sigma}^{(\beta)}(x,t)$) given in equations (2.21), is not an exact solution for the discrete EoM, we expect it to be a good approximate solution in the regime where the typical soliton length $\lambda_\beta$ is much larger than the lattice spacing $d$, i.e. $\lambda_\beta \gg d$.

subjected to the different forcing terms. The detailed description of the method used as well as the results for the different situations considered can be found in the next section.

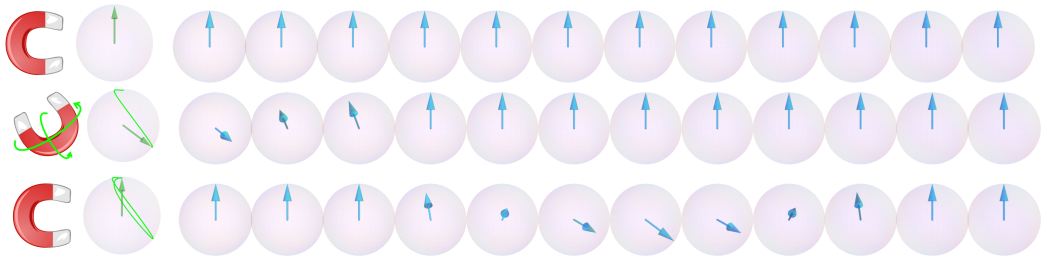

**Figure 3.2:** Schematic representation of the chain dynamics induced by the time-dependent boundary condition described in the text. The magnet and the green arrow represent the external magnetic field acting on the first spin of the chain (blue arrows are the chain spins): as the field varies, the chain spins starts moving accordingly.

## 3.2 Numerics and results

The resolution of the system dynamics, and the consequent verification of our injection scheme, has to pass through the integration of the set of equations described in equation (3.4). This kind of equations for the discrete chain have to be solved numerically, since no analytical solution can be found: though the numerical integration is not particularly expensive in terms of computing resources (at least for chains made up by $10^3 \div 10^4$ spins), some attention must be paid to the choice of the algorithm to be used for this task, in order to get the best results (in term of numerical precision and accuracy) with the least expense in resources and, especially, to avoid some issues related to the constraints given by the conservation laws which must be fulfilled during each step of the evolution, such as the conservation of the spin modulus and of the system total energy. In our case, trying to use, for example, some Runge-Kutta algorithms, the necessity of conserving the modulus of each spin leads us to consider the integration of the polar angle variables [3], which also reduces the total number of equations from $3(2L+1)$, considering the cartesian components, to $2(2L+1)$. Although this choice appears to be convenient, it turns out not to be so because of some terms $\propto (\sin\theta_j)^{-1}$ which cause numerical issues whenever some $\theta_j$ get close to zero (which are common occurrences in our system); this results in a dramatic loss of accuracy and in an uncontrolled increase of the system energy. This fact can be partially cured decreasing the size of the integration step or by using a higher order, more sophisticated, algorithm but in both cases the needed resources drastically increase. Our solution to this problem has been that of performing the integration of the chain EoM us-

[3] We refer to change of representation for the spin vectors $\boldsymbol{s}_j = (s_j^x, s_j^y, s_j^z) = (\sin\theta_j\cos\phi_j, \sin\theta_j\sin\phi_j, \cos\theta_j)$ from the cartesian components, to polar angles $\theta_j$ and $\phi_j$.

ing a specific algorithm [96–100] based on the Suzuki-Trotter decomposition of exponential operators which, unlike more commonly used algorithms, in our specific case allows for conservation of the single-spin magnitude and the total energy, still representing the spin vectors using cartesian components. We will now briefly explain how this algorithm works: imagine to divide the 1-d lattice representing the chain into two sub-lattices, the odd-sites lattice and even-sites lattice, and call them respectively $A$ and $B$. Now the system of EoM (2.16) can be rewritten as two sets of equations

$$\partial_t \boldsymbol{s}_{l\in A} = \Omega_l^B[\{\boldsymbol{s}\}] \times \boldsymbol{s}_{l\in A}\,, \qquad \partial_t \boldsymbol{s}_{l\in B} = \Omega_l^A[\{\boldsymbol{s}\}] \times \boldsymbol{s}_{l\in B}\,, \tag{3.5}$$

where $\Omega_l^{\{\cdot\}} = -[JS(\boldsymbol{s}_{l+1} + \boldsymbol{s}_{l-1}) + \gamma \boldsymbol{H}]$, and $\boldsymbol{s}_{l\pm1}$ belongs to $A(B)$ if $\boldsymbol{s}_l \in B(A)$. If the spin configuration in one sub-lattice were somehow fixed then the EoM of spin belonging to the other sub-lattice would be a linear equation readily solvable in term of a suitable exponential operator representing single spin rotations of the sub-lattice considered along the axes identified by the local fields $\Omega_l^{\{\cdot\}}$ (which would be fixed as they depend on the spin configuration of the fixed sub-lattice). Obviously this is not our case, but, if we represent a complete configuration of the system as one large vector $\boldsymbol{y}$ ordering the components belonging to subset $A$ and $B$ according to $\boldsymbol{y} = (\boldsymbol{y}_A, \boldsymbol{y}_B)$, we can express the cross products in the equations (3.5) as matrices $\hat{A}$ and $\hat{B}$ representing the generators of rotations of the spin configuration of one sub-lattice while the other is kept fixed. Now we can still formally express the system configuration at a time $t + \delta t$ ($\delta t$ is an infinitesimal time interval) as a function of the configuration at time $t$:

$$\boldsymbol{y}(t + \delta t) = e^{(\hat{A}+\hat{B})\delta t}\boldsymbol{y}(t)\,. \tag{3.6}$$

Obviously this is only a formal expression because the exponential operator has no simple explicit form as a consequence of the non-linearity of the original system (i.e., the operator itself depends on the spin configuration of each sub-lattice). By contrast, the expression of the single sub-lattice rotations $e^{\hat{A}\delta t}$ and $e^{\hat{B}\delta t}$ can be explicitly written and the action on the single spin of the specific sub-lattice calculated. In our case, beginning from one of the equations (3.5), we can demonstrate that

$$\begin{aligned}\boldsymbol{s}_l(t + \delta t) \;=\; & \frac{\Omega_l(\Omega_l \cdot \boldsymbol{s}_l(t))}{\Omega_l^2} \;+\; \left[\boldsymbol{s}_l(t) - \frac{\Omega_l(\Omega_l \cdot \boldsymbol{s}_l(t))}{\Omega_l^2}\right] \cos(|\Omega_l|\delta t) + \\ & \frac{\Omega_l \times \boldsymbol{s}_l(t)}{|\Omega_l|} \sin(|\Omega_l|\delta t)\,,\end{aligned} \tag{3.7}$$

where $\Omega_l$ is the same as $\Omega_l^{\{\cdot\}}$ in Eq. (3.5), where we have dropped the superscripts $A(B)$ for the sake of simplicity. Taking into account equation (3.7) and using the well known

Suzuki-Trotter decomposition of the exponential operator (3.6) we can give an approximate estimate of the exact dynamics to any order in $\delta t$. In particular we have chosen to use the second order approximation

$$e^{(\hat{A}+\hat{B})\delta t} = e^{\hat{A}\delta t/2} e^{\hat{B}\delta t} e^{\hat{A}\delta t/2} + \mathcal{O}(\delta t^3)\,, \tag{3.8}$$

which allows us to calculate each step of the dynamics with a local error of order $\delta t^3$. Thus each step of the integration is made by the following three parts: first one sub-lattice, say $A$ is updated by $\delta t/2$ using (3.7), then sub-lattice $B$ is updated by an increment $\delta t$ using sub-lattice $A$ configuration, previously updated, to calculate the local fields $\Omega_l$; finally sub-lattice $A$ is again updated by $\delta t/2$ using the updated version of sub-lattice $B$. Moreover we want to note that according to (3.7) we have

$$|\boldsymbol{s}_l(t+\delta t)|^2 = |\boldsymbol{s}_l(t)|^2 \quad \text{and} \quad \Omega_l \cdot \boldsymbol{s}_l(t+\delta t) = \Omega_l \cdot \boldsymbol{s}_l(t)\,,$$

explicitly confirming both spin length and energy conservation.

Thanks to equations (3.7) and (3.8), we can reconstruct the chain evolution once the initial configuration has been provided. We thus integrated the EoM for different injected shapes $\Sigma^{(\beta)}$ with the additional condition that $2Ld \gg \lambda_\beta$ and choosing an integration time $T \geq 2Ld/v$ [$v$ is the injected shape velocity according to Eq. (2.23)], i.e., the chain has to be much longer than the soliton typical length, leaving enough room for appreciating the soliton propagation for a significant space-time interval. The results of the integration for the different initial conditions considered are discussed in the next paragraphs as follows: in section *Ideal Dynamics* the results obtained starting from the ferromagnetic minimum energy configuration as initial condition are presented; section *Noisy Dynamics* is instead devoted to the discussion of the results for the soliton injection in presence of noise in the system, obtained starting the evolution from an initial condition given by a configuration which reproduces the thermal correlators of spin waves at a given temperature. In order to avoid misunderstandings, it is worth noticing here that, despite we introduce a parameter $\mathcal{T}$, which will be called "reduced temperature" for reasons that will be clear later, our treatment of the spin-chain dynamics do not involve the "temperature" in the usual meaning, i.e. in relation to the interaction of our system with an external heat bath defining its thermodynamic properties. In fact, the EoM here considered are the Hamilton equations for the discrete Heisenberg spin chain as an isolated system, i.e. it has no interaction with any external object. A proper treatment including also the temperature would mean to exchange the ordinary differential equations representing the EoM (3.4), with a set of *stochastic differential equations* including, besides the terms already discussed, a damping term and a stochastic noise term which would schematize the interaction of the chain with

a thermal bath at a given temperature [101–105]. Although this approach can be useful for studying the mean (with respect to different noise realizations) properties of generated solitons in a more realistic situation, it is behind the scope of this thesis. We here want to verify the possibility of injecting soliton-like shapes with the proposed scheme with the aim of using these generated solitons for some practical purpose. For this reason, we are more interested to study the single-shot evolution related to a determined forcing term, rather than the mean properties of the possibly generated solitons.

### 3.2.1 Ideal Dynamics ($\mathcal{T} = 0$)

We now discuss the results obtained by the integration of EoM (3.4) with the chain initialized in the ferromagnetic minimum energy configuration, $\{\boldsymbol{s}_l = \hat{\boldsymbol{z}}\}\ \forall l$. This situation represents an ideal condition in order to test the possibility of injecting a soliton in the chain and also to highlight the features of the generated configurations in comparison with the injected ones and the possible effects related to the discreteness of the support. Remembering the considerations made in section 3.1.1, the perfect ferromagnetic order is the best situation to be encountered by a soliton coming into the chain from $-\infty$, since it represents exactly the asymptotic condition under which the exact soliton solution have been derived. As it has been anticipated we will relate the intensity of the noise present in the system with the *reduced temperature* $\mathcal{T} \equiv k_{\mathrm{B}}T/JS^2$, i.e. the ratio between the energy associated with the temperature $T$ ($k_{\mathrm{B}}T$), and the typical chain interaction energy ($JS^2$): the situation described in this section can be regarded as the realization of a microcanonical (i.e. the system is isolated) evolution starting from the minimum energy configuration, the ferromagnetic order corresponding to zero reduced temperature, $\mathcal{T} = 0$.

Having analyzed the solutions resulting from the numerical integration described in the previous section, we found that when the field $\boldsymbol{b}^{(\beta)}(t)$ is applied to $\boldsymbol{s}_{-L+1}$, i.e., after the injection of $\boldsymbol{\Sigma}_l^{(\beta)}(t)$, dynamical configurations $\boldsymbol{\Gamma}_l(\beta; t)$, identifiable as soliton-like, actually appear in the chain. In order to better characterize these configurations, we have numerically measured their velocity $v'$ and, assuming the validity of Eq. (2.23), we have obtained values for the respective amplitudes, $2\beta' = 2\arccos[v'/(JS\gamma H)]$. These values have been found to agree with those independently determined by fitting $\Gamma_l(\beta; t)$ with Eqs. (2.21), for almost all values of $\beta$ considered [4]. Moreover, by monitoring the chain energy throughout the numerical integration, we have calculated the total work made by the forcing term, and found it very close to $\varepsilon_{\beta'}$, meaning that the work done on the chain does actually correspond to the energy needed to generate a soliton $\boldsymbol{\Sigma}_l^{(\beta')}(t)$. Summarizing, the above analysis confirms that:

[4] Exceptions are encountered when the values of the reduced field $h \equiv \gamma B/(JS)$ and $\beta$ are such that the corresponding soliton width is of the order of the lattice spacing, $\lambda_\beta \simeq d$, see for example the last panel of figure 3.3. This situation is commented at the end of this section.

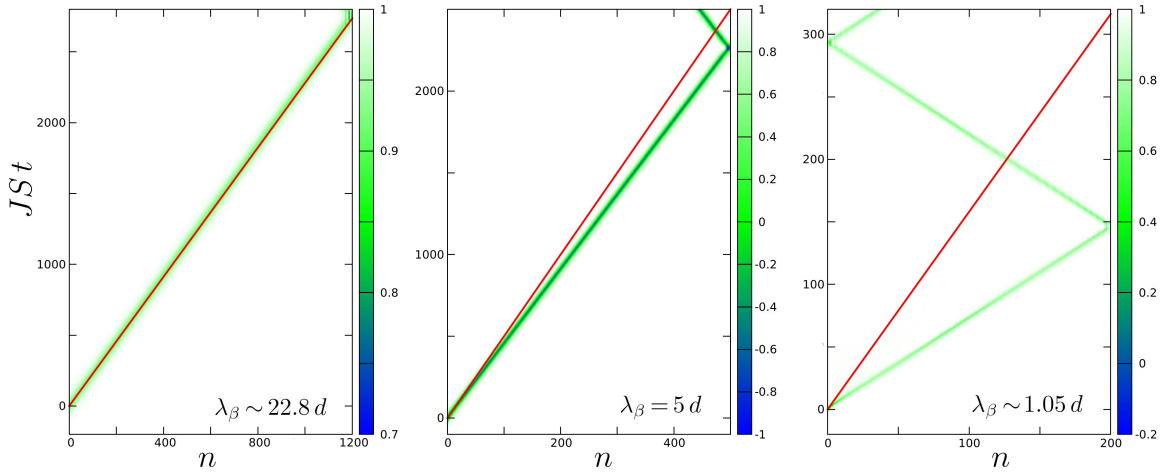


**Figure 3.3:** Evolution of $s_n^z(t)$ for solitons generated in discrete chains by injection of $\beta$-soliton shapes $\Sigma^{(\beta)}(t)$ with three different lengths: $\lambda_\beta \sim 22.8\,d$ ($h = 0.05$, $\tan\beta = 0.2$), $\lambda_\beta = 5\,d$ ($h = 0.05$, $\tan\beta = 2$), $\lambda_\beta \sim 1.05\,d$ ($h = 1$, $\tan\beta = 3$). The white-to-green-to-blue shading corresponds to the progressive deviation of the spin direction from the $z$-direction, and permits to appreciate how the excitation is localized in space and time (reflection occurs at the open chain end). The red lines' slope corresponds to the velocity of the injected $\beta$-soliton.

- by applying the field $\boldsymbol{b}^{(\beta)}(t)$ defined in Eq. (3.2) to the left tail of the chain,
- a dynamical configuration $\boldsymbol{\Gamma}_l(\beta; t)$ is generated inside the chain itself,
- with the essential features of a soliton $\boldsymbol{\Sigma}_l^{(\beta')}(t)$.

Finally we notice that $\beta'$ is closer to $\beta$ when $\lambda_\beta \gg d$, which means that discreteness effects are more evident when the typical length of the injected shape is closer to the lattice spacing. In figure 3.3 the evolutions of $\Gamma_l^z(t)$, corresponding to the injection of three different shapes, are shown in comparison with a slope representing the velocity of injected solitons so that the latter feature can be appreciated. An example of the described analysis for the data sets of figure 3.3 is given in table 3.1, reporting the values, $(\tan\beta)^{\text{fit}}$, obtained through the best fit obtained by minimizing the distance of the numerical data from the function $\boldsymbol{\Sigma}_l^{(\beta)}(t - t_0)$, using $\beta$ and $t_0$ as free parameters in the minimization process. The other quantities are obtained as follows [$h \equiv \gamma B/(JS)$ is the reduced uniform field acting on the whole spin chain]:

- The velocity obtained reversing Eq. (2.23):

$$v^{\text{fit}} = 2\sqrt{\frac{h}{1 + [(\tan\beta)^{\text{fit}}]^2}}$$

- The "measured" velocity, $v^{\text{meas}} \equiv N/(2t_0^{\text{fit}})$ obtained dividing half the length of the chain by the time interval occurred to the generated shape to reach that position, i.e.

the time corresponding to maximum of the peak in figure 3.4 (the soliton is injected at $t = 0$), which numerically correspond to $t_0^{\text{fit}}$.

- The energy of a shape $\mathbf{\Sigma}^{(\beta^{\text{fit}})}$ obtained from eq. 2.25

$$\frac{\varepsilon^{\text{fit}}}{JS^2} = 8\sqrt{h}\,\sin\beta^{\text{fit}}$$

- Energy difference $(\Delta E)^{\text{meas}}$ between the initial configuration energy $E_0 = -JS^2\,N(1+h)$ and the constant value of the chain energy after the soliton injection, evaluated during the numerical integration.

| Injected shape | $(\tan\beta)^{\text{fit}}$ | $v^{\text{fit}}/(JSd)$ | $v^{\text{meas}}/(JSd)$ | $\varepsilon^{\text{fit}}/(JS^2)$ | $(\Delta E)^{\text{meas}}/(JS^2)$ |
|---|---|---|---|---|---|
| $\tan\beta = 0.2;\ h = 0.05$ | 0.200 | 0.439 | 0.435 | 0.359 | 0.348 |
| $\tan\beta = 2.0;\ h = 0.05$ | 1.74 | 0.223 | 0.219 | 1.55 | 1.54 |
| $\tan\beta = 3.0;\ h = 1.0$ | 0.432 | 1.84 | 1.36 | 3.17 | 3.00 |

**Table 3.1:** Different quantities of the generated shapes, for the data sets of figure 3.3. The first row corresponds to an injected soliton with $\lambda_\beta = 22.8d$ and $v \simeq 0.43JSd$, the second row $\lambda_\beta = 5d$ and $v \simeq 0.2JSd$, the third row $\lambda_\beta = 1.05d$ and $v \simeq 0.63JSd$. The values of the first two rows show good correspondence between the quantities graphically measured for the generated shapes and those obtained from eq. (2.23) and following, using $\beta^{\text{fit}}$. The third row corresponds to the extremely short soliton case discussed in the text.

Figure 3.4 shows the time-dependence of the $z$-component of the central spin of the chain compared with the corresponding best fit (see table 3.1), using the set of data of figure 3.3. The quantities reported in table 3.1 confirm the previous expectations: for the injected shape with $\lambda_\beta = 22.8d$ there is an almost perfect match with the generated shape; for $\lambda_\beta = 5d$ the generated soliton is slightly different from the injected one, but the relation $\mathbf{\Gamma}_l(\beta; t) = \mathbf{\Sigma}_l^{(\beta')}(t)$ as well as those in equations (2.23)-(2.26) still hold very well with $\beta' = \beta^{\text{fit}}$; the last case presented, $\lambda_\beta = 1.05d$, shows different features: the generated shape do not perfectly match the function $\mathbf{\Sigma}_l^{(\beta')}(t)$, $\beta^{\text{fit}}$ is far from the $\beta$ of the injected shape and also the other relations are poorly respected. The last case is not particularly worrying for the generation scheme proposed, since an injected shape with $\lambda_\beta = 1.05d$ represents a rather extreme situation for the discrete chain. Conversely, the fact that even in this extreme case a soliton-like dynamical configuration is found travelling along the chain after the injection, though its features look somehow different from the continuous chain exact solution, contributes to strengthen our scheme, since it proves that soliton generation is possible also when $\lambda_\beta$ is comparable with $d$ and that the discrete Heisenberg chain can sustain soliton-like excitations that are not simply the discrete counterpart of the solutions described at the end of the previous chapter.

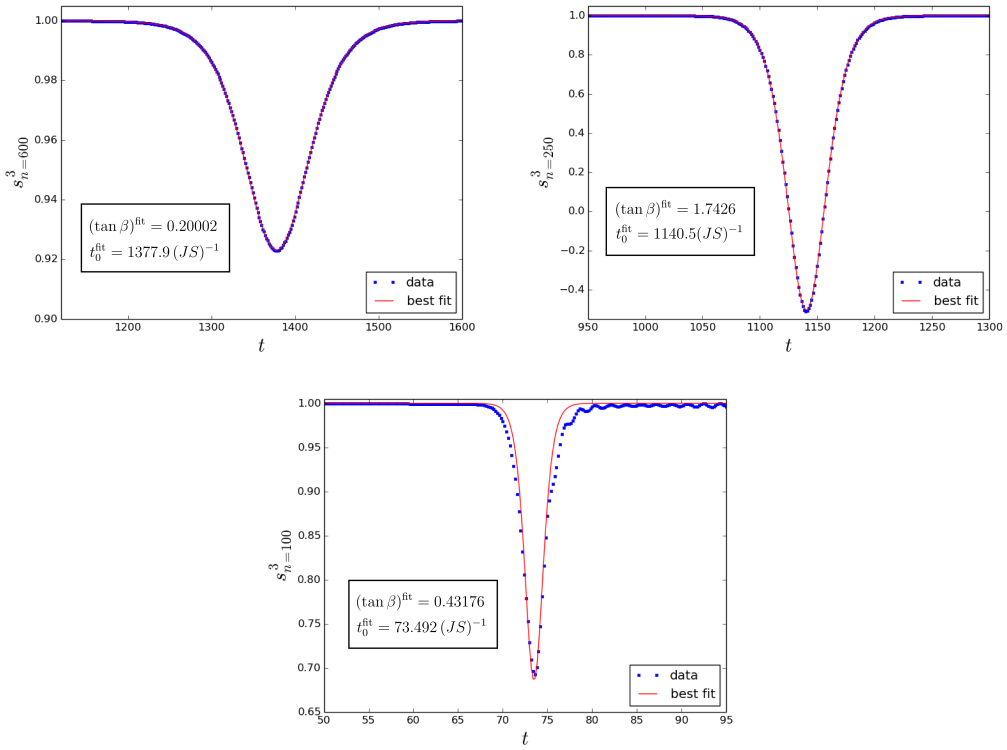


**Figure 3.4:** $s_l^z$ time-dependence for the central spin of the chain, the set of data are those of figure 3.3; the red solid curve is the best fit of the underlying data with the function $\mathbf{\Sigma}_l^{(\beta)}(t - t_0)$ ($\beta$ and $t_0$ free parameters). The values obtained for the best fit parameters are reported in the insets. As noted in the text there is a good match between the analytical solution for the continuous chain and the generated shapes, except for the case of a soliton with a width $\simeq d$.

### 3.2.2 Noisy Dynamics ($\mathcal{T} > 0$)

In this section we analyse the robustness of the injection scheme and that of the resulting generated shapes with respect to the noise or the imperfections possibly present in the spin chain. To accomplish this goal we choose different initial conditions with respect to the ferromagnetic configuration considered in the previous paragraph. The new initial conditions will correspond to statistical spin distributions reproducing the spin-wave correlators which in turn are related to a given value of the reduced temperature ($\mathcal{T} \equiv k_{\rm B}T/JS^2$) of the system. In this way we obtain again a sort of microcanonical evolution (the system is still isolated) but, this time, the system initial energy is not the chain minimum energy associated with the uniform configuration, but that corresponding to a certain "thermal" configuration like that described in the following. The construction technique here adopted is useful not only because it allows to construct physically meaningful configurations, but also because it connects the strength of the noise present in the system to a control parameter (the temperature) which can be easily given a physical interpretation. Let us illustrate the method we use to build one of these configurations. First we need to introduce the

canonical Holstein-Primakoff variables $\{q_l, p_l\}$:

$$s_l^x = \sqrt{1 - \frac{z_l^2}{2}}\, q_l\,, \quad s_l^y = \sqrt{1 - \frac{z_l^2}{2}}\, p_l\,, \quad s_l^z = 1 - z_l^2 \quad \text{with} \quad z_l^2 = \frac{q_l^2 + p_l^2}{2}\,. \tag{3.9}$$

By such a change of variables, provided that $z_l^2 \ll 1$, we can take the quadratic approximation of the Hamiltonian (2.15) which results diagonal in Fourier space and in particular

$$\mathcal{H}_{\text{chain}} \simeq \frac{1}{2}\sum_k \omega_k (q_k^\star q_k + p_k^\star p_k) = \sum_{k\geq 0} \omega_k \left( {q'_k}^2 + {q''_k}^2 + {p'_k}^2 + {p''_k}^2 \right)\,, \tag{3.10}$$

where $\omega_k = 2JS(1-\cos k) + \gamma H$; in the last equivalence we used the fact that, being the $q_j(p_j)$ real, $q_k = q'_k + iq''_k = q^\star_{-k}$ (analogously for the $p_k$). We thus have $4L$ (notice that $q''_{k=0} = p''_{k=0} = 0$) independent Gaussian-distributed stochastic variables with variances

$$\langle {q'_k}^2 \rangle = \langle {q''_k}^2 \rangle = \langle {p'_k}^2 \rangle = \langle {p''_k}^2 \rangle = \frac{k_{\text{B}}T}{2S\omega_k} = \frac{\mathcal{T}}{2}\left[h + 4\sin^2(2k)\right]^{-1} \tag{3.11}$$

where $\mathcal{T} = k_{\text{B}}T/JS^2$ and $h = \gamma H/JS$. So, using a Gaussian random number generator, we generate the set of $4L$ variables corresponding to the $\{q'_k, q''_k, p'_k, p''_k\}$ with the corresponding variances (3.11), then, back-transforming to the direct space we get the $\{q_l, p_l\}$ which, inserted in equations (3.9), give the desired spin components. With this technique we obtain spin configurations characterized by thermal correlators $\left\langle (s_l^x - s_{l+1}^x)^2 \right\rangle = \left\langle (s_l^y - s_{l+1}^y)^2 \right\rangle \simeq \mathcal{T}$ and $\left\langle (s_l^x)^2 \right\rangle = \left\langle (s_l^y)^2 \right\rangle \simeq \mathcal{T}/h$. Being the above construction valid for $z_l^2 \ll 1$, attention has been paid to use values of $\mathcal{T}$ and $h$ such that $\mathcal{T}/h \ll 1$ so that the fluctuations of the in-plane spin components were small and the former condition resulted satisfied.

Integrating again the EoM with these initial conditions we found that, injecting the usual soliton shape $\Sigma^{(\beta)}$, a soliton-like configuration $\Gamma^{(\beta')}$ is again generated in the chain; this time however, the new $\beta'$ is dependent on the initial configuration, and in particular on the reduced temperature value. Another fundamental aspect we can learn by observing the dynamics resulting from these initial conditions is that, although the generated shape can somehow interact with the underlying noise, the soliton dynamics is not spoiled by it. In figure 3.5 we show the colour-density plot of $\Gamma_l^z(\beta; t)$ as a function of $l$ and $JSt$, for different $\mathcal{T}$. The strong resilience of the generated signal is evident: even when fully embedded and barely recognizable within the thermal noise, as in the last panel, its time propagation along the chain can still be easily followed.

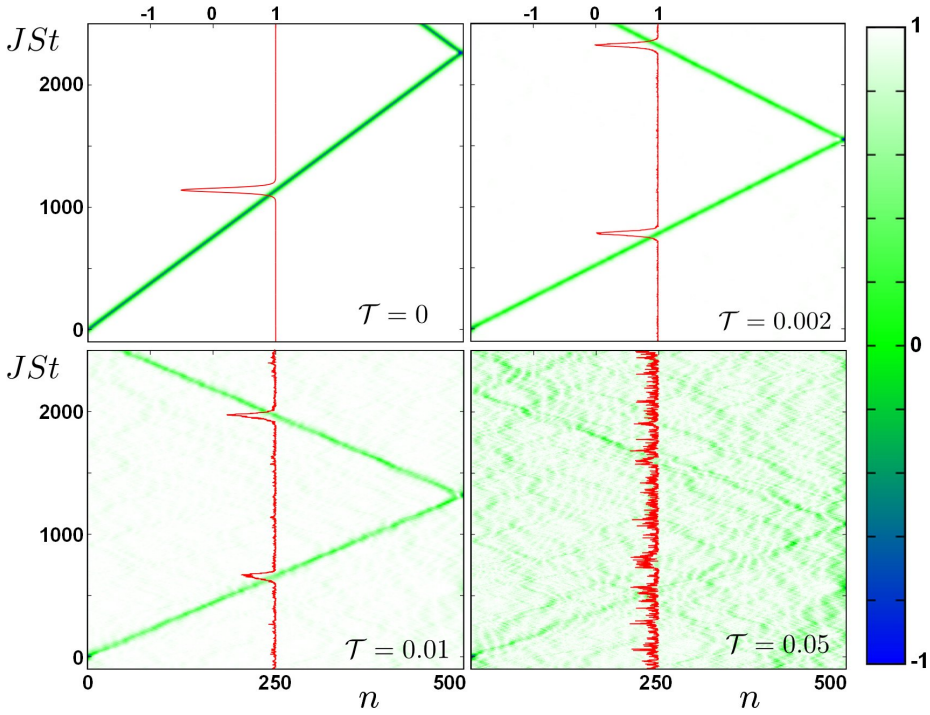


**Figure 3.5:** Samples of generated soliton-like excitations $\mathbf{\Gamma}_l(\beta;t)$ in a discrete chain of 500 spins; the parameters of the injected soliton $\mathbf{\Sigma}_l^{(\beta)}(t)$ are $\gamma H/JS = 0.05$ and $\tan\beta = 2$. Density plots are shown for the space-time evolution of $s_l^z(t)$ at zero (upper left panel) and finite temperature, indicated in the lower, right edge of each panel. The propagating soliton is reflected by the open boundary at site $n = 500$. The thin, red line reports the time dependence of $s_l^z(t)$ at the site $n = 250$.

## 3.3 Penetrating field generation

In this chapter it has already been numerically demonstrated that systems of interacting magnetic moments on one-dimensional lattices, possibly of finite length, support dynamical configurations which are the discrete counterparts of $\beta$-solitons. This is true in particular if the soliton has typical length that is much larger than the lattice spacing, $\lambda_\beta \gg d$, i.e. [referring to (2.24)], $\sqrt{\gamma H/JS}\sin\beta \ll 1$, which has also to be compared with $H \neq 0$, necessary for getting $v > 0$. Given the values of $S$ and $J$ typically observed in magnetic compounds, it is $JS^2 \sim 1 \div 10^3$ K meaning that, as $\mu_B = 0.67$ K/Tesla, only very large fields could break the above inequality. Unfortunately the same argument tells us that in our scheme the time-dependent magnetic field we want to use for generating the soliton must have a rather large modulus. However, we must take into account that, in order to put forward the features related to the mechanism of soliton generation, we have kept things very simple considering the external magnetic field acting only on the first spin of the chain: in a more realistic situation the field applied to the chain edge will act on a certain number of spins, depending on the nature of the system embodying the spin chain. Hence, the effect of $\boldsymbol{b}^{(\beta)}(t)$ is amplified by the effective number of spins it affects and its intensity can well be comparable with $H$.

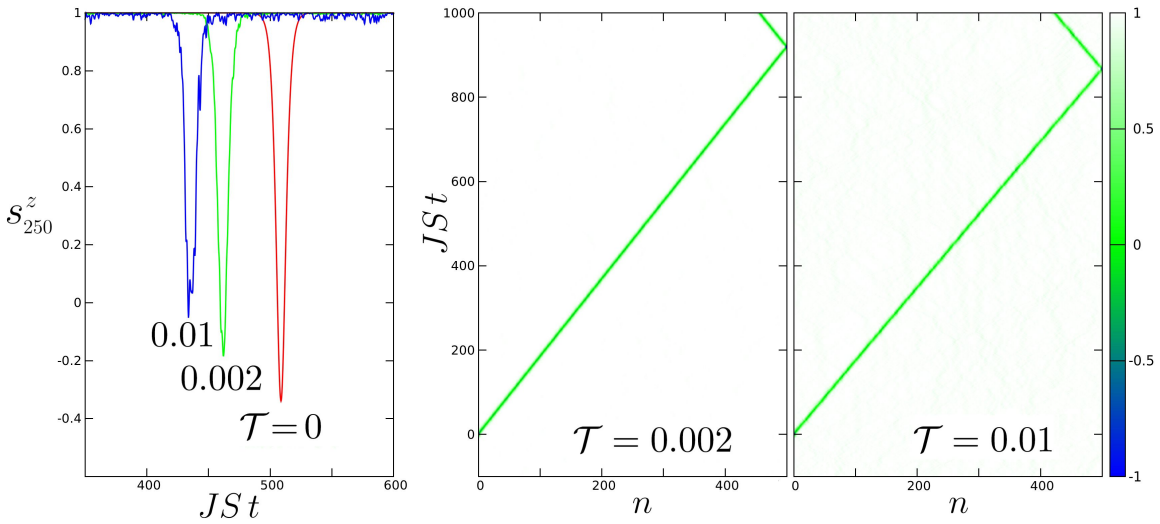


**Figure 3.6:** Solitons generated in a discrete chain of $N=500$ spins by injecting a TW shape $\boldsymbol{s}_\beta(t)$ with $h=0.2$ and $\tan\beta=2$. Left, line plot: $s^z_{250}(t)$ for $\mathcal{T}=0$ (red line), $\mathcal{T}=0.002$ (green line), $\mathcal{T}=0.01$ (blue line). Density plots: evolution of $s^z_n(t)$ for two different temperatures with shading as in figure 3.5.

We here present some unpublished results confirming that our proposal keeps being effective when the action of the field pulse $\boldsymbol{b}^{(\beta)}(t)$ is not punctual but rather extends to a finite part of the chain end, as required in a realistic set-up. In order to represent the described situation we have to change Eq. (3.2) with the following

$$\tilde{b}^{(\beta)}_l(t) \;=\; \frac{JS}{\gamma} w_l\, \Sigma^{(\beta)}_{-L}(t)\,, \tag{3.12}$$

where $w_l$ is a function describing the decreasing intensity of the field along the chain; the boundary term is now given by the sum of all the contributions of the external field on different spins as follows

$$-\,\gamma \sum_l \tilde{b}^{(\beta)}_l \cdot \boldsymbol{s}_l\,. \tag{3.13}$$

EoM (2.16) will also change according to

$$\partial_t \boldsymbol{s}_l = \boldsymbol{s}_l \times \left[ JS \left( \boldsymbol{s}_{l+1} + \boldsymbol{s}_{l-1} + w_l \Sigma^{(\beta)}_{-L}(t) \right) + \gamma \boldsymbol{H} \right]\,. \tag{3.14}$$

At this point we only need to specify the function $w_l$, then, being the new terms of the EoM functions of time and position independent of the spin configuration, we can still integrate them using the same algorithm presented before. Having to represent how the intensity of the magnetic field decreases going deeper inside the chain, we can reasonably choose a simple exponential shape for the function $w_l$, as this kind of law is typical in absorption

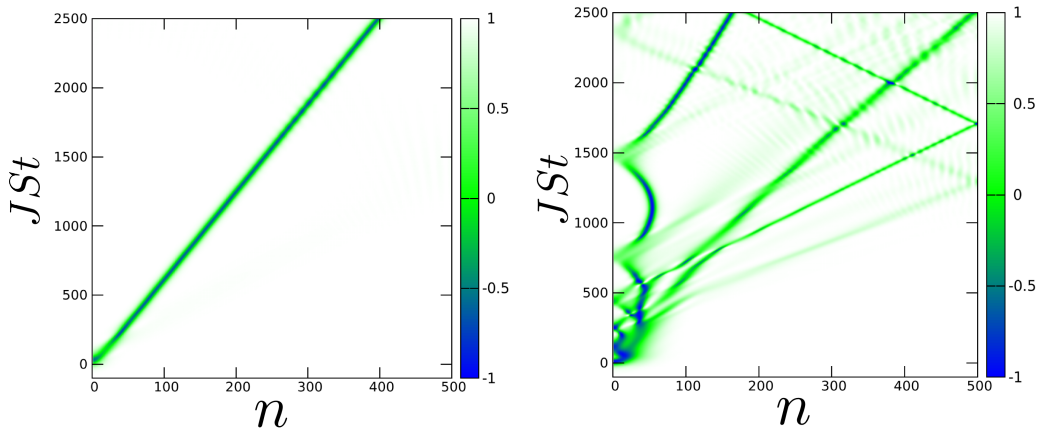


**Figure 3.7:** Generated shape $z$-component $\Gamma_l^z(\beta, t)$ in a chain of 500 spins with respect to position $n$ and scaled time $JSt$; the parameters of the injected soliton are $\tan\ \beta = 2$ and $h = 0.05$. Left panel: $V_{\text{ampl}} = 0.05$ and $\ell = 10$. Right panel: $V_{\text{ampl}} = 0.1$ and $\ell = 20$.

phenomena. In particular we set $w_l$ as

$$w_l \ = \ V_{\text{ampl}} \ \exp\left[\frac{-(l+L-1)}{\ell}\right] \ , \tag{3.15}$$

where $V_{\text{ampl}}$ is a dimensionless constant which determines the amplitude of the field acting on the spin sitting in position $l = -L+1$, and $\ell$ represent the characteristic penetration length of the magnetic field inside the system.

The first results concerning the dynamics obtained from the numerical integration of equations (3.14) with the "zero-temperature" initial configuration show that for the different values of $\ell$ we can still have the generation of one single soliton tuning the parameter $V_{\text{ampl}}$. In particular we find that $V_{\text{ampl}}$ should be set to a value $< \ell^{-1}$ in order to obtain this result, confirming the expected amplification effect and the corresponding reduction in the needed field strength. Moreover when $V_{\text{ampl}} \gtrsim \ell^{-1}$ we observe the generation of several solitons with different energies together with a completely new feature which is a temporary spatial localization of the magnetization in a finite region at the beginning of the chain. This new feature is still unexplained and we are currently studying the physical conditions under which this sort of "bouncing" of the magnetization takes place. In figure 3.7 two density plot of $\boldsymbol{s}_l^z$, as function of $l$ and $JSt$, are presented showing an example of the described phenomenology. Finally, as a proof of consistency of the correct implementation of the penetrating field condition, we find that, setting $\ell \ll 1$, the results of the punctual interaction condition are exactly recovered.

## 3.4 Conclusions

In view of exploiting the robustness features of solitons for the realization of quantum operations, we have here examined a method for injecting soliton-like dynamical configurations in classical discrete spin chains through the application, at one of the chain ends, of a magnetic field with a peculiar time-dependence.

It has been shown that soliton-like dynamical configurations are indeed generated in the chain: these configurations resemble the known analytical solitons of the continuous model when the soliton length is much larger than the lattice spacing, and they are stable with respect to the thermal noise present in the system. Moreover, it is found that the generating scheme still keeps working when considering the finite penetration length of the injecting field inside the chain, and this, besides alleviating the need of high values of field intensity, introduces some new interesting phenomenology that is still under analysis.

We want also to point out that the results about the penetrating injecting field, together with some tests, that have been performed using external fields with a slightly different time dependence with respect to $\Sigma^{(\beta)}$, show that the scheme here proposed for generating solitons is not extremely sensitive to the peculiar time-shape of the injecting field, indicating that a deeper study in this direction aiming to establish necessary or sufficient conditions on the external field time dependence in order to obtain soliton generation could be of particular interest in view of an experimental application of the presented scheme.

Finally, it is worth noticing that the magnetic soliton propagation we have studied is an energy-conservative phenomenon and has proved to be robust against thermal noise up to a reduced temperature $\mathcal{T} \sim 0.01$: this suggests that, besides the specific proposal presented in this work, using solitons for transferring either classical or quantum information in solid-state devices might strongly alleviate the heat dissipation requirements that seriously affect more conventional solutions, without requiring a highly demanding lowering of the operating temperature.

# Chapter 4

# Qubit state control

The ability of addressing, initializing, and possibly controlling one single qubit without spoiling its quantum features or disturbing other nearby qubits is a necessary prerequisite for putting a quantum device into operation. Depending on the specific device architecture, however, this can be a most challenging task, as it implies the opening of the qubit towards an environment that, in a way or another, embodies some macroscopic apparatus. One possibility for avoiding that this opening alter the fragile properties of the qubit is that of placing the apparatus at a distance, and use a transmission line for conveying a proper signal to the qubit itself. In particular, when the qubit is represented by a localized magnetic particle [17, 19, 22, 106] it comes quite natural that the above signal be a time-dependent magnetic field; in fact, as it has been pointed out in chapter 1, any unitary action on a single qubit can be represented in terms of a Zeeman interaction lasting for a precise time interval. This nonetheless leaves the question open on how to realize the transmission line.

To this purpose, we here propose the use of classical spin chains featuring soliton-like excitations, a choice suggested by these observations: *i*) A soliton faithfully represents a signal in so far as it is a finite-energy excitation which is well localized in space at any given time, and can travel at fixed velocity with constant profile; *ii*) Solitons are known to travel undisturbed along their medium, which allows us to put the apparatus that generates the pulse at great distance from the qubit and yet be sure that the signal will pass near its target undeformed; *iii*) Solitons relative to the very same model can have different shapes and energies, which gives us the freedom of choosing the signal that best controls the qubit, without modifying the transmission line.

The scheme here proposed is one where the transmission lines, one for each qubit, depart from a control apparatus and convey to the qubits a suitable signal to accomplish the assigned task: a practical realization of such scheme can be found, e.g., in nanofabricated microwave transmission lines recently used to manipulate electron and nuclear spin of phosphorus donors in silicon [107].

In this chapter, the wire will be modelled as an Heisenberg spin-chain while the signals will be the solitons described in the former chapters; a control apparatus, allowing for soliton injection, is supposed to be placed at one end of the chain, i.e. far enough from the quantum register in order to avoid any disturbance, but that mediated by the wire. We thus thoroughly analyse the effects of the soliton transit on the spin state of the spin-$\frac{1}{2}$ localized particle embodying the qubit, considering both an ideal and an injected soliton, as well as the possibility of noise along the chain.

The results will be divided according to the different physical situations considered, i.e. the specific types of interaction between the qubit and the spin-chain, which determine the effective magnetic field sensed by the qubit. Finally, comments upon possible experimental implementations of the scheme are put forward in the conclusive part, with attention focused on the validity of the assumptions we have made in order to make the scheme work.

## 4.1 Model

Having already demonstrated that a soliton-like signal can be successfully generated in a spin-chain, we now turn our attention on the effects that the propagation of this kind of signal has on a qubit interacting with the chain. In fact, the transit of the soliton near to the qubit produces a time-varying distortion in the, otherwise uniform, spin-chain configuration resulting in an effective magnetic field on the qubit which is given by the sum of the contributions from all the spins, weighted by the strength of their interaction with the qubit, and whose effects on the qubit-state dynamics is what we are interested in.

Let us now introduce the model we consider to represent this situation, starting from the qubit. As stated in chapter 1, a qubit is a physical system that can be described by the spin-1/2 operator [1] $\frac{\hbar}{2}\hat{\boldsymbol{\sigma}}$ represented by the Pauli matrices $\hat{\boldsymbol{\sigma}} = (\hat{\sigma}^x, \hat{\sigma}^y, \hat{\sigma}^z)$; its state $\hat{\rho}(t)$ in terms of the Bloch's vector $\boldsymbol{n}(t) \equiv \mathrm{Tr}\big[\hat{\rho}(t)\,\hat{\boldsymbol{\sigma}}\big]$, reads

$$\hat{\rho}(t) = \frac{1}{2}\big[\mathbb{1} + \hat{\boldsymbol{\sigma}}\cdot\boldsymbol{n}(t)\big] \ . \tag{4.1}$$

In our scheme, the qubit is realized by a localized spin-$\frac{1}{2}$ particle, sitting near the site of the chain labelled by the index "0". We assume that the way the qubit feels the presence of the chain magnetic moments, as depicted in figure 4.1, can be generally described as a Zeeman interaction with an effective magnetic field proportional to

$$\tilde{\boldsymbol{s}}(t) \equiv \sum_l p_l \boldsymbol{s}_l(t) \ , \tag{4.2}$$

[1] Hereafter we will denote every operator $\mathcal{O}$ as $\hat{\mathcal{O}}$, with the "hat" superscript in order to distinguish them from the other quantities.

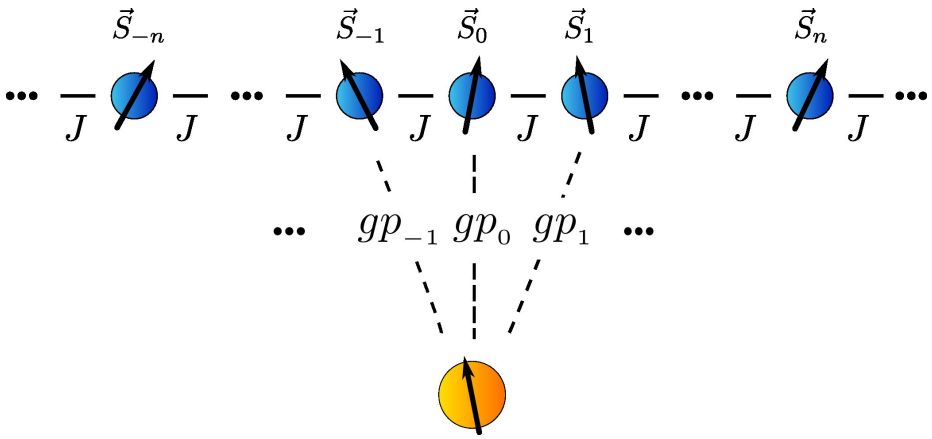


**Figure 4.1:** The qubit interacts with a bunch of moments of the classical spin-chain, with couplings $j_l = g\, p_l$; a constant uniform field is applied to the overall system.

where $\boldsymbol{s}_l$ are the unit vectors entering Eq. (2.15), and $p_l$ is expected to decrease rapidly with $|l|$. In fact, the detailed dependence of $p_l$ on $l$ is not relevant, particularly if, as in the present scheme, the time dependence of the magnetic moments is primarily due to the transit of a signal whose length equals a finite number of lattice spacings.

From Sec. 2.2 we have learned that the presence of a constant and homogeneous magnetic field $\boldsymbol{H}$ is necessary for the Heisenberg spin chain to support solitons with finite velocity: therefore, we take $\boldsymbol{H} \neq 0$ and identify its direction with the quantization axis used for encoding the qubit states into the spin degree of freedom of the spin-$\frac{1}{2}$ localized particle. The qubit Hamiltonian thus reads

$$\hat{\mathcal{H}}_{\text{qubit}} = -\big[\gamma_\sigma H\, \boldsymbol{z} + g\, S\, \tilde{\boldsymbol{s}}(t)\big] \cdot \frac{\hbar \hat{\boldsymbol{\sigma}}}{2} \ , \tag{4.3}$$

where $\boldsymbol{z} = (0, 0, 1)$, $\gamma_\sigma$ is the gyromagnetic ratio of the particle realizing the qubit, and $g$ is an overall coupling constant. The corresponding evolution of the qubit Bloch's vector is ruled by the equation

$$\partial_\tau \boldsymbol{n} = \boldsymbol{n} \times \big[\delta\, \hat{\boldsymbol{z}} + \mu\, \tilde{\boldsymbol{s}}(\tau)\big] \ , \tag{4.4}$$

where $\tau \equiv \gamma H\, t$ is the (chain) dimensionless time that will be hereafter used. The two dimensionless parameters

$$\delta \equiv \frac{\gamma_\sigma}{\gamma} \ , \qquad \mu \equiv \frac{gS}{\gamma H} \tag{4.5}$$

characterize the qubit interactions with the external and the effective field, $\boldsymbol{H}$ and $\tilde{\boldsymbol{s}}(t)$, respectively. Notice that, despite the chain parameter $\gamma$ does not appear in the qubit-Hamiltonian (4.3), it does enter the EoM for the qubit Bloch's vector via the definition of the dimensionless time $\tau$; in fact, the relevant time-scale of the overall dynamics is exclusively set by the chain-Hamiltonian (2.15), a statement based on the implicit assumption that the presence of the qubit has no effect (no 'back-action') on the chain itself. This assumption

can be formalized by saying that the maximal qubit energy gain (occurring for a complete flip), $\Delta E = \hbar(gS + \gamma_\sigma H)$, should be much smaller than the soliton energy $\varepsilon_\beta$, i.e., by requiring that the following relation is satisfied:

$$\frac{\Delta E}{\varepsilon_\beta} = \frac{gS+\gamma_\sigma H}{8\gamma H}\frac{\hbar}{S}\frac{\sqrt{h}}{\sin\beta} \ll 1 . \tag{4.6}$$

We notice that the above requirement is satisfied when the conditions of quasi-classical spins, $S \gg \hbar$, and of "quasi-continuum" support, $\lambda_\beta \gg d \Rightarrow \sqrt{h} \ll \sin\beta$, are assumed. As shown in the following, it is indeed found that, for parameter values flipping the qubit-state, the ratio $\Delta E/\varepsilon_\beta \sim 10^{-2}$.

## 4.2 General results

Suppose now that a magnetic signal in the form of $\mathbf{\Gamma}_l(\beta;\tau)$, i.e. a generated soliton-like dynamical configuration (see section 3.2.1), runs through the chain. In the early stage of the process, at a time when the soliton is still far from the site 0, it is $\tilde{\boldsymbol{s}}(\tau) \propto \boldsymbol{z}$ and the qubit Bloch's vector undergoes a uniform precession around $\boldsymbol{z}$, unless it is not initially aligned along the $z$-axis itself. In order to isolate the qubit evolution exclusively due to the soliton transit, it is convenient to choose $\boldsymbol{n}(\tau_\mathrm{i})=\boldsymbol{z}$, with $\tau_\mathrm{i}$ the earlier time when $\boldsymbol{s}_{-L} = \boldsymbol{z}$. Notice that this does not imply adding a previous single-qubit manipulation step in the overall scheme, but rather preparing the whole system in a globally aligned state, which is readily obtained as $\boldsymbol{H} \neq 0$.

Consider now a time $\tau_\mathrm{f}$ during the final stage of the process, i.e. after the soliton has travelled along the chain far beyond the qubit: the qubit Bloch's vector, set in motion by the soliton transit, can *1)* align back to $\boldsymbol{z}$, *2)* tilt-up and hence precess around $\boldsymbol{z}$, or *3)* perfectly flip and anti-align along $-\boldsymbol{z}$. Situations *2)* and *3)* are those in which we are most interested, as they represent the possibility of permanently modifying the qubit state, which is in fact the final goal of our scheme. In order to analyse the conditions under which they are obtained, one must numerically integrate Eqs. (4.4) with the effective field $\tilde{\boldsymbol{s}}(\tau)$ as from Eq. (4.2) with

$$\boldsymbol{s}_l(\tau) = \mathbf{\Gamma}_l(\beta;\tau) . \tag{4.7}$$

For the sake of clarity, in what follows we will specifically concentrate on the case when the qubit response to the signal consists in a permanent flip, which means that, for all times such that $\tau > \tau_\mathrm{f}$, we have $n^z(\tau) = n^z(\tau_\mathrm{f}) \neq 1$. Figure 4.2 shows an example of the above dynamics. In the following paragraphs (except the last one) we will take $\mathbf{\Gamma}_l(\beta;\tau) = \mathbf{\Sigma}_l^{(\beta)}(\tau)$ and the chain initially prepared in the ferromagnetic state, since, as shown in previous chapter, the generated solitons $\mathbf{\Gamma}_l(\beta;\tau)$ are almost equal to the analytical shape $\mathbf{\Sigma}_l^{(\beta)}$ in the

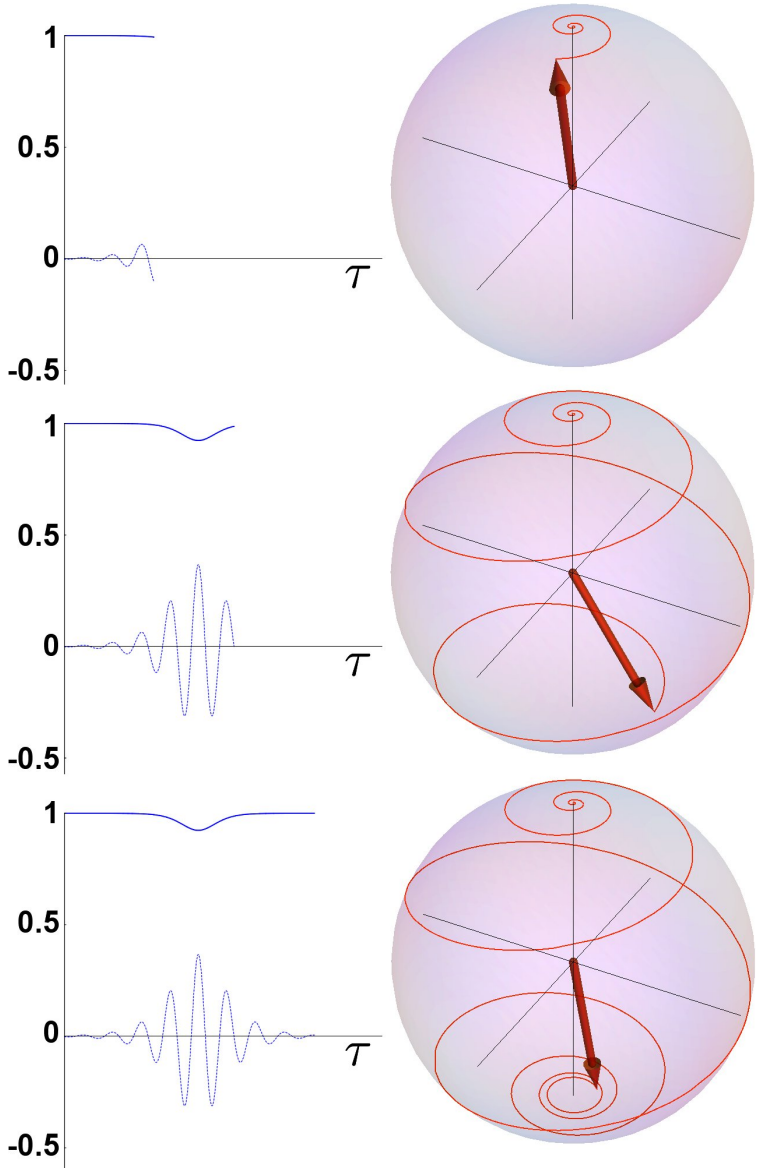


**Figure 4.2:** Snapshots of the qubit state trajectory [represented by $\boldsymbol{n}(\tau)$] on the Bloch's sphere while a $\beta$-soliton propagates along the chain. The graphs on the left display $\tilde{s}^z(\tau)$ (full lines) and $\tilde{s}^x(\tau)$ (dashed lines), i.e., the components of the effective field acting on the qubit as a consequence of the soliton transit. The parameter values are: $h = 0.01$, $\tan\beta = 0.2$, $\mu = 1$, $\delta = 1$, and $\alpha = 3$.

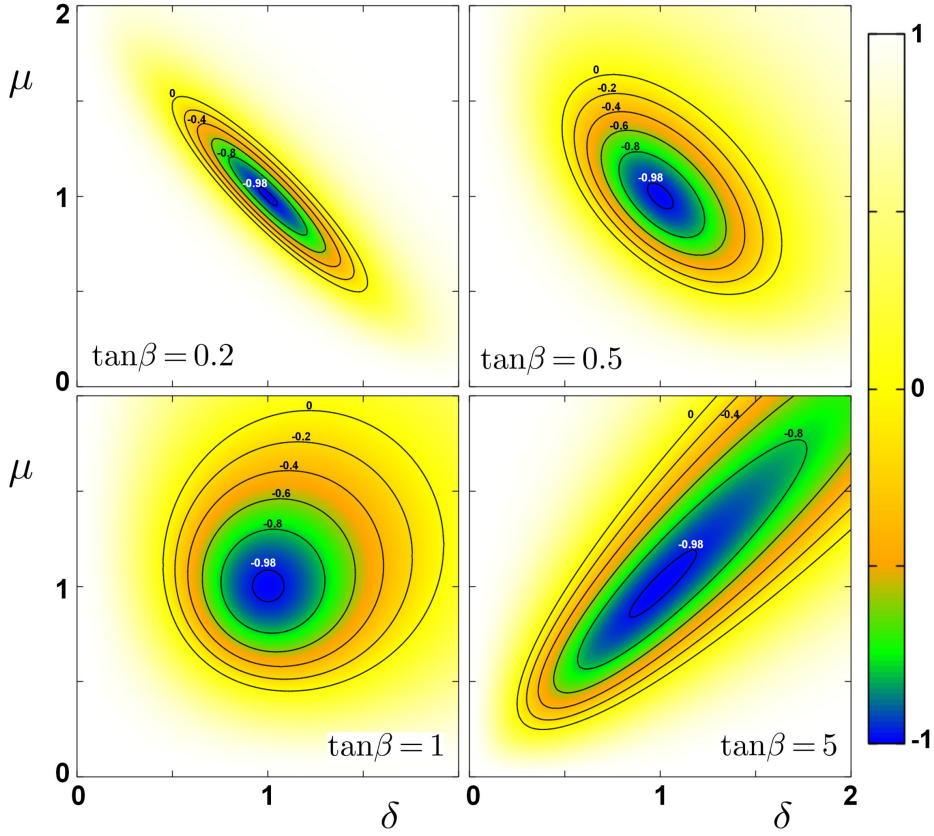


**Figure 4.3:** Contour plots of $n^z(\tau_f)$ as a function of $\delta$ and $\mu$, for $\alpha = 0$. In each panel the magnetic signal acting on the qubit is that produced by an ideal $\beta$-soliton, $\mathbf{\Sigma}_l^{(\beta)}(t)$.

case $\mathcal{T} = 0$.

## 4.3 Zero range interaction dynamics

We start considering the case of zero interaction length $p_l = \delta_{l0}$: in this case the qubit state for $\tau > \tau_f$ can be represented as follows:

$$\hat{\rho}(\tau) = \frac{1}{2}\begin{pmatrix} 1+n^z(\tau_f) & \sqrt{1-(n^z(\tau_f))^2}\, e^{-i[(\mu+\delta)\tau+\delta_0]} \\ c.c. & 1-n^z(\tau_f) \end{pmatrix} , \tag{4.8}$$

with $n^z(\tau_f)$ being a function of the relevant parameter $\delta$, $\mu$ and $\beta$. Equation (4.8) shows that, in order to characterize the final state of the qubit, it is sufficient to study the behaviour of $n^z(\tau_f)$ with respect to the parameters. We also know [43] that, whenever $\delta = 0$, the qubit goes back to its initial state ($n^z(\tau_f) = 1$): therefore, in order to obtain a permanent flip, the physical object embodying the qubit must have a finite gyromagnetic ratio. Since studying $n^z(\tau_f)$ suffices to distinguish the above situations *1)*, *2)*, and *3)*, in figure 4.3 we plot $n^z(\tau_f)$ in the plane $(\delta, \mu)$: when $\delta = \mu = 1$ the flip is complete (figure 4.4), while the change in $n^z(\tau_f)$ decreases monotonically when getting far from this point. Remarkably, for $\delta = \mu = 1$

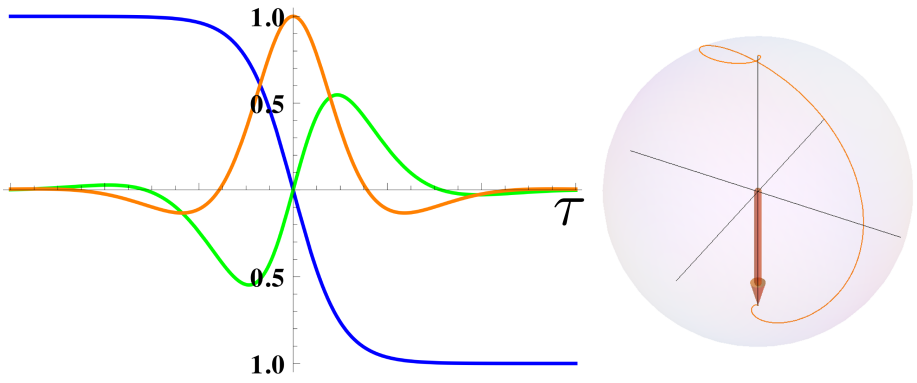


**Figure 4.4:** Qubit perfect flip situation obtained for $\delta = \mu = 1$. Left panel: Bloch's vector components as function of $\tau$ (green $n^x$, orange $n^y$ and blue $n^z$). Right panel: trajectory of the Bloch's vector on Bloch's sphere.

there is no dependence on $\beta$: the qubit is flipped whatever the amplitude of the signal running through the chain [2]. An additional feature, numerically observed and clearly seen in figure 4.3, is that $n^z(\tau_f)$ is symmetric in the exchange $\delta \leftrightarrow \mu$, even though the evolution of the qubit is different in the two cases. The most relevant feature displayed by figure 4.3, however, is the presence of a region where almost complete flip occurs: this means that fine-tuning is not necessary and if $\delta$ is difficult to alter one can still act on $\mu$, or viceversa, depending on the specific physical realization of the scheme.

## 4.4 The dipolar interaction

Before analysing the finite-range interaction case, we want to show that the qualitative dynamics described above holds independently of the specific shape of the function $p_l$ and in particular that $p_l$ should not be exponentially decaying with the distance from the qubit but it is sufficient that it decays fast enough to let the sum $\sum_l p_l \boldsymbol{s}_l$ be well defined. In particular we are going to study the case where $p_l$ represents a typical magnetic interaction, namely the dipolar interaction between magnetic moments. A magnetic dipole of corresponding moment $\boldsymbol{m}$ will generate at a distance $\boldsymbol{r}$ a magnetic field

$$\boldsymbol{B}_{\text{dipole}} = \frac{\mu_0}{4\pi}\left[\frac{3\boldsymbol{r}\,(\boldsymbol{m}\cdot\boldsymbol{r})}{r^5} - \frac{\boldsymbol{m}}{r^3}\right],$$

where $\mu_0$ is the magnetic permeability constant. Considering now the magnetic moment of one of the chain spins $(\gamma S)\boldsymbol{s}_l$, the magnetic field generated by the spin-chain at the qubit position is

$$\boldsymbol{B}_{\text{chain}}(t) = \frac{\gamma S \mu_0}{4\pi d^3}\sum_l \left[\frac{3\boldsymbol{r}_l\,(\boldsymbol{s}_l(t)\cdot\boldsymbol{r}_l)}{r_l^5} - \frac{\boldsymbol{s}_l(t)}{r_l^3}\right], \tag{4.9}$$

[2] It is important to remember that all these results have been derived under the no back-action assumption, i.e., equation (4.6) must be satisfied: this implies that $\beta$ cannot become too small.

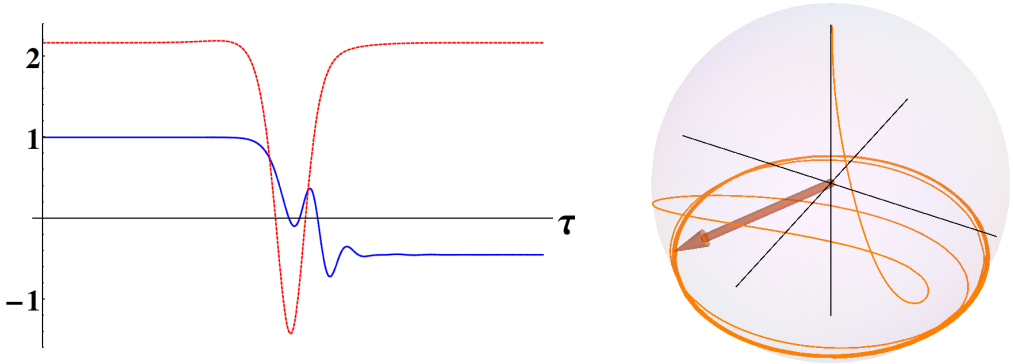


**Figure 4.5:** Left panel: time evolution of $n^z(\tau)$ (solid blue line) and $\tilde{B}^z_{\rm chain}(\tau)$ (dashed red line) for $\tan\beta = 2$; $\tilde{\mu} = 1$, $\delta = 1$, $h = 0.05$ and $r_0 = 1$. Right panel: trajectory of the qubit state on the Bloch's sphere.

where dimensionless vectors $\boldsymbol{r}_l$ indicate the position of the spins $\boldsymbol{s}_l$ with respect to the qubit position. In this situation the Hamiltonian (4.3) is replaced by

$$\hat{\mathcal{H}}_{\rm qubit} = -\gamma_\sigma \left[ H\,\boldsymbol{z} + \frac{\gamma S \mu_0}{4\pi d^3}\,\tilde{\boldsymbol{B}}_{\rm chain}(t) \right] \cdot \frac{\hbar \hat{\boldsymbol{\sigma}}}{2}\,, \tag{4.10}$$

where we have introduced the dimensionless field $\tilde{\boldsymbol{B}}_{\rm chain}(t) \equiv (4\pi d^3)/(\gamma S \mu_0)\boldsymbol{B}_{\rm chain}(t)$, which takes the place of the effective field $\tilde{\boldsymbol{s}}(t)$. The equation for the evolution of the qubit Bloch's vector (4.4) also changes according to

$$\partial_\tau \boldsymbol{n} = \boldsymbol{n} \times \left[ \delta\,\hat{\boldsymbol{z}} + \tilde{\mu}\,\tilde{\boldsymbol{B}}_{\rm chain}(\tau) \right]\,, \tag{4.11}$$

where $\tau$, $\delta$ and $\boldsymbol{z}$ are the same of equation (4.4) while

$$\tilde{\mu} = \frac{\gamma_\sigma S \mu_0}{4\pi d^3 H}\,, \tag{4.12}$$

represents the new interaction parameter of the qubit with the spin chain. We will now take into account the results concerning the Bloch's vector evolution in the situation here described, considering in particular the following spatial configuration of the system: the spin-chain lies on the $\boldsymbol{x}$-direction, while the qubit is again placed near the spin $\boldsymbol{s}_0$ at a distance $r_0$ in such a way that the position of $\boldsymbol{s}_0$ with respect to the qubit is identified by the vector $(0, 0, r_0)$ (i.e. along the $\boldsymbol{z}$-axis). In this configuration the position of each $\boldsymbol{s}_l$ is identified by the vector $(l, 0, r_0)$. The qubit state dynamics emerging from this situation setting $\boldsymbol{s}_l(t) = \boldsymbol{\Sigma}_l(t)$ is perfectly analogous to that already described in previous sections: the Bloch's vector is again characterized by the constant value of its third component $(n^z(\tau_{\rm f}))$ plus a precession with a constant frequency depending on the uniform field value and on the other parameters through the expression (4.9) evaluated at $\tau_{\rm f}$. Here, besides the

values of $\delta$, $\tilde{\mu}$ and $\beta$, also the values of $r_0$ and $h = \gamma H/JS$ play a role in determining the value of $n^z(\tau_f)$: the first gives the intensity of the dipolar field and the second (as it will be further commented in the next section) fixes the soliton characteristic length. Figure 4.5 shows an example of the Bloch's vector dynamics when the qubit is subjected to a dipolar interaction with the spin chain, confirming that the scheme is still effective for manipulating a qubit state also considering a finite range interaction decaying with power law with the distance from the qubit.

## 4.5 Finite range interaction dynamics

Finally, although the dipolar interaction is a pretty typical among magnetic moments, we will characterize the dependence of $n^z(\tau_f)$ on parameters using an interaction whose spatial behaviour $p_l$ is described by a gaussian shape. The reason behind this choice is that using the gaussian shape we can easily identify the interaction range with its standard deviation: this gives us an easy way to check both the final state dependence on the interaction range and the interplay with the other length-scale (soliton length, $\lambda_\beta$). Using the dipolar-law shape we do not have the same control on this parameter and this would make the analysis more difficult. Moreover, in the dipolar interaction case, a crucial role is played by the specific spatial configuration of the system; this fact would thus limit our conclusions to a specific system set-up and leads us to the aforementioned choice, being not our aim that of comparing our results with a specific experimental realization, but rather that of obtaining a general characterization of the qubit dynamics in the proposed theoretical scheme.

We consider the finite-range case, and take

$$p_l = A \exp(-l^2/2\alpha^2) \tag{4.13}$$

in equation (4.2), where $A$ is such that $\sum_l p_l = 1$ . In this way the standard deviation $\alpha$ characterizes the interaction range, in units of $d$. When $\alpha \neq 0$, as in the case shown in figure 4.2, the qubit dynamics is qualitatively similar to that observed for $\alpha = 0$ [42], but the value of $n^z(\tau_f)$ is found to be quite sensitive to $\alpha$ itself. However, an almost complete flip, even better than that observed in figure 4.2, can be obtained by further adjusting the available parameters. To this respect, notice that the ratio $h = \gamma H/JS$ is a relevant quantity when $\alpha \neq 0$, as it contributes to set the length-scale of the soliton: for example, $h = 0.05$ and $\tan\beta = 2$, 1, 0.5, 0.2 define $\beta$-solitons with $\lambda_\beta = 5d$, $6.3d$, $10d$, $22.8d$, respectively.

In figure 4.6 we show a contour-plot relative to $n^z(\tau_f)$ in the plane ($\tan\beta$,$\mu$), for $\delta = 1$ and different values of $h$. As expected, for smaller $\tan\beta$ the qubit dynamics is less affected by the finite interaction range, as the effective field acting on the qubit, when a broad soliton ($\lambda_\beta \gg \alpha d$) is considered, is little modified by the 'smearing' entailed by Eq. (4.2).

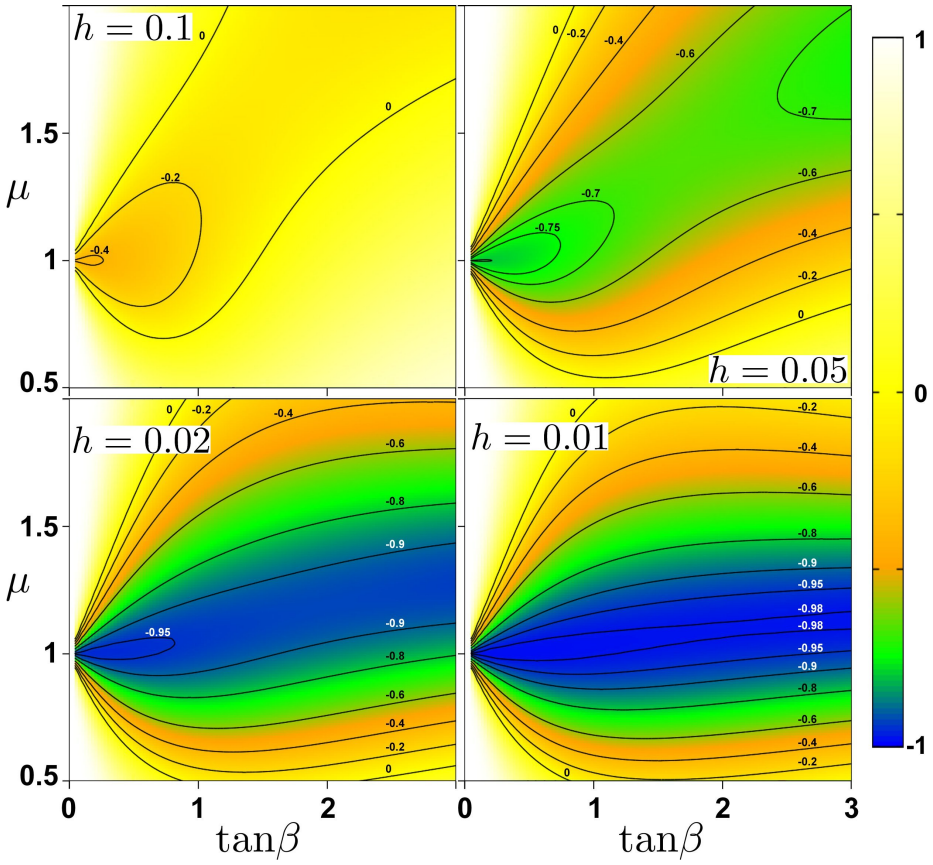


**Figure 4.6:** Contour plots of the final magnetization $n^z(\tau_f)$ as a function of the parameters $\tan\beta$ and $\mu$, for $\alpha = 3$ and $\delta = 1$. In each panel a different value of $h$ is considered.

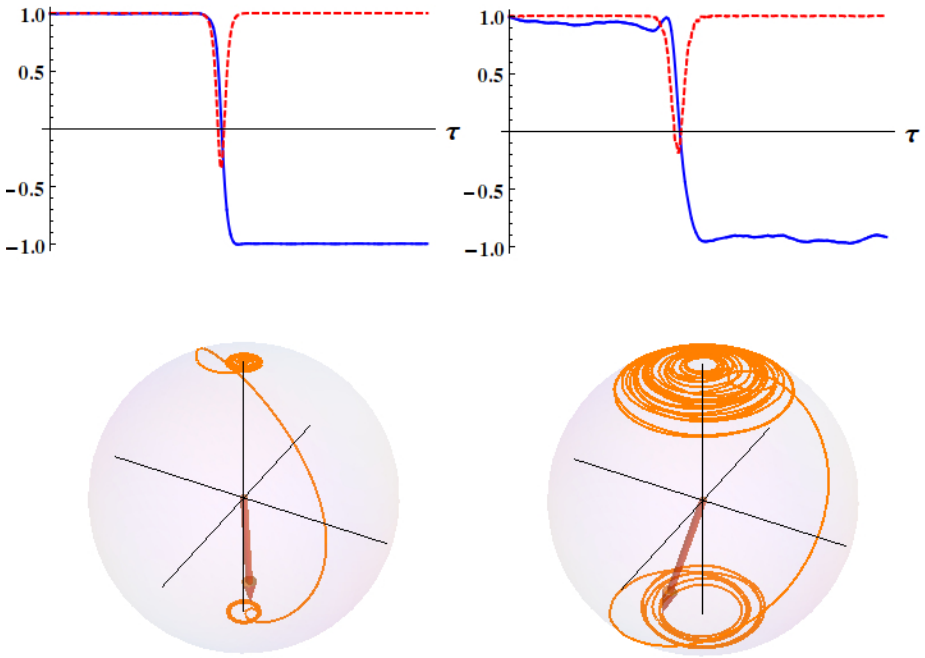


**Figure 4.7:** Top panels: time-evolution of $n^z(\tau)$ (solid blue line) for the qubit interacting with the soliton (dashed red line) generated by injecting TW-shape ($\tan\beta = 2$, $h = 0.2$) with $\mathcal{T} = 0$ (left panel) and $\mathcal{T} = 0.002$ (right panel); $\mu = 1$, $\delta = 1$, and $\alpha = 0$. Bottom panels: parametric plots of the qubit state evolution on the Bloch's sphere, under the same conditions of the respective upper panel.

In particular, the plot for $h = 0.02$ shows that the partial flip seen in figure 4.2 can be improved by taking smaller $\beta$, i.e. longer solitons, or increasing $\mu$, i.e. the qubit-chain coupling. The flip quality decreases also when, due to the phase term $\xi \cot\beta$ appearing in Eq. (2.21), the $x$ and $y$ components of $\tilde{\boldsymbol{s}}(t)$ shrink under the smearing (4.2). This effect can be reduced, as suggested by Eq. (2.27), requiring $\alpha\sqrt{h} \ll \cos\beta$, i.e., for small $\beta$, $h \ll \alpha^{-2}$. In fact, figure 4.6 shows that by taking a smaller $h$ the flip quality can be made to approach optimal values in an extended region of the $\beta$-$\mu$ plane. Referring to the definitions (4.5), this optimization can be typically performed by driving the external field only. The freedom from the necessity of a fine tuning of parameters, due to the above feature, makes the scheme here described a suitable proposal for the experimental realizations.

## 4.6 Generated soliton induced dynamics

Let us now consider the case when the soliton running through the chain is not ideal, but rather a generated one, $\boldsymbol{\Gamma}_l(\beta;\tau) \simeq \boldsymbol{\Sigma}_l^{(\beta')}(\tau)$. In figure 4.7 we show the qubit-state evolution when $\tan\beta = 2$ and $\lambda_\beta = 5$ ($\alpha = 0$): in the left panels one can appreciate that the evolution of $n^z(\tau)$ follows that of the generated soliton, both for zero (left) and finite (right) temperature; the right panels display the overall trajectory of the qubit Bloch's

vector on the Bloch's sphere. The qubit behaviour under the action of a generated soliton looks similar to that described in the previous sections for ideal solitons: in particular, for $\mathcal{T}=0$ an almost complete flip is obtained. More pronounced differences emerge for $\mathcal{T}\neq 0$, where the value of $n^z(\tau_\mathrm{f})$ is no more constant in time but fluctuates, being subjected to the thermal fluctuations of the spin chain. However, we note that such fluctuations are conceptually different from the decoherence phenomena commonly met when dealing with open quantum systems, as the (whatever noisy) effective field acting on the qubit is still classical, keeping the qubit evolution *on* the Bloch's sphere.

## 4.7 Conclusions

In this chapter we have proposed a scheme to manipulate a qubit state at distance by means of magnetic solitons running through a spin chain. The solitons here considered are both the analytical shapes of the continuous chain $\mathbf{\Sigma}_l^{(\beta)}(\tau)$, evaluated at the lattice sites (as anticipated in section 2.2), and the dynamical configurations $\mathbf{\Gamma}_l(\beta;\tau)$ generated through the method described in the chapter 3.

We have considered the dynamics of the qubit state subjected to the soliton transit in different physical situations: a point-like interaction with one spin of the chain, the dipolar interaction and a general finite-range interaction. We found that in all the three cases the resulting dynamics shows similar features; in particular, after the soliton has run by, the qubit is left in a state which can be significantly different from the initial one depending on the values of these parameters which are relevant for the specific case. We have then characterized the qubit final state finding that, even in the case of finite range interaction, we can recover a quasi-perfect flip of the qubit state in a broad region of the parameters manifold, implying that a fine tuning is not necessary in order to achieve the goal of significantly modifying the qubit state.

In virtue of these results we can conclude that using dynamical solitons as magnetic signals running through spin chains is quite a promising prospect, though it still needs an in-depth analysis in order to become a more solid possibility. In fact, besides checking intuitions, quantitative conditions must also emerge and be tested, with specific reference to the realization one has in mind. To this respect, the scheme presented in this chapter might find several different applications, as spin chains are versatile models that can be used for describing the most diverse real situations.

Finally we comment upon the conditions identifiable as essential in our analysis, in the case of an implementation based on solid-state systems [20, 23, 107–109].

Although having already discussed about soliton generation in the former chapter, we want to point out here that solitons exist and run also in anisotropic spin chains [24, 27], which makes our scheme potentially efficient in the case of anisotropic quasi one-dimensional

real compounds. In fact, this is quite a relevant feature when thinking of implementations based on one-dimensional monoatomic metal chains deposited on surfaces [110] where the system geometry inevitably makes the intra-chain exchange anisotropic [111].

Having shown that a controlled action on the qubit can actually be obtained by its interaction with the nearby running magnetic soliton, we notice that the condition required by the continuum approximation is fully consistent with the small values of $\sqrt{\gamma H/JS}$ that are found to produce a permanent variation of the qubit state, according to the analysis presented in Sec. 4.2 and in the following. Moreover, the energy exchanged between qubit and chain in the case of complete flip (obtained by, say, $\gamma H/JS = 0.05$, $\alpha = 0$, $\tan\beta = 0.2$, $\mu = \delta = 1$) amounts to $\Delta E = \hbar(gS + \gamma_\sigma H) \simeq 10^{-2} JS^2$; as the soliton energy is of the order of $JS^2$, the chain dynamics results unaffected by the evolution of the qubit, essentially validating the 'no back-action' approximation described in equation (4.6). As for the limits dictated by the typical coherence times attainable in solid-state qubit realizations, an additional relevant quantity is the time $t_{\mathrm{prop}}$ required by the soliton to reach the qubit after its injection: for a time-scale of $(JS)^{-1} \sim 10^{-13}\,\mathrm{s}$, we can estimate $t_{\mathrm{prop}} \sim 1\,\mathrm{ns}$, if the qubit lies around $10^3$ lattice constants away from the chain end.

# Chapter 5

# Entanglement generation via semi-classical channels

Creating and transferring entanglement between distant qubits are fundamentals of quantum computation and, for this very reason, finding a practical method to accomplish these operations and the directly related applications (e.g. implementing a two-qubit entangling gate) is a central problem of any tentative realization of a quantum computer.

Whenever we deal with quantum devices, we have to accommodate apparently contradictory requirements: indeed, in order to get a truly quantum behaviour for a suitably extended time interval, we have to select a microscopic object well protected from external disturbances, which could otherwise destroy its delicate, coherent quantum evolution; but, at the same time, the given object has to be able to communicate with the outside world, if it has to accomplish some useful task. We propose a possible way to meet both requirements by means of a hybrid scheme, where the fragile quantum component (a qubit) is accompanied by a robust, almost classical, partner (a spin chain), mediating its dialogue with the external world without exposing it, but still being able to convey quantum correlations.

We already showed in the previous chapters that the soliton features of robustness against disturbances can be used for applications where the spin-chain dynamics can be regarded as classical, e.g. to drive a qubit state. The question here is if the same features can be exploited for accomplishing some tasks which are intimately quantum, i.e. tasks where the quantum nature of the spin chain has to be necessarily considered. An example of such a task is the generation of entanglement between distant qubits. Purely quantum-channels constituted by many interacting qubits are usually the key players for entanglement generation/transfer. In fact, spin-1/2 chains have been fruitfully used for generating and transferring entanglement in the realization of entangling gates and perfect state-transfer protocols [112–118]. They provide very good results but they are really sensitive to decoherence, thus requiring protection against external disturbances, not only as

far as the interaction between the channel and the qubit is concerned but also during the channel dynamical evolution.

In view of these considerations, we ask ourselves if a semi-classical system, i.e. a system made of many interacting degrees of freedom whose behaviour is known to be well described by (semi-)classical equations, can accomplish the goal in a comparable way with respect to fully quantum systems. If so, it would be possible to obtain quantum devices which are less sensitive to the unwanted external disturbances taking advantage of the robustness properties of the classical systems.

This situation can be far more complicated than considering systems of interacting qubits only, where the study of how correlations are moved within the system from one point A to another point B is of straightforward interpretation, since the homogeneity of its constituents allows one to use the same definitions to characterize each of the system components. A completely different situation is met in the cases where qubits are present, being the targets of some quantum operation, but the system designated for accomplishing those operations is constituted by a set of different objects (typically more complex than qubits). This situation set two more issues, the first provided by the complexity and the second by the heterogeneity of the considered system. In fact a full quantum description of systems like those just cited, usually, cannot be pursued, and approximations must be taken into consideration. Moreover, attention must also be paid to the specific choice of the approximations to be undertaken, since a standard semi-classical approach does not usually fit well for describing purely quantum objects like qubits.

For these reasons, finding a method to describe the interaction of some qubits with a semi-classical system is a challenging goal on its own, which is worth to be followed, and can pave the way for several applications.

The aim of the present chapter is thus to demonstrate the possibility of generating entanglement between distant, and not directly interacting, qubits through their interaction with a large-$S$ spin chain. In particular, we want to introduce a method which is capable to give an approximate description of such an hybrid system still retaining enough of the spin-chain quantum nature in order to account for entanglement transfer between the qubits, but also to keep a strong relation with the chain classical description, in order to take advantage from the robustness properties of non-linear classical dynamics. The success of this method, as it will be clarified later, relies on the careful choice of the initial states of the spin chain.

We now describe the particular model considered in this chapter, and the specific states leading to the *semi-classical approximation* of the chain dynamics, that allows us to complete calculations and keep an open link between the quantum behaviour and the classical picture.


**Figure 5.1:** Schematic representation of the system described in the text: the connected blue spheres represent spin-$S$ of the Heisenberg chain, while the orange ones are the two qubits.

## 5.1 Model

The system considered is formed by a discrete Heisenberg chain, henceforth referred to as $\Xi$, made by quantum objects with spin quantum number $S \gg 1/2$ (namely large-$S$) [1]) interacting via a ferromagnetic isotropic nearest-neighbour interaction, and two distant qubits, A and B, both close to the chain, interacting with two spins of the chain, $\boldsymbol{S}_A$ and $\boldsymbol{S}_B$, respectively, as shown in figure (5.1.

Due to the large value of $S$, the Hilbert space of the spin chain has a huge dimension already for $\Xi$ longer than a few spins, which makes the exact description of the chain dynamics out of reach, even numerically. For this reason we will need to introduce the set of states given by the tensor product of the spin-$S$ SSCS (see section 1.4.2 for SSCS definition and properties). These states will be called the *semi-classical states* of the spin chain $\Xi$, since it is possible to set a one-to-one correspondence between them and the configurations of the classical chain. In fact, any configuration of a classical spin chain, of length $N$ and spin modulus $S$, is completely determined by the set of $2N$ values, $\Omega_n \equiv \{\theta_n, \phi_n \mid n = 1, \dots, N\}$, defining the directions of each spin-vector [2]. Making reference to section 1.4.2 we can thus associate to the classical configuration of each spin the corresponding SSCS as follows

$$\Omega_n \quad \longrightarrow \quad |\Omega_n\rangle \tag{5.1}$$

where $|\Omega_n\rangle$ is defined in equation (1.55). The semi-classical state for $\Xi$ will be given by the tensor product over the chain index $n$ of the SSCS of each spin, in this way every classical configuration defines a semi-classical separable state for the quantum spin-chain (and vice versa), via

$$\{\, \Omega_n,\, \forall n = 1, \dots, N \,\} \quad \longleftrightarrow \quad \bigotimes_{n=1}^{N} |\Omega_n\rangle \ . \tag{5.2}$$

The chain-state will be approximated at the semi-classical level as a product of single-spin coherent states, belonging to a subspace of the Hilbert space of states for $\Xi$; this entails a

[1] As it is shown in the literature, the behaviour of 1-d spin system is well represented by classical renormalized equations down to $S = 1$ (see consideration in section 2.1. Of course, the bigger the value of $S$, the stronger correspondence with classical behaviour.

[2] A classical spin is nothing but a vector of fixed modulus $S$, its configuration is thus defined by the polar angles $\theta$ and $\phi$ in the usual way $\boldsymbol{S} = S(\sin\theta\cos\phi, \sin\theta\sin\phi, \cos\theta)$.

one-to-one correspondence with the configurations of the classical counterpart of the chain [3].

Starting with a completely factorized state of the chain $\Xi$ and the two qubits, we want to study whether the system dynamics can lead A and B in an entangled state; i.e., whether the entanglement locally created by the interaction between A and $\boldsymbol{S}_{\mathrm{A}}$ is propagated by the chain evolution up to $\boldsymbol{S}_{\mathrm{B}}$ and finally transferred to the second qubit B, the net result being the generation of entanglement between the two qubits.

According to the scheme outlined above, our picture of the system dynamics, leading to the desired outcome, unfolds in three subsequent time intervals: in the first one, only the interaction between A and the spin $\boldsymbol{S}_{\mathrm{A}} \equiv \boldsymbol{S}_{n=n_{\mathrm{A}}}$ at site $n_{\mathrm{A}}$ of the chain is relevant; in the second interval the chain is let to evolve, neglecting its interaction with the qubits, and in the last one the only relevant interaction is that between the qubit B and the spin $\boldsymbol{S}_{\mathrm{B}} \equiv \boldsymbol{S}_{n=n_{\mathrm{B}}}$. As discussed in the following sections, such three-stage dynamics could be approximately realized if A and B interact with $\boldsymbol{S}_{\mathrm{A}}$ and $\boldsymbol{S}_{\mathrm{B}}$, respectively, and the initial state of the overall system, as well as the free chain Hamiltonian, are properly chosen: Indeed, if $\Xi$ is able to sustain the propagation of Heisenberg solitons like those of equations (2.21), i.e. well-localized, stable, pulse-shaped excitations, we will show that soliton propagation will be the player able to switch on (and off) the interaction with the relevant qubit in the first and third stage, and the conveyor of the information during the second stage.

In order to get a first insight about the potentiality of the proposed scheme, in the actual calculation we implement the three-stage dynamics by assuming a very simplified model, where the qubit-chain interaction constants $g_{\mathrm{A}}(t)$ and $g_{\mathrm{B}}(t)$ depend on time, and are switched on and off according to step functions:

$$\begin{aligned} g_{\mathrm{A}}(t) &= g\,\vartheta(t-t_0)\,\vartheta(t_1-t) \\ g_{\mathrm{B}}(t) &= g\,\vartheta(t-t_2)\,\vartheta(t_3-t)\,, \end{aligned} \tag{5.3}$$

where $\vartheta(t)$ is the Heaviside function, and $g$ is the interaction strength (see figure 5.2). In the interval $[t_1, t_2]$ the chain quantum state evolves according to the approximated semi-classical evolution introduced in section 5.3 below.

In more detail, assuming an initial factorized state, the three different stages of the system evolution from $t = t_0$ to $t = t_3$ are described as follows :

(1) $[t_0, t_1]$: $g_{\mathrm{A}}(t) = g$ while $g_{\mathrm{B}}(t) = 0$. Starting from the factorized initial state the joint evolution of $(\mathrm{A}, \boldsymbol{S}_{\mathrm{A}})$ is evaluated in a fully quantum way. During this stage the spin

[3] As it will be discussed later on, among all the classical dynamical configurations of the spin chain $\Xi$, we are particularly interested in the Heisenberg solitons discussed in the previous chapters: they will be crucial in the scheme proposed, embodying the robust classical part of our "hybrid device".

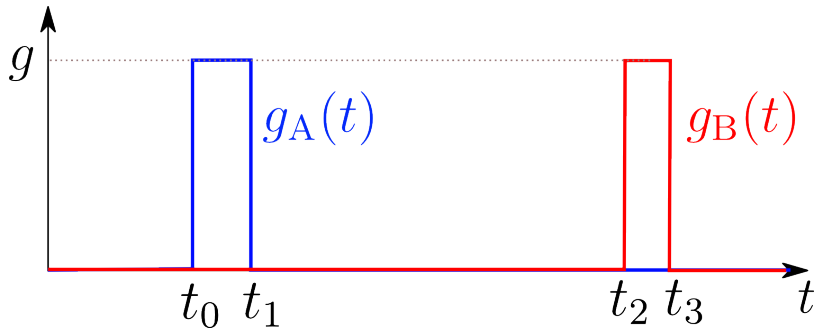


**Figure 5.2:** Time dependence of the interaction constants.

chain is frozen, i.e., the spins $\{\boldsymbol{S}_n\}$, except $\boldsymbol{S}_A$, are not evolving [4]. This leads to an entangled state of A and $\boldsymbol{S}_A$, while the remaining part of the overall state is still factorized.

(2) $[t_1, t_2]$: $g_A(t) = g_B(t) = 0$. The semi-classical evolution of the chain $\Xi$ results in an entangled state of A with the entire chain, while the quantum state of B is still pure.

(3) $[t_2, t_3]$: $g_B(t) = g$ and $g_A(t) = 0$. The evolution only concerns the $(B, \boldsymbol{S}_B)$ pair, while the spin chain is frozen as during the first stage. The eventual result is a non-separable state of the whole system.

In the final overall state, the reduced density matrix of the two qubits generally develops entanglement, namely the concurrence between A and B is found to be non-zero. The three stages described above are discussed in detail in the following three sections; section 5.5 is devoted to an overall discussion about the results and to some concluding remarks.

## 5.2 First dynamical stage

During the first stage of the evolution we will consider the qubit A interaction with the spin $\boldsymbol{S}_A$ of the chain.

The evolution of the system during the time interval $[t_0, t_1]$ is given by the following unitary operator (hereafter $\hbar = 1$):

$$\hat{\mathcal{U}}^{(1)}(t) = \hat{\mathcal{U}}_{A,\boldsymbol{S}_A}(t) \otimes \mathbb{1}_{\Xi\setminus\boldsymbol{S}_A} \otimes \hat{\mathcal{U}}_B(t) \tag{5.4}$$

where

$$\hat{\mathcal{U}}_{A,\boldsymbol{S}_A}(t) = \exp(-i\,\hat{\mathcal{H}}_{A,\boldsymbol{S}_A}\,t)\ , \tag{5.5}$$

[4] The validity of this approximation in a realistic set-up sets constraints on the ratios of the interaction constants $g_A$, $g_B$ and the spin-chain time-scale, which will be discussed later. Nevertheless, it is worth to point out that the extreme simplification is aimed at demonstrating the possibility of entanglement transfer by a semi-classical channel.

is the evolution operator of the subsystem (A,$\boldsymbol{S}_{\mathrm{A}}$), the Hamiltonian describing their interaction being

$$\hat{\mathcal{H}}_{\mathrm{A},\boldsymbol{S}_{\mathrm{A}}} = g\,\hat{\boldsymbol{S}}_{\mathrm{A}}\cdot\hat{\boldsymbol{\sigma}}_{\mathrm{A}} + h_{\mathrm{A}}\hat{\sigma}^{z}_{\mathrm{A}}\ . \tag{5.6}$$

The constant $g$ fixes the strength of the interaction between A and $\boldsymbol{S}_{\mathrm{A}}$, as well as the time-scale related to this stage of the evolution, while $h_{\mathrm{A}}$ is a uniform field term. Finally, the term

$$\hat{\mathcal{U}}_{\mathrm{B}}(t) = \exp(-i\,h_{\mathrm{B}}\hat{\sigma}^{z}_{\mathrm{B}}\ t) \tag{5.7}$$

is a local operation describing the action of a uniform field $h_{\mathrm{B}}$ acting only on the second qubit. Before evaluating the dynamics it is a compelling matter to discuss the initial state of the system, i.e. the system state at $t = t_0$.

### 5.2.1 The initial state

In order to better account for the generation of entanglement in the different parts of the system as a result of the related dynamics, the evolution will start from a completely factorized state of the whole system in the form

$$|\Psi(t_0)\rangle \;=\; |\mathrm{A}\rangle \otimes \left[\bigotimes_{n} \left|\Omega^{0}_{n}\right\rangle\right] \otimes |\mathrm{B}\rangle\ , \tag{5.8}$$

where $|\mathrm{A}\rangle$ and $|\mathrm{B}\rangle$ are two vectors, belonging respectively to the Hilbert spaces $\mathscr{H}_{\mathrm{A}}$ and $\mathscr{H}_{\mathrm{B}}$, which define the initial states of the two qubits; the state in brackets represents the chain state and deserves a more detailed description. In fact, it is given by a specific semi-classical state, i.e. a tensor product of SSCS according to equation (5.2), whose corresponding classical configuration is given by an Heisenberg soliton shape

$$\Omega^{0}_{n} \quad\longleftrightarrow\quad \boldsymbol{\Sigma}^{(\beta)}_{n}(t_0)\,, \tag{5.9}$$

where the function $\boldsymbol{\Sigma}^{(\beta)}$, given in equations (2.21), is evaluated at the discrete positions $n$, and the value of the time $t_0$ is chosen as $t_0 = n_{\mathrm{A}}/v$, with $v$ the soliton velocity, i.e. so as to have the soliton centred at position $n_{\mathrm{A}}$ at time $t = t_0$. The choice of a soliton-shaped semi-classical configuration is fundamental for the realization of the hybrid scheme here proposed, and stems from the idea that solitons are stable with respect to perturbations, and remain localized during their propagation. In our specific situation, the robustness may assure that the chain state evolves "maintaining" more or less the same localization features despite the interaction with the first qubit; the localization of the soliton may, instead, help keeping the possible quantum correlations between A and $\Xi$ localized on a finite number of spins, making an efficient transfer to B conceivable.

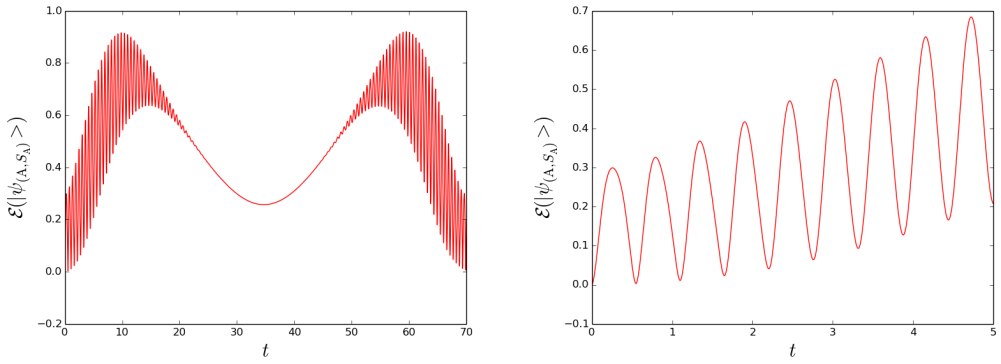


**Figure 5.3:** Von Neumann entropy of $A$ with $\boldsymbol{S}_A$ as a function of time, for $S = 5$, $g_A = 1$, $h_1 = 0.5$. The right panel is a zoom of the small-time part of the left panel.

### 5.2.2 Evolution $(A, \boldsymbol{S}_A)$

The evolution during the first dynamical stage is obtained by calculating the effect of the operator $\hat{\mathcal{U}}^{(1)}(t_1 - t_0)$ on the initial state (5.8). This gives a trivial evolution for $\Xi \setminus \boldsymbol{S}_A$ (i.e. all the chain except $\boldsymbol{S}_A$) and for the qubit B, while in general the subsystem $(A, \boldsymbol{S}_A)$ evolves to an entangled state, as shown in figure 5.3, where the Von Neumann entropy [5] of A is shown as a function of time for a given choice of parameter values and initial state of $\boldsymbol{S}_A$: it is clearly convenient to chose the time $t_1$ such as to maximize the numerically evaluated entropy between A and $\boldsymbol{S}_A$ at the end of the first dynamical stage. The formal expression of the state of the subsytem $(A, \boldsymbol{S}_A)$ can be obtained reminding the assumed separable structure of the overall state (5.8), so that:

$$\left|\psi_{A,\boldsymbol{S}_A}(t_0)\right\rangle = |A\rangle \otimes |\Omega_A\rangle \ , \tag{5.10}$$

where $\Omega_A \equiv \Omega^0_{n=n_A} = \boldsymbol{\Sigma}^{(\beta)}_{n_A}(t_0)$ is the initial "direction" of $\boldsymbol{S}_A$; letting the above state to evolve according to Eq. (5.5) the entangled state

$$\left|\psi_{A,\boldsymbol{S}_A}(t_1)\right\rangle = \sum_{\sigma m} c_{\sigma m}(t_1) \, |\sigma\rangle \otimes |m\rangle \tag{5.11}$$

is reached, where the following representation for $\mathscr{H}_{(A,\boldsymbol{S}_A)}$

$$\left\{ \, |\sigma\rangle \otimes |m\rangle \, \middle| \, \sigma \in \{+,-\}; m \in \{-S, -S+1, ..., S-1, S\}, \, \right\},$$

i.e., the Dicke state representations both for A and $\boldsymbol{S}_A$ is used. This representation, being finite-dimensional, is particularly convenient for the explicit evaluation of the coefficients $c_{\sigma m}(t_1)$, obtained by the numerical diagonalization of the Hamiltonian (5.6). Using the completeness relation (1.62), the state (5.11) can be rewritten in the coherent state repre-

[5] $\mathcal{E}(\rho_A)$ is evaluated from equation (1.15) starting from the state $\left|\psi_{A,\boldsymbol{S}_A}(t)\right\rangle$ as defined in (5.11) for $t = t_1$.

sentation for $\boldsymbol{S}_{\mathrm{A}}$:

$$\big|\psi_{\mathrm{A},\boldsymbol{S}_{\mathrm{A}}}(t_1)\big\rangle = (2S{+}1)\sum_{\sigma}\int\frac{d\Omega}{4\pi}\; f_{\sigma}^{\Omega}\;\; |\sigma\rangle\otimes|\Omega\rangle\;\;, \tag{5.12}$$

where

$$f_{\sigma}^{\Omega} = \sum_{m} c_{\sigma m}(t_1)\;\; \langle\Omega|m\rangle \tag{5.13}$$

and the overlap $\langle\Omega|m\rangle$ is defined in Eq. (1.59).

Turning the attention back to the overall system, we write its state at time $t_1$ in the density operator formalism:

$$\begin{aligned}\big|\Psi(t_1)\big\rangle\big\langle\Psi(t_1)\big| \;=& \big|\psi_{\mathrm{A},\boldsymbol{S}_{\mathrm{A}}}(t_1)\big\rangle\big\langle\psi_{\mathrm{A},\boldsymbol{S}_{\mathrm{A}}}(t_1)\big|\otimes \\ & \Big[\bigotimes_{n\neq n_{\mathrm{A}}}\big|\Omega_n^0\big\rangle\big\langle\Omega_n^0\big|\Big]\otimes\big|B(t_1)\big\rangle\big\langle B(t_1)\big|\,,\end{aligned} \tag{5.14}$$

where $\big|B(t_1)\big\rangle = \hat{\mathcal{U}}_{\mathrm{B}}(t_1)\,|B\rangle$, and the term in brackets is the state of $\Xi\setminus\boldsymbol{S}_{\mathrm{A}}$, that is left unchanged by the first stage dynamics. The projector onto the state $\big|\psi_{\mathrm{A},\boldsymbol{S}_{\mathrm{A}}}(t_1)\big\rangle$ can be rewritten using the coherent state representation (5.12),

$$\big|\psi_{\mathrm{A},\boldsymbol{S}_{\mathrm{A}}}(t_1)\big\rangle\big\langle\psi_{\mathrm{A},\boldsymbol{S}_{\mathrm{A}}}(t_1)\big| = (2S{+}1)^2\sum_{\sigma\sigma'}\int\frac{d\Omega}{4\pi}\frac{d\Omega'}{4\pi}\; C_{\sigma\sigma'}^{\Omega\Omega'}\;\; |\sigma\rangle\langle\sigma'|\otimes|\Omega\rangle\langle\Omega'|\;, \tag{5.15}$$

with

$$C_{\sigma\sigma'}^{\Omega\Omega'} \equiv f_{\sigma}^{\Omega} f_{\sigma'}^{\Omega'\star} = \sum_{mm'} c_{\sigma m}(t_1)\, c^{*}_{\sigma' m'}(t_1)\big\langle\Omega\big|m\big\rangle\big\langle m'\big|\Omega'\big\rangle\,. \tag{5.16}$$

Eq. (5.14) clearly reminds us that, due to the specific form of $\hat{\mathcal{U}}^{(1)}(t)$, the only correlations generated during this stage are those between A and $\boldsymbol{S}_{\mathrm{A}}$, as the states corresponding to the other part of the system keep being factorized (see Eq. (5.14)).

## 5.3 Second stage: the semi-classical chain evolution

At $t = t_1$ the interaction $g_{\mathrm{A}}(t)$ of the first qubit is quenched and, until $t = t_2$ when $g_{\mathrm{B}}(t)$ is switched on, the evolution operator of the system can be split as

$$\hat{\mathcal{U}}^{(2)}(t) = \hat{\mathcal{U}}_{\mathrm{A}}(t)\otimes\hat{\mathcal{U}}_{\Xi}(t)\otimes\hat{\mathcal{U}}_{\mathrm{B}}(t)\,, \tag{5.17}$$

where $\hat{\mathcal{U}}_{\mathrm{A}}(t)$ is a local operator on A, analogous to Eq. (5.7), due to the presence of the local uniform field $h_{\mathrm{A}}$, and $\hat{\mathcal{U}}_{\Xi}(t)$ is the evolution operator of the spin chain. The aim of this section is to introduce a suitable approximation for $\hat{\mathcal{U}}_{\Xi}(t)$ able to account for entanglement transfer between A and B.

In order to proceed, the chain $\Xi$ is modelled by the Heisenberg Hamiltonian

$$\hat{\mathcal{H}}_{\Xi} = -J \sum_{n} \hat{\boldsymbol{S}}_n \cdot \hat{\boldsymbol{S}}_{n+1} - \gamma H \sum_{n} \hat{S}^z_n \,, \tag{5.18}$$

with a nearest-neighbour isotropic ferromagnetic exchange $J$, a uniform magnetic field $H$ and a gyromagnetic ratio $\gamma$.

As the spins of the chain have a large-$S$ value, it is practically impossible to explicitly evaluate the evolution induced by the Hamiltonian (5.18). However, the large value of $S$ makes the chain "semiclassical" (see, e.g. the discussion at the end of section 2.2), suggesting the adoption of the following approximation. We start by observing that upon identifying the dynamical group of the Heisenberg Hamiltonian Eq.(5.18), the procedure outlined in section 1.4.3 would lead to the definition of generalized coherent states $|\Omega_{\Xi}\rangle$ of the full chain, whose dynamics is known to be ruled by classical equations of motion [73]: again, such procedure can not be implemented exactly, but the high value of the spin $S$ makes sensible to approximate the true generalized coherent state of the chain by the product of SSCS (the semi-classical configuration), i.e.

$$|\Omega_{\Xi}\rangle \simeq \bigotimes_{n} |\Omega_n\rangle \ , \tag{5.19}$$

and to consider the dynamics of the single $|\Omega_n\rangle$ well approximated by the solution of the equations of motion for the classical vectors $\Omega_n$ appearing in the classical counterpart of Eq.(5.18), i.e. EoM (2.15), as it would happen for the coherent states of the full chain. Of course, such classical dynamics of product coherent states cannot generate nor transfer quantum correlations if one starts from one single configuration of the chain, but in view of Eq. (5.12), the starting state is, on the side of $\Xi$, a *superposition* of configurations with different value of $\Omega$ for the spin $\boldsymbol{S}_{\mathrm{A}}$.

More in detail, an initial product state

$$\bigotimes_{n} |\Omega^0_n\rangle \ , \tag{5.20}$$

evolves following the dynamics of the associated classical configuration $\{\boldsymbol{S}_n(t) = S\,\Omega_n(t)\}$, defined according to (5.2), with the classical equations of motion. This operation gives the corresponding evolved classical configuration for any $t$ and, hence, the evolved quantum state as reported in the following scheme:

$$\begin{array}{ccc} \{\Omega^0_n\} & \xrightarrow{\text{classical}} & \{\Omega_n\big(t;\{\Omega^0_n\}\big)\} \\ \bigotimes_n |\Omega^0_n\rangle & \xrightarrow{\text{semi-classical}} & \bigotimes_n \big|\Omega_n\big(t,\{\Omega^0_n\}\big)\big\rangle \ . \end{array} \tag{5.21}$$

This prescription for the chain evolution essentially neglects the entanglement among spins possibly generated by the chain dynamics. Nevertheless, it provides a dynamics that reproduces the correct evolution of the spin expectation values in the classical limit ($S \gg 1$) and still keeps the quantum structure of the chain states. Moreover, it can be shown that the above rule gives the exact evolution in the limit $S \to \infty$, since the semi-classical states becomes the correct GCS of the chain in such limit (see section 5.5 and appendix B).

Within this approximation scheme, in order to write the evolution of a generic chain state it is therefore sufficient to expand it in the overcomplete basis provided by the (tensor product of) coherent states and then apply the evolution Eq. (5.21) to each vector in the decomposition.

Before using this procedure in our case, let us briefly explain what it means by a simple example that allows for some general comments about the approximation. Imagine that the chain $\Xi$ is in the state

$$\big|\Xi\big\rangle \;=\; \big|\psi_{\boldsymbol{S}_k}\big\rangle \otimes \left[\bigotimes_{n\neq k} \big|\Omega_n^0\big\rangle\right] \,, \tag{5.22}$$

for some fixed $k$, where $|\psi_{\boldsymbol{S}_k}\rangle$ is not in a coherent state

$$\big|\psi_{\boldsymbol{S}_k}\big\rangle = (2S+1)\int \frac{d\Omega}{4\pi}\; c(\Omega)\,\big|\Omega\big\rangle \,, \tag{5.23}$$

where the coefficients $c(\Omega)$ satisfy the following normalization condition:

$$(2S+1)^2 \int \frac{d\Omega}{4\pi}\int \frac{d\Omega'}{4\pi}\; c(\Omega)\, c^*(\Omega')\,\big\langle\Omega'\big|\Omega\big\rangle \;=\; 1\,. \tag{5.24}$$

According to (5.21), the chain configurations defined by the different components $\Omega$ evolve through the classical EoM:

$$\big\{\,\Omega_n^0 \mid \Omega_k = \Omega\big\} \quad \xrightarrow{\text{classical}} \quad \big\{\,\Omega_n(t,\Omega)\,\big\}\,, \tag{5.25}$$

where we have dropped the explicit dependence of $\Omega_n(t)$ on all $\{\Omega_n^0\}$ with $n \neq k$, retaining only the more meaningful one on $\Omega_k \equiv \Omega$. The approximation introduced here is that one can classically evolve the chain for *all* the configurations defined by the set $\big\{\,\Omega_n \mid \Omega_k = \Omega\big\}$ varying $\Omega$, i.e., perform several dynamical evolutions, finally keeping the same superposition for the evolved configurations. Of course, from the 'quantum' viewpoint, this dynamics associates to any initial state, belonging to the set of tensor products of single-spin coherent states, an evolved state inside the same set. We thus find the time-evolution of the state $\big|\Xi\big\rangle$ in the form

$$\big|\Xi(t)\big\rangle \;=\; \tilde{\mathcal{N}}\int d\Omega\; c(\Omega)\left(\bigotimes_n \big|\Omega_n(t,\Omega)\big\rangle\right) \,, \tag{5.26}$$

where the factor $\tilde{\mathcal{N}}$ restores the normalization of the evolved state, which is no more implicitly assured. In fact, evaluating the squared norm of the state (5.26) without the normalization constant, we find

$$(2S+1)^2 \int \frac{d\Omega}{4\pi} \int \frac{d\Omega'}{4\pi}\, c(\Omega)\, c^*(\Omega') \prod_n \big\langle \Omega_n\big(t,\Omega'\big)\big|\Omega_n\big(t,\Omega\big)\big\rangle\,, \tag{5.27}$$

which is in general different from one [6].

Turning back our attention to the specific case, we note that our situation is similar to the one described above with $k = n_{\rm A}$ but the state $\big|\psi_{{\rm A},\boldsymbol{S}_{\rm A}}(t_1)\big\rangle$ also involve A degrees of freedom. Since our approximation scheme does not affect the qubit Hilbert space we can straightforwardly apply the described procedure to our initial state

$$\big|\psi_{{\rm A},\Xi}(t_1)\big\rangle = \big|\psi_{{\rm A},\boldsymbol{S}_{\rm A}}(t_1)\big\rangle \bigotimes_{n\neq n_{\rm A}} |\Omega_n^0\rangle\ , \tag{5.28}$$

where $\big|\psi_{{\rm A},\Xi}(t_1)\big\rangle$ is given by Eq.(5.12), so that we finally get:

$$\big|\psi_{{\rm A},\Xi}(t_2)\big\rangle = \mathcal{A}\sum_\sigma \int d\Omega\ f_\sigma^\Omega \big|\sigma(t_2)\big\rangle \bigotimes_n \big|\Omega_n(t_2,\Omega)\big\rangle\,, \tag{5.29}$$

[6] This observation suggests that the semi-classical evolution is not unitary. In fact, we find that angles between different vectors are, in general, not preserved by the evolution. Start, for example, from two chain semi-classical states that differ only for the configuration of the $k$-th spin

$$\big|\Xi_1\big\rangle = \big|\Omega_k=\Omega\big\rangle \otimes \left[\bigotimes_{n\neq k} \big|\Omega_n\big\rangle\right] \quad \text{and} \quad \big|\Xi_2\big\rangle = \big|\Omega_k=\Omega'\big\rangle \otimes \left[\bigotimes_{n\neq k} \big|\Omega_n\big\rangle\right]\,,$$

where $\Omega \neq \Omega'$. The overlap between these two states is

$$\big\langle\Xi_2\big|\Xi_1\big\rangle \,=\, \big\langle\Omega'\big|\Omega\big\rangle\,,$$

since the configurations of all spins are equal, except the $k$-th; $\big\langle\Omega'\big|\Omega\big\rangle$ is given in (1.60). Applying now the evolution rule (5.21) to $\big|\Xi_1\big\rangle$ and $\big|\Xi_2\big\rangle$, one finds the following overlap between the chain states at the generic time $t$

$$\big\langle\Xi_2(t)\big|\Xi_1(t)\big\rangle \,=\, \prod_n \big\langle\Omega_n(t,\Omega')(t)\big|\Omega_n(t,\Omega)(t)\big\rangle\,.$$

Unitarity would require the evolution to be an isometry of the chain Hilbert space i.e. the overlap between any couple of states belonging to $\mathscr{H}_\Xi$ must be preserved during the evolution. This means, in our example, that the following equation,

$$\big\langle\Xi_2\big|\Xi_1\big\rangle = \big\langle\Xi_2(t)\big|\Xi_1(t)\big\rangle \quad\Rightarrow\quad \big\langle\Omega'\big|\Omega\big\rangle = \prod_n \big\langle\Omega_n(t,\Omega')(t)\big|\Omega_n(t,\Omega)(t)\big\rangle\,,$$

should hold for any couple $\Omega,\Omega'$, which is not true in general. This can be expected, since semi-classical evolution is not the exact chain evolution for finite $S$ values, while it becomes exact in the limit $S\to\infty$, as noted before.Recovery of unitarity in the spin classical limit $S\to\infty$ is also evident from the last equation, since the overlap (1.60) tends to $\delta(\Omega-\Omega')$ and different trajectories of a Hamiltonian system never cross each other. In fact, the integral of Hamiltonian EoM represents a bijection of the classical phase space in itself for any fixed time $t$ [119], and this also implies that semi-classical evolution (5.21) is, in principle, invertible. Thus, we account for the non-unitarity of the semi-classical evolution normalizing the system state after the second dynamical stage, i.e. at $t=t_2$. Further comments about the semi-classical approximation can be found in section 5.5.

where $|\sigma(t_2)\rangle = \hat{\mathcal{U}}_{\rm A}(t_2 - t_1)\,|\sigma\rangle = \exp[-ih_{\rm A}\sigma(t_2 - t_1)]\,|\sigma\rangle$, $\mathcal{A}$ is the overall normalization. Using the last expression one can finally write the projector for the whole system after the second stage of the evolution,

$$\big|\Psi(t_2)\big\rangle\!\big\langle\Psi(t_2)\big| = \big|\psi_{\rm A,\Xi}(t_2)\big\rangle\!\big\langle\psi_{\rm A,\Xi}(t_2)\big| \otimes \big|B(t_2)\big\rangle\!\big\langle B(t_2)\big| \tag{5.30}$$

where $|B(t_2)\rangle = \hat{\mathcal{U}}_{\rm B}(t_2 - t_0)\,|B\rangle$ and, using Eq. (5.15),

$$\begin{aligned}\big|\psi_{\rm A,\Xi}(t_2)\big\rangle\!\big\langle\psi_{\rm A,\Xi}(t_2)\big| =& \mathcal{N}\sum_{\sigma\sigma'}\int d\Omega\, d\Omega'\; C_{\sigma\sigma'}^{\Omega\Omega'} \\ &\times\; |\sigma(t_2)\rangle\langle\sigma'(t_2)| \bigotimes_n \big|\Omega_n(t_2,\Omega)\big\rangle\!\big\langle\Omega_n(t_2,\Omega')\big|\;.\end{aligned} \tag{5.31}$$

The normalization constant $\mathcal{N}$, which can be obtained from expression (5.29), reads [7]:

$$\frac{1}{\mathcal{N}} = \sum_{\sigma}\int d\Omega\, d\Omega'\, C_{\sigma\sigma}^{\Omega\Omega'} \prod_n \big\langle\Omega_n(t_2,\Omega')\big|\Omega_n(t_2,\Omega)\big\rangle\;. \tag{5.32}$$

We underline the fact that the explicit dependence on the initial conditions $\{\Omega\}$ of the spin-chain state (5.29), which makes $|\psi_{q_1+\rm chain}(t_2)\rangle$ explicitly not separable, testifies to the fact that the entanglement, originally generated only between A and $\boldsymbol{S}_{\rm A}$, is now spread over all the chain spins as a consequence of the chain evolution.

### 5.3.1 Some comments about the state at $t = t_2$

In order to check the generation of entanglement between the qubits A and B, one has to trace away the chain degrees of freedom, obtaining the two-qubit density matrix representing the joint state of (A, B), for which one can then evaluate, e.g., the concurrence. Since the chain minus the spin $\boldsymbol{S}_{\rm B}$, which experiences the interaction with B, does not evolve during this stage (the third stage is analogous to the first one with the exchanged roles between A and B), tracing away those degrees of freedom can be done equivalently on the state at $t_2$ as well as on that at $t_3$. Of course, it is more convenient to perform the partial tracing before the evolution, in such a way to work with a smaller Hilbert space during the third stage. Consider, then, the partial trace on $\Xi \setminus \boldsymbol{S}_{\rm B}$, which gives the reduced density matrix for the system $({\rm A}, \boldsymbol{S}_{\rm B}, {\rm B})$,

$$\hat{\rho}_{{\rm A},\boldsymbol{S}_{\rm B},{\rm B}}(t_2) = {\rm Tr}_{\boldsymbol{S}_n \neq \boldsymbol{S}_{\rm B}}\,\big|\Psi(t_2)\big\rangle\!\big\langle\Psi(t_2)\big|\;. \tag{5.33}$$

[7] The same expression for $\mathcal{N}$ is obtained performing the trace of the projector (5.30) (see consideration about the trace over the $\boldsymbol{S}_n$ degrees of freedom in the next section)

$${\rm Tr}(|\Psi_{sys}(t_2)\rangle\langle\Psi_{sys}(t_2)|)\,.$$

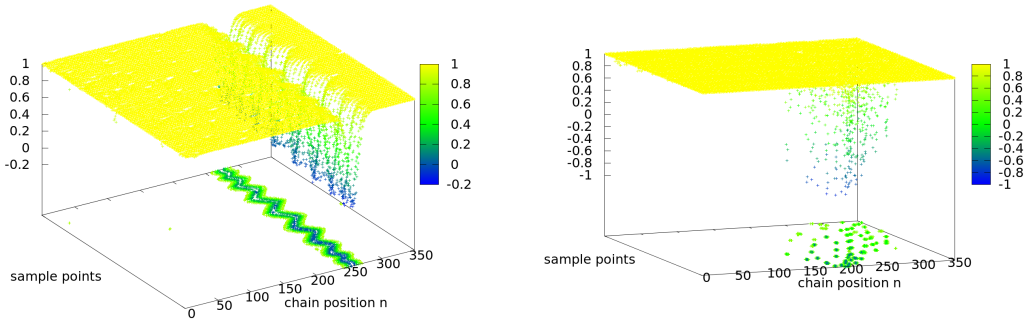


**Figure 5.4:** Comparison of different configurations obtained in a fixed integration time $(t_2 - t_1)$. The $z$-component $\cos[\theta_n(t_2 - t_1, \Omega)]$ is reported (third-axis and color) as a function of chain position $n$ by sampling $\Omega$ on the whole sphere (second axis, ordered by subsequent 'parallels'). The contour plot in color scale is reported in the base. The two panels show evolved configurations obtained starting with two solitons differing in the typical width $\lambda$ (lattice spacing units): left, $\lambda = 10$; right $\lambda = 2.5$.

One realizes that all partial traces over different spins $\boldsymbol{S}_n$ are trivially factorized [8], the contribution for each $n$ being of the form

$$\mathrm{Tr}_{\boldsymbol{S}_n} \left|\Omega_n(t_2,\Omega)\right\rangle \left\langle\Omega_n(t_2,\Omega')\right| = \left\langle\Omega_n(t_2,\Omega')\middle|\Omega_n(t_2,\Omega)\right\rangle \,, \tag{5.35}$$

namely, the overlap between the coherent states at the same position $n$ as evolved according to different initial conditions, $\Omega'$ and $\Omega$; the expression for this overlap is given in Eq. (1.60). After this operation on the state (5.30) one obtains

$$\hat{\rho}_{\mathrm{A},\boldsymbol{S}_\mathrm{B},\mathrm{B}}(t_2) \;=\; \hat{\rho}_{\mathrm{A},\boldsymbol{S}_\mathrm{B}}(t_2) \otimes \left|B(t_2)\right\rangle\!\left\langle B(t_2)\right| , \tag{5.36}$$

with

$$\begin{aligned} \hat{\rho}_{\mathrm{A},\boldsymbol{S}_\mathrm{B}}(t_2) \;=& \mathcal{N} \sum_{\sigma\sigma'} \int d\Omega d\Omega'\, C^{\Omega\Omega'}_{\sigma\sigma'} \left|\sigma(t_2)\right\rangle\!\left\langle\sigma'(t_2)\right| \\ & \times \left[\prod_{n\neq n_\mathrm{B}} \left\langle\Omega_n(t_2,\Omega')\middle|\Omega_n(t_2,\Omega)\right\rangle\right] \otimes \left|\Omega_\mathrm{B}(t_2,\Omega)\right\rangle \left\langle\Omega_\mathrm{B}(t_2,\Omega')\right| \,. \end{aligned} \tag{5.37}$$

Imagine a set of evolved configurations $\{\Omega_n(t,\Omega)\}$, depending on the initial value $\Omega$, that look very similar among themselves whatever the value of $\Omega$ in a large part of the chain (e.g., most spins aligned along the $z$-axis). In such a case a large number of the overlaps

[8] The trace over a generic spin $\boldsymbol{S}$ can be written, in the coherent state representation, as

$$\mathrm{Tr}_{\boldsymbol{S}}(\cdots) = (2S{+}1) \int \frac{d\Omega}{4\pi} \left\langle\Omega\right| \cdots \left|\Omega\right\rangle . \tag{5.34}$$

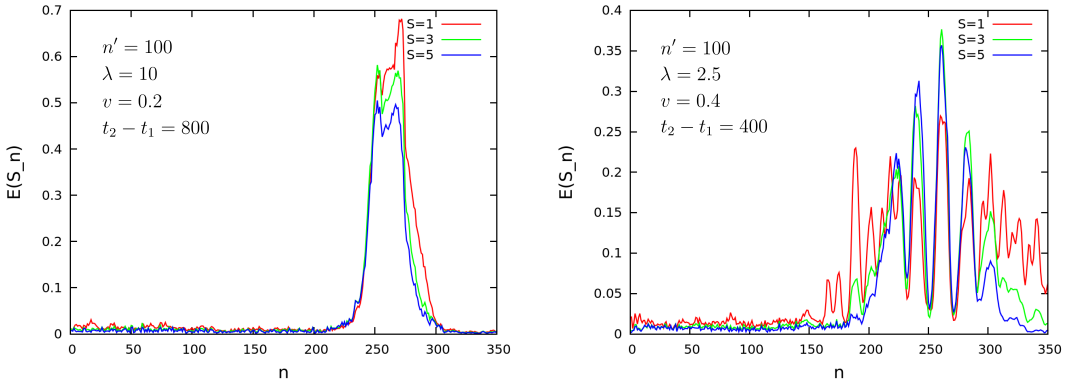


**Figure 5.5:** Comparison of $E_{\boldsymbol{S}_n}$ as a function of $n$ for different values of $S$, spin modulus of the chain spins. Left panel: initial configuration soliton-shape with $\lambda_\beta = 10$ ($T = 800$, $v = 0.2$, initially centered in $n_{\mathrm{A}} = n' = 100$); Right panel: initial configuration soliton-shape with $\lambda_\beta = 2.5$ ($T = 400$, $v = 0.4$, initially centered in $n_{\mathrm{A}} = n' = 100$).

appearing in the partial trace are equal to one and the corresponding spins are uncorrelated from the rest of the system: being independent of $\Omega$ they indeed disappear from the state expression. Thus, the entanglement originally generated by the interaction of A with $\boldsymbol{S}_{\mathrm{A}}$ is not spread along all the chain, but remains confined to the portion which carries dependence on the initial condition $\Omega$. Such situation happens, for instance, starting with the chain in a Heisenberg soliton shape localized around $n_{\mathrm{A}}$ (hence our choice for the initial state). If the soliton width is larger than the chain spacing, changing the configuration $\Omega$ of the spin at one single site $n_{\mathrm{A}}$ will not significantly affect its propagation; the evolved configurations will be similar, as shown in figure 5.4. Moreover, the soliton moves forward with invariant shape and hauls the deformation of $\Omega_{\mathrm{A}}$, imposed while it travelled through site $n_{\mathrm{A}}$. The time $t_2$ is thus chosen when the soliton crosses $n_{\mathrm{B}}$ [9] and the superposition Eq. (5.37) of the evolved configurations, obtained from different deformations $\Omega$, is expected to concentrate around $n_{\mathrm{B}}$ the entanglement collected at time $t_1$ in $n_{\mathrm{A}}$. During the evolution the soliton thus behaves as a carrier that keeps the entanglement localized while travelling along the chain. Numerical results do indeed confirm this behavior: figure 5.5 shows snapshots of $E_{\boldsymbol{S}_n}$, the *normalized* entropy of entanglement [10] $E_{\boldsymbol{S}_n}$, which quantifies the entanglement that the spin $\boldsymbol{S}_n$ has with the rest of the system (i.e. $\Xi \setminus \boldsymbol{S}_n$, A), and is defined as

$$E_{\boldsymbol{S}_n} = -\operatorname{Tr}_{\boldsymbol{S}_n} \hat{\rho}_{\boldsymbol{S}_n} \log_{\mathrm{d}} \hat{\rho}_{\boldsymbol{S}_n} \tag{5.38}$$

[9] Assuming that the different evolutions of the deformed soliton-shape still keeps, more or less, also the same velocity $v_{\mathrm{sol}}$ of the original soliton, their superposition will look like an "enlarged" solitonic shape who center moves again, more or less, like that of the original soliton.

[10] Differently from definition (1.15), we here report its normalized version, i.e. we evaluate the logarithm in base d, where d represent the dimension of $\mathscr{H}_S$. With this choice the entropy of entanglement assume values $\leq 1$, regardless the dimension of the Hilbert space.

where d = 2$S$+1 and

$$\hat{\rho}_{\boldsymbol{S}_n} = \mathrm{Tr}_{\mathrm{A},\Xi\setminus\boldsymbol{S}_n} \left|\psi_{\mathrm{A},\Xi}(t_2)\right\rangle\!\left\langle\psi_{\mathrm{A},\Xi}(t_2)\right| . \tag{5.39}$$

In the left panel of figure 5.5 a bump is clearly visible whose center is at about $v_{\mathrm{sol}}(t_2 - t_1)$, this meaning that only the spins around the soliton are significantly entangled with the rest of the system, while the others are almost uncorrelated. The different curves report the same quantity for different values of $S$: the shape is almost unchanged, but the values monotonically decrease with increasing $S$, according to the fact that in the limit $S \to \infty$ the entanglement disappears [11] as the spins become completely classical.

## 5.4 Third dynamical stage: evolution of (B, $S_B$)

During the third time interval $[t_2, t_3]$ the second qubit B interacts with the spin $\boldsymbol{S}_{\mathrm{B}}$ with the coupling strength $g_{\mathrm{B}}(t) = g$, while the first qubit is affected only by a uniform field and the spin chain does not evolve, except for $\boldsymbol{S}_{\mathrm{B}}$. Apart from the different initial state, this stage is analogous to the first one, with exchanged roles between A and B, and the evolution operator is

$$\hat{\mathcal{U}}^{(3)}(t) = \hat{\mathcal{U}}_{\mathrm{A}}(t) \otimes \mathbb{1}_{\Xi\setminus\boldsymbol{S}_{\mathrm{B}}} \otimes \hat{\mathcal{U}}_{\mathrm{B},\boldsymbol{S}_{\mathrm{B}}}(t) , \tag{5.40}$$

where $\hat{\mathcal{U}}_{\mathrm{A}}(t)$ is the same of the previous stage and $\mathbb{1}_{\Xi\setminus\boldsymbol{S}_{\mathrm{B}}}$ is the identity on the Hilbert space $\mathscr{H}_{\Xi\setminus\boldsymbol{S}_{\mathrm{B}}}$.

Consider now that, having traced out all the spins of the chain but $\boldsymbol{S}_{\mathrm{B}}$, as explained in the previous section, for $t > t_2$ one has to deal with the Hilbert space of the two qubits and the spin $\boldsymbol{S}_{\mathrm{B}}$, which has dimension equal to only 4(2$S$+1). The evolution operator acting on $\hat{\rho}_{\mathrm{A},\boldsymbol{S}_{\mathrm{B}},\mathrm{B}}(t_2)$ is given by

$$\hat{\mathcal{U}}^{(3)} = \hat{\mathcal{U}}_{\mathrm{A}}(t) \otimes \hat{\mathcal{U}}_{\boldsymbol{S}_{\mathrm{B}},\mathrm{B}}(t) = e^{-i\hat{\mathcal{H}}_{\mathrm{A},\boldsymbol{S}_{\mathrm{B}},\mathrm{B}}\, t} , \tag{5.41}$$

with the Hamiltonian

$$\hat{\mathcal{H}}_{\mathrm{A},\boldsymbol{S}_{\mathrm{B}},\mathrm{B}} = h_{\mathrm{A}}\hat{\sigma}^z_{\mathrm{A}} + g\,\hat{\boldsymbol{S}}_{\mathrm{B}}\cdot\hat{\boldsymbol{\sigma}}_{\mathrm{B}} + h_{\mathrm{B}}\hat{\sigma}^z_{\mathrm{B}} , \tag{5.42}$$

which can be diagonalized numerically using the basis $\{|m\rangle\}$ of the eigenvectors [12] of $\boldsymbol{S}^z_{\mathrm{B}}$;

[11] Entanglement, should increase its value as the dimension of the Hilbert space is increased. Evidently, the same do not happens for the "density of entanglement" with respect to the number of degrees of freedom: remember, in fact, that we are here normalizing the entanglement entropy with respect to $\dim \mathscr{H}_S$.

[12] For numerical calculations, it is obviously convenient to use a finite representation of the Hilbert space.

the generic element of the density matrix for $(\mathrm{A}, \boldsymbol{S}_\mathrm{B})$ can be written as

$$\begin{aligned}\left[\hat{\rho}_{\mathrm{A},\boldsymbol{S}_\mathrm{B}}(t_2)\right]^{\sigma\sigma'}_{mm'} =& \mathcal{N} e^{-ih(t_{12})(\sigma-\sigma')} \int d\Omega\, d\Omega'\, C^{\Omega\Omega'}_{\sigma\sigma'} \\ &\times \left[\prod_{n\neq n_\mathrm{B}} \left\langle \Omega_n(t_{12},\Omega') \middle| \Omega_n(t_{12},\Omega)\right\rangle\right] \mathcal{D}^{\Omega\Omega'}_{mm'}(t_2)\end{aligned} \tag{5.43}$$

with

$$\mathcal{D}^{\Omega\Omega'}_{mm'}(t_2) = \left\langle m \middle| \Omega_\mathrm{B}(t_{12},\Omega)\right\rangle \left\langle \Omega_\mathrm{B}(t_{12},\Omega') \middle| m'\right\rangle . \tag{5.44}$$

Since $\hat{\rho}_{\mathrm{A},\boldsymbol{S}_\mathrm{B},\mathrm{B}}(t_2) = \hat{\rho}_{\mathrm{A},\boldsymbol{S}_\mathrm{B}}(t_2) \otimes \left|B(t_2)\right\rangle\left\langle B(t_2)\right|$, making use of the relations (1.59) and (1.60) one can numerically compute the state $\hat{\rho}_{\mathrm{A},\boldsymbol{S}_\mathrm{B},\mathrm{B}}(t_2)$ and the evolution (5.41) in the time interval $t_3 - t_2$. The evolved state $\hat{\rho}_{\mathrm{A},\boldsymbol{S}_\mathrm{B},\mathrm{B}}(t_3)$ is finally obtained. It is, in general a non separable state of the subsystems B and $(\mathrm{A}, \boldsymbol{S}_\mathrm{B})$, meaning that B is entangled with $(\mathrm{A}, \boldsymbol{S}_\mathrm{B})$. Nevertheless, this does not necessarily mean that the A and B are directly entangled: their entanglement might also be "diluted" along the spin chain. In order to settle this, one has to trace out $\boldsymbol{S}_\mathrm{B}$, yielding the two-qubit density matrix

$$\hat{\rho}_{\mathrm{A},\mathrm{B}}(t_3) = \mathrm{Tr}_{\boldsymbol{S}_\mathrm{B}}\, \hat{\rho}_{\mathrm{A},\boldsymbol{S}_\mathrm{B},\mathrm{B}}(t_3) \ , \tag{5.45}$$

and use it to calculate the *concurrence*, $\mathcal{C}(\hat{\rho}_{\mathrm{A},\mathrm{B}}(t_3))$, whose definition is given in section 1.2.

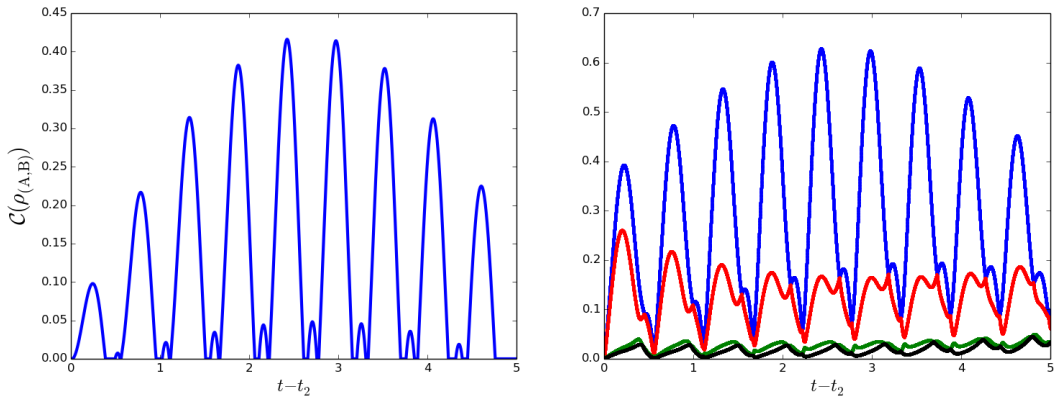


**Figure 5.6:** Concurrence of the state for the (A,B) system as a function of $t-t_2$. The first panel reports the difference $\lambda_1-\lambda_2-\lambda_3-\lambda_4$ (the concurrence is the positive part of the blue curve). The second panel reports the four eigenvalues $\{\lambda_1, \lambda_2, \lambda_3, \lambda_4\}$ separately: cusps in the first panel correspond to eigenvalue crossings. Values of parameters: $g = 1$, $h_\mathrm{A} = h_\mathrm{B} = 0.5$, $S = 5$; initial semi-classical state: soliton shape with $\lambda = 10$.

An example of the concurrence of $\hat{\rho}_{\mathrm{A},\mathrm{B}}$, obtained starting from an initial state defined by $|A\rangle = |B\rangle = |+\rangle$ and the chain initial configuration taken as the Heisenberg soliton of width $\lambda = 10$ (lattice spacings) initially centred at $\boldsymbol{S}_\mathrm{A}$ is shown in figure 5.6 as a function of $t-t_2$: it appears that the two qubits are indeed entangled. We want to note that the periodic time dependence is due to the fact that A and B never interact directly, and that

the interaction of ($\boldsymbol{S}_B$,B) is ruled by the simple Hamiltonian (5.42), giving raise to a simple periodic dynamics as it happens for ($\boldsymbol{S}_A$,A) during the first dynamical stage. As a result the consequent oscillations evidently transfer the entanglement with A back and forth between B and $\boldsymbol{S}_B$.

We observe that changing parameters (the spin value $S$, the coupling intensities $g_A$ or $g_B$, which we here set both equal to $g$ but that can be in principle different, the local fields $h_A$ and $h_B$ etc.) as well as the the initial semi-classical state for $\Xi$, the results are qualitatively the same; numerical values of the different quantities, such as the peak value or the frequency in the concurrence between A and B, do indeed change, but an oscillating behaviour like that shown in figure 5.6 is always found.

Moreover, values of the concurrence significantly different from zero are obtained only if $t_2$ is chosen $\sim n_B/v_{sol}$, i.e. the spin $\boldsymbol{S}_B$ interacting with B is among those that are correlated with the rest of the chain and A, and if the initial semi-classical configuration is such that superposition (5.31) allows for the entanglement to be localized on a small number of spins rather than a large portion of the chain, e.g., referring to figure 5.5, better results (i.e. higher values of the concurrence) are obtained in the situation depicted in the left panel rather than in that of right panel, as shown in figures 5.6 and 5.7.

Therefore, choosing $t_3$ such that $\mathcal{C}\big[\hat{\rho}_{A,B}(t_3)\big] \neq 0$, the evolution of the proposed model system in the interval $[t_0, t_3]$, takes a separable state into an entangled state of the two qubits. The entanglement, dynamically generated between A and a single spin of the chain, $\boldsymbol{S}_A$, is successfully transferred through to B by means of the semi-classical evolution of the spin chain. In other words, the dynamics of a semi-classical channel is able to transfer quantum correlations, generating entanglement between distant and non interacting qubits. This is possible thanks to the coherent-state mapping between classical configurations and quantum product states for $\Xi$, which allows us to approximately evaluate the quantum evolution of the channel. The most interesting fact, however, is that, in order to obtain the final quantum state, many of these semi-classical evolutions must be superimposed: this simultaneous existence of "parallel classical histories" is thus the key point to explain why our hybrid channel can transfer quantum correlations.

As a last remark, we notice that for $t > t_3$, i.e. after the last qubit-spin interaction has been quenched, the evolution of the three subsystems is strictly local implying that the entanglement of the state $\hat{\rho}_{A,B}(t)$ is no more varied. Thus, the scheme proposed, realizing an entangling channel acting on a two-qubit state, can be exploited for the realization of specific two-qubit entangling gates, by the proper choice of the initial state of the spin chain and of the other parameters.

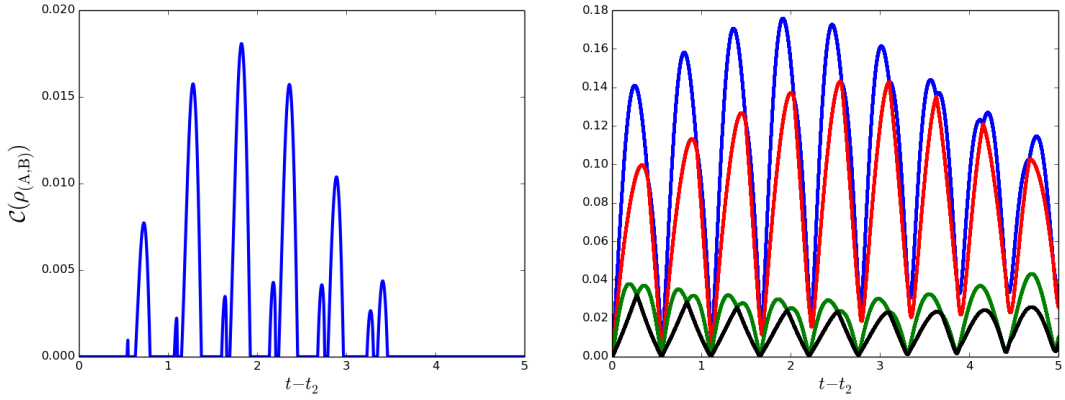


**Figure 5.7:** Concurrence of the state for the (A,B) system as a function of $t-t_2$. The first panel reports the difference $\lambda_1-\lambda_2-\lambda_3-\lambda_4$ (the concurrence is the positive part of the blue curve). The second panel reports the four eigenvalues $\{\lambda_1, \lambda_2, \lambda_3, \lambda_4\}$ separately: cusps in the first panel correspond to eigenvalue crossings. Values of parameters: $g = 1$, $h_A = h_B = 0.5$, $S = 5$; initial semi-classical state: soliton shape with $\lambda = 2.5$.

## 5.5 Conclusions

In this chapter we showed that a semi-classical system, embodied by a large-$S$ spin chain, can generate entanglement between distant qubits. In particular, it has been shown that, starting from a factorized state of the whole system with the state of $\Xi$ represented by the semi-classical state corresponding to a $\beta$-soliton of the Heisenberg chain, the quantum correlations dynamically established during the first stage of the evolution between A and $\boldsymbol{S}_A$ can be transferred efficiently, i.e. keeping them "localized" on a small number of spins (related with the soliton width), in such a way that the second qubit B, after its interaction with $\boldsymbol{S}_B$, is indeed entangled with A. Moreover, it has been shown that these features do not qualitatively depend neither on the specific values of the parameters nor on the specific chain initial state, which affect only the efficiency of the channel.

Reaching these results requires some simplifications, that make the explicit calculations feasible. In particular, the proposed theoretical scheme relies on three simplifying assumptions: the first is the qubit-spin interactions time-dependence, i.e. interaction must be somehow turned on/off; the second is related to the duration of the qubit-spin interactions; while the third is the semi-classical approximation for the chain evolution. Let us comment each of them.

The first assumption implies somehow the ability of switching on and quenching the qubit-chain interactions: although this is a typical approximation in theoretical schemes, it is not always clear how to realize such a situation in the diverse realizations, especially for the solid-state ones. One possibility, limiting the above requests only to the capacity of quenching the qubit-spin interactions, can be that of starting the dynamics (well before $t = t_0$) with both the qubit-chain interactions already present; in fact, if the qubits and the

spins $\boldsymbol{S}_{\mathrm{A}}$, $\boldsymbol{S}_{\mathrm{B}}$ are all in the maximum $z$-projection state, the presence of the interactions does not affect their states (except for an overall phase factor) unless the transit of the soliton modifies the state of $\boldsymbol{S}_{\mathrm{A}}$. The first stage would start, for A and $\boldsymbol{S}_{\mathrm{A}}$, when the soliton reach $\boldsymbol{S}_{\mathrm{A}}$ and start modifying its state, in the meanwhile B and $\boldsymbol{S}_{\mathrm{B}}$ are still not affected by presence of the interaction since the soliton deformation is far from $\boldsymbol{S}_{\mathrm{B}}$. Quenching the first qubit-spin interaction when A and $\boldsymbol{S}_{\mathrm{A}}$ are entangled, the dynamics of the chain continues as described in section 5.3 transferring the quantum correlations to B. When the deformed soliton reaches $\boldsymbol{S}_{\mathrm{B}}$, its dynamics with B starts as for A and $\boldsymbol{S}_{\mathrm{A}}$ and the third stage is realized. This would result in a smoother time-dependence than that shown in figure 5.2, at least for the interaction starting, which should not result in a dramatic change of the qualitative behaviour of our scheme if, however, the ability of quenching the interactions is still maintained.

As for the second one, in order to obtain a significant effect on the spin $\boldsymbol{S}_{\mathrm{A}}(\boldsymbol{S}_{\mathrm{B}})$, during the first(third) stage, while the rest of the chain is not evolving, it is necessary that the typical time-scale of the qubit-spin interaction, $(gS)^{-1}$, is much smaller than that of $\Xi$. When a $\beta$-soliton represents the chain dynamical state, the corresponding time-scale will be provided by equation (2.26) and hence, for the assumed condition to be met, the relation

$$\frac{(gS)^{-1}}{\tau_\beta} = \frac{J}{g}\frac{\gamma H}{JS}\sin 2\beta \ll 1$$

must be satisfied. The above relation can be satisfied both if $g \gg J$, i.e. the chain coupling is much weaker than the qubit-spin coupling, or if $\frac{\gamma H}{JS} \ll 1$, i.e. the uniform field intensity must be weak compared with the chain coupling. This second requirement is usually met, if the spin chain is thought to be some solid state system; in fact, being $\gamma \propto \mu_{\mathrm{B}}$ with $\mu_{\mathrm{B}}$ the Bohr magneton, given the typical exchange energies and the small value of $\mu_{\mathrm{B}}$, very high values of the field intensity $H$ are needed in order to break the above inequality.

Let us now comment on the semi-classical approximation for the chain evolution. It was already noted that taking the expectation values of the chain spin operators (in the Heisenberg picture) on the semi-classical states, the correct classical evolution of spin vectors was recovered for the isotropic Heisenberg case [120, 121]; moreover, it has been also shown in the literature [36, 37, 39, 120, 121] that choosing the semi-classical states for the spin chain (also in the anisotropic cases), a good description of magnetic one-dimensional systems can be given and accordance with experimental results have also been found [30–34].

Finally we provide a proof that semi-classical configurations become the true spin-chain generalized coherent states in the limit of $S \to \infty$: referring to Hamiltonian (5.18), we note that, in order to keep the chain energy finite in the $S \to \infty$ limit, the coupling $J$ must scale as $1/S^2$. Successive commutation operations between operators appearing the Hamiltonian (5.18), originate the infinite operator set containing the products, to any order,

of spin operators $S_n^\alpha$ ($\alpha = \pm, z$), whose scaling order with respect to $J$ and $S$ is $J^n S^m$. Since this set contains an infinite number of operators it is impossible to explicitly build a set of GCS as described in section 1.4.3, without approximations. However, it is found that, as a consequence of being $J \sim 1/S^2$, it is possible to neglect all commutators of order $J^n S^m$ with $2n > m$. It is thus possible to close an algebra containing a finite number of chain operators, and to repeat the GCS construction, to finally show that the proper GCS in this limit are given by the tensor product of SSCS, i.e. the semi-classical states (the explicit construction is shown in the appendix B). Thus, according to the GCS properties, the exact chain dynamics is provided by (5.21) in the $S \to \infty$ limit.

Using the semi-classical approximation for finite $S$ values is still an approximation, but we now have put the basis to estimate the resulting error as some function of $1/S$.

# Concluding remarks and future perspectives

Leitmotiv of this work is the proposal of an *hybrid* scheme where a *classical* or *large-S* spin chain play the role of the robust (semi-)classical partner, while magnetic qubits represent the delicate systems which are the agents of the quantum operation to be accomplished. According to this general idea we introduced three schemes, each corresponding to a different action to be achieved.

Aiming at exploiting the robustness feature of some particular dynamical configuration of non-linear classical systems, i.e. solitons, we first faced the problem of how to generate solitons in a discrete, classical Heisenberg chain. In order to achieve this goal we have proposed a scheme where a suitable time-dependent magnetic field, acting on one of the chain ends, inject the desired dynamical configuration. The numerical analysis of the model, which has been accomplished employing a specific symplectic algorithm, shows that soliton can be indeed generated, with features resembling those of the known analytical soliton solutions of the continuous model. We have also shown that the injection scheme as well as the generated dynamical configurations are robust with respect to the presence of noise in the system, and the generated solitons propagate along the chain despite the noise intensity.

Moreover, when considering a finite penetration length of the injecting field inside the spin chain, results show also some new dynamical features, such as temporary localization of the magnetization in the first segment of the spin chain, that are worth to be investigated further.

Successively, we focused on how to exploit the generated solitons to reach and control the state of a single qubit without the necessity of acting directly on it: a soliton, generated at the spin-chain extremity, travels along the chain producing a deformation in the, otherwise uniform, chain configuration. A distant (from the chain extremity) qubit is interacting with a finite portion of the spin chain, and feels the deformation produced by the soliton transit as a time-dependent, effective magnetic field.

The numerical study of the resulting qubit dynamics shows that, as the soliton runs on the chain section interacting with the qubit, the qubit state is modified; after the soliton transit, the qubit is left in a final state characterized by a constant value of the Bloch's vector third component $n^z(\tau_f)$. The classification of the final qubit states according to their $n^z(\tau_f)$ value, with respect to different types of interaction and to the relevant parameters, shows that basically any final state can be reached within the proposed scheme, without the necessity of a fine tuning of all parameters.

Besides giving the possibility of successfully addressing and controlling the states of distant qubits, the above result make the described scheme suitable for realizing qubit register preparations or to realize selective single-qubit gates in a proposal where each qubit of the register in coupled with a magnetic wire embodied by the spin chain.

We finally addressed the problem of generating quantum correlations in distant qubits through their interaction with a large-$S$ spin chain. The model is made up by a large-$S$ spin chain and two distant, and non interacting qubits, each coupled with a different spin of the chain. The scheme works as follows: the spin chain is in a semi-classical (tensor product of SSCS) state corresponding to the classical spin configuration representing a soliton, centred around the position of the spin interacting with the first qubit; as the first qubit interacts with the chain, quantum correlations establish between the qubit and the chain. The chain evolution transfers correlations along the chain, and the second qubit interacting, in turn, with the chain, becomes entangled with the whole system and, thus, also with the first qubit.

The qubit spin-$S$ evolution are solved exactly, by numerical diagonalization of the corresponding Hamiltonian, while, for the chain evolution, a specific approximation has been introduced, which has been demonstrated to reproduce exact dynamics in the $S \to \infty$ limit. It is found that the correlations generated between the first qubit and the respective spin-$S$ are, indeed, efficiently transferred along the chain, due to the chain evolution. This happens if the initial chain state is chosen to correspond to a soliton whose typical width is large compared with the lattice spacing. In such a case the soliton propagation is not substantially altered by the change of the configuration of a single spin, and, as a result, the quantum correlations generated during the first dynamical stage remain confined to a small, and moving portion of the chain.

Numerical results show that, if the previous condition is met, during the chain evolution the first qubit remain correlated, at any time, only with a finite number spin, following the propagation of a deformed soliton; finally, after the second qubit has interacted with the chain, values of the two-qubit concurrence are found, which are significantly different from zero, meaning that the two qubits are indeed entangled.

The above results confirm that a semi-classical system, such as a large-$S$ spin chain, can

be fruitfully used as an entangling channel for distant qubits. Since the system dynamics can transform a two-qubit separable state in an entangled state, the hybrid scheme here proposed, with the proper choice of parameters, can be exploited for the realization of specific, robust two-qubit entangling gates.

# Appendix A

# Derivation of eq. (3.7)

In this appendix we show how to derive the exact expression given in equation 3.7, i.e. the expression for the infinitesimal rotation generated by the evolution of a magnetic moment making precession motion around a magnetic field $\boldsymbol{B}$. Consider a magnetic moment $\boldsymbol{m}$ in a magnetic field $\boldsymbol{B} = (B_1, B_2, B_3)$, its EoM will be given by

$$\dot{\boldsymbol{m}} = \boldsymbol{m} \times \boldsymbol{B} \equiv \hat{\boldsymbol{R}}\boldsymbol{m}\,, \tag{A.1}$$

where

$$\hat{\boldsymbol{R}} = \begin{pmatrix} 0 & B_3 & -B_2 \\ -B_3 & 0 & B_1 \\ B_2 & -B_1 & 0 \end{pmatrix}. \tag{A.2}$$

Defining the matrix $\hat{\boldsymbol{R}}$ we explicitly wrote equation A.1 as a linear equation whose solution is given in term of the exponential operator $\exp(\hat{\boldsymbol{R}}t)$ as follows

$$\boldsymbol{m}(t) = \exp(\hat{\boldsymbol{R}}t)\boldsymbol{m}(0) = \left(\sum_{n=0}^{\infty} \frac{t^n}{n!}\hat{\boldsymbol{R}}^n\right)\boldsymbol{m}(0)\,. \tag{A.3}$$

From equation A.4 we realize that all the powers of the matrix $\hat{\boldsymbol{R}}$ can be rewritten in terms of $\hat{\boldsymbol{R}}$, $\hat{\boldsymbol{R}}^2$ and the modulus of the field $\boldsymbol{B}$. In fact, it is found

$$\hat{\boldsymbol{R}}^2 = \begin{pmatrix} -(B_2^2 + B_3^2) & B_1B_2 & B_1B_3 \\ B_1B_2 & -(B_1^2 + B_3^2) & B_2B_3 \\ B_1B_3 & B_2B_3 & -(B_1^2 + B_2^2) \end{pmatrix} \quad \text{and} \quad \hat{\boldsymbol{R}}^3 = -|\boldsymbol{B}|^2\hat{\boldsymbol{R}}\,. \tag{A.4}$$

We can thus write

$$\begin{aligned} \boldsymbol{m}(t) \;=\; & \left[\mathbb{1} + \frac{1}{|\boldsymbol{B}|}\left(|\boldsymbol{B}|t - \frac{t^3}{3!}|\boldsymbol{B}|^3 + \dots\right)\hat{\boldsymbol{R}}\right. \\ & \left. + \frac{1}{|\boldsymbol{B}|^2}\left(\frac{t^2}{2!}|\boldsymbol{B}|^2 - \frac{t^4}{4!}|\boldsymbol{B}|^4 + \dots\right)\hat{\boldsymbol{R}}^2\right]\boldsymbol{m}(0) \\ =\; & \left[\mathbb{1} + \frac{\hat{\boldsymbol{R}}^2}{|\boldsymbol{B}|^2} + \frac{\sin\left(|\boldsymbol{B}|t\right)}{|\boldsymbol{B}|}\hat{\boldsymbol{R}} - \frac{\cos\left(|\boldsymbol{B}|t\right)}{|\boldsymbol{B}|^2}\hat{\boldsymbol{R}}^2\right]\boldsymbol{m}(0)\,. \end{aligned} \tag{A.5}$$

The last thing to do is to evaluate the action of the matrix part on the vector $\boldsymbol{m}(0)$. According to equation (A.1) and (A.4) we have

$$\begin{aligned} \hat{\boldsymbol{R}}\boldsymbol{m}(0) \;\equiv & \boldsymbol{m}(0)\times\boldsymbol{B} \\ \hat{\boldsymbol{R}}^2\boldsymbol{m}(0) \;=\; & -|\boldsymbol{B}|^2\left[\boldsymbol{m}(0) - \boldsymbol{B}\frac{(\boldsymbol{B}\cdot\boldsymbol{m}(0))}{|\boldsymbol{B}|^2}\right]. \end{aligned} \tag{A.6}$$

Substituting the above equation in the last line of equation (A.5) we finally obtain

$$\begin{aligned} \boldsymbol{m}(t) \;=& \boldsymbol{B}\,\frac{(\boldsymbol{B}\cdot\boldsymbol{m}(0))}{|\boldsymbol{B}|^2} + \frac{\boldsymbol{m}(0)\times\boldsymbol{B}}{|\boldsymbol{B}|}\sin\left(|\boldsymbol{B}|t\right) \\ & - \left[\boldsymbol{m}(0) - \boldsymbol{B}\frac{(\boldsymbol{B}\cdot\boldsymbol{m}(0))}{|\boldsymbol{B}|^2}\right]\cos\left(|\boldsymbol{B}|t\right), \end{aligned} \tag{A.7}$$

which is the same as equation (3.7) with the substitutions $\boldsymbol{B} \leftrightarrow \Omega_l$ and $\boldsymbol{m} \leftrightarrow \boldsymbol{s}_l$ and evaluated for the infinitesimal time-interval $\delta t$ from $t$ to $t+\delta t$. We note here that the derivation of equation (A.7) is exact for any time value $t$ since the magnetic field $\boldsymbol{B}$ is fixed. In chapter 3, the use of small interval is fundamental because it allows us to use and truncate the Suzuki-Trotter expansion knowing the magnitude of the committed error and it also allows, while updating one sub-lattice configuration, to treat the other sub-lattice as constant and thus to use equation (3.7).

# Appendix B

# Large-$S$ limit Heisenberg chain GCS

In this appendix we demonstrate that, in the limit of large $S$, the GCS of the spin chain are well approximated by a tensor product of SSCS, i.e. the semi-classical states defined in chapter 5, and we provide the explicit construction of the GCS for an isotropic Heisenberg spin chain in the limit of $S \to \infty$. The basic scheme of the construction was already discussed for the two simple examples of the FCS and SSCS in section 1.4.3; for the details not included there, we refer to reference [73], where the guidelines for the general construction are given rigorously.

We will consider a quantum Heisenberg spin chain made by $N$ spin-$S$ interacting through a ferromagnetic, isotropic interaction of intensity $J$. Let's start from rewriting the Heisenberg Hamiltonian of equation (5.18) in terms of the raising(lowering) operators $S_n^{\pm} = S_n^x \pm i S_n^y$ [1]

$$\hat{\mathcal{H}}_{\Xi} = -\frac{J}{2} \sum_n \left( S_n^+ S_{n+1}^- + S_n^- S_{n+1}^+ + 2 S_n^z S_{n+1}^z \right) - \gamma H \sum_n \hat{S}_n^z \,. \tag{B.1}$$

As described in section 1.4.3, the GCS construction requires three elements: a group $G$ and the corresponding algebra of its generators $\boldsymbol{g}$; an Hilbert space containing a unitary irreducible representation of $G$; a normalized reference state belonging to this Hilbert space. While the second and the third request are readily satisfied by the following two natural choices: $\mathscr{H}_{\Xi}$ as the Hilbert space, and, as the reference state, the following

$$\big|\Lambda\big\rangle \equiv \bigotimes_n |m_n = S\rangle \ , \tag{B.2}$$

[1] The spin operator $S_n^{\alpha}$ represent the natural extension to the whole chain space of the single-spin operator $\bar{S}_n^{\alpha}$, according to:

$$S_n^{\alpha} = \mathbb{1}_1 \otimes \cdots \otimes \bar{S}_n^{\alpha} \otimes \cdots \otimes \mathbb{1}_N \,.$$

where $S_n^z \left|m_n\right\rangle = m_n \left|m_n\right\rangle$, i.e. the product of the Dicke states with maximum $z$-projection value. The last choice is motivated by the final result we want to achieve, since the states $|m_n = S\rangle$ are the reference states for the SSCS.

What we still need to start the construction, is to find a transformation group acting on $\mathscr{H}_\Xi$ whose generators include all the operators appearing in the Hamiltonian (B.1), i.e. the dynamical group $G$. In order to find this particular group, we can work directly on the generators and their algebra. We take the operators appearing in the Hamiltonian

$$JS_n^+ S_{n+1}^-,\ JS_n^- S_{n+1}^+,\ JS_n^z S_{n+1}^z,\ S_n^z\,, \quad n = 1, \ldots, N\,, \tag{B.3}$$

where we have included the coupling $J$ in the definition of the quadratic terms since it will be fundamental for introducing the large-$S$ approximation. In order to build the Lie Algebra $\boldsymbol{g}$ of the dynamical group generators, we calculate the commutators between the above operators in $\boldsymbol{g}$ (commutators are the operators Lie brackets), and add all the possible new operators we get; such enlargement of $\boldsymbol{g}$ continues until new operators are generated from the commutators of the elements already present in $\boldsymbol{g}$.

Repeating this procedure we realize that successive commutation operations introduce higher order terms in the form

$$J^k \prod_{n,\alpha} (S_n^\alpha)^{k_n^\alpha}\,, \tag{B.4}$$

where $\alpha = \pm, z$. It is clear that the algebra we are trying to build is not closed at any finite order, and has thus infinite terms. This is the reason why an exact explicit construction of Heisenberg chain GCS is not possible.

To overcome this problem we exploit the fact that $S$ has to be large in our application. In particular, considering the limit $S \to \infty$, we find that, in order to keep the chain interaction energy, $JS^2$, finite, the coupling $J$ must scale as $1/S^2$. For the operators, we define the reduced spin operator $S_n^\alpha \equiv S s_n^\alpha$ and their commutation relation

$$[s_n^z, s_m^\pm] \,=\, \pm\delta_{nm} \frac{1}{S} s_m^\pm\,, \quad [s_n^+, s_m^-] \,=\, \delta_{nm} \frac{1}{S} 2 s_m^z\,, \tag{B.5}$$

showing that any commutation operation carries a factor $1/S$. The above considerations allow us to introduce a criterion for neglecting a subset of the terms like those in equation (B.4).

In particular, being interested in the limit $S \to \infty$, we decide to neglect all terms (B.4) with

$$k > 2m \quad \text{where} \quad m \equiv \sum_{n,\alpha} k_n^\alpha\,, \tag{B.6}$$

This implies that all the commutators like $[JS_n^\alpha S_{n+1}^\beta, JS_n^{\alpha'} S_{n+1}^{\beta'}]$, vanish; the only non trivial

commutators remaining are those involving at least one term $S_n^z$.

According to the former assumption, we find that the closed, non-trivial, finite algebra, $\boldsymbol{g}$, is constituted by the following set

$$\left\{ \mathbb{1},\, S_i^z,\, JS_i^z S_{i+1}^z,\, JS_i^{\pm} S_{i+1}^{\mp},\, JS_i^z S_{i+1}^{\pm},\, JS_i^{\pm} S_{i+1}^z \;\middle|\; i = 1, \ldots, N \right\}, \tag{B.7}$$

which generates the chain dynamical group $G$ through the exponential map of its elements.

Having already chosen the Hilbert space $\mathscr{H}_{\Xi}$ and the reference state $\big|\Lambda\big\rangle$, we can readily continue with the construction by identifying the stability subgroup $H$. It is evident that the stability subgroup is the subgroup generated by the following generators

$$\left\{ \mathbb{1}, S_i^z, JS_i^z S_{i+1}^z \mid i = 1, \ldots, N \right\}, \tag{B.8}$$

being $\big|\Lambda\big\rangle$ an eigenstate of this operators, all the group elements, generated by their exponential map, will change the reference state only up to a phase factor.

Now, in order to complete the construction, we must find the displacement operators, that acting on the reference state give the CGS, and that correspond to the representatives of the coset $G/H$ of $G$ with respect to $H$. The displacement operators are obtained as the exponential maps of the anti-hermitean combinations of the elements, $T_i$, of $\boldsymbol{g}$ minus the generators of $H$, which do not annihilate the reference state $\big|\Lambda\big\rangle$, in the form $\eta_i T_i - \text{h.c.}$, with $\eta_i$ a complex coefficient. In our case the operators $T_i$ are the following

$$\left\{ JS_n^z S_{n+1}^-, JS_n^- S_{n+1}^z \mid n = 1, \ldots, N \right\}. \tag{B.9}$$

Thus the general displacement operator read

$$\begin{aligned} D(\eta, \zeta) \;&\equiv \exp\left[ \sum_n J \left( \eta_n S_n^z S_{n+1}^- + \zeta_n S_n^- S_{n+1}^z - \text{h.c.} \right) \right] \\ &= \exp J(\eta_1 S_1^z S_2^- + \zeta_1 S_1^- S_2^z - \eta_1 S_1^z S_2^+ - \zeta_1 S_1^+ S_2^z \\ &\quad + \eta_2 S_2^z S_3^- + \zeta_2 S_2^- S_3^z - \eta_2 S_2^z S_3^+ - \zeta_2 S_2^+ S_3^z + \ldots) \\ &= \exp\{ J(\zeta_1 S_2^z S_1^- - \zeta_1^\star S_2^z S_1^+) + J[(\eta_1 S_1^z + \zeta_2 S_3^z)\, S_2^- - \text{h.c.}] + \ldots \} \end{aligned} \tag{B.10}$$

where $\eta \equiv (\eta_1, \ldots, \eta_N)$ and $\zeta \equiv (\zeta_1, \ldots, \zeta_N)$. The GCS for the spin chain are, thus, readily

obtained by applying the above operator to the reference state:

$$\begin{aligned}\big|\Xi\big\rangle \equiv & D(\eta,\zeta)\big|\Lambda\big\rangle \\ = & \exp\{J(\zeta_1 S_2^z S_1^- - \zeta_1^\star S_2^z S_1^+) + J[(\eta_1 S_1^z + \zeta_2 S_3^z)\, S_2^- - \text{h.c.}] + \ldots\}\big|\Lambda\big\rangle \\ = & \, e^{JS(\zeta_1 S_1^- - \zeta_1^\star S_1^+)}\,|m_1 = S\rangle \otimes e^{JS[(\eta_1+\zeta_2)\, S_2^- - (\eta_1+\zeta_2)^\star\, S_2^+]}\,|m_2 = S\rangle \otimes \cdots \\ & \cdots \otimes e^{JS(\eta_{N-1} S_1^- - \eta_{N-1}^\star S_N^+)}\,|m_N = S\rangle \\ = & \big|\xi_1\big\rangle \otimes \big|\xi_2\big\rangle \otimes \cdots \otimes \big|\xi_n\big\rangle \otimes \cdots \otimes \big|\xi_N\big\rangle\,,\end{aligned} \tag{B.11}$$

where in the third line we have exploited the fact that the reference state is the product of the $S_n^z$ eigenstate with $m_n = S$ and that all the operators at the exponent commute according to our approximation, allowing any factorization of the exponential. In the last line we introduced the complex coefficients $\xi_n$ as

$$\begin{aligned}\xi_1 &= JS\zeta_1 \\ \xi_n &= JS(\zeta_n + \eta_{n-1}) \quad \text{for} \quad n = 2, \ldots, N-1 \\ \xi_N &= JS\eta_{N-1}\end{aligned} \tag{B.12}$$

and the corresponding state

$$\big|\xi_n\big\rangle = e^{\xi_n S_n^- - \xi_n^\star S_n^+}\,|m_n = S\rangle\,, \tag{B.13}$$

which are the SSCS of the $n$-th spin of the chain with parameter $\xi_n$. We note that the first and the last coefficients are different from the other because of the chain open boundaries (if the periodic boundary conditions are assumed the difference disappears). Finally, we note that the last line of equation (B.11) shows that the GCS for the chain $\Xi$ are, indeed, a tensor product of SSCS in the limit of $S \to \infty$.

Since it has been demonstrated that GCS evolve according to the corresponding classical EoM if the Hamiltonian ruling the evolution is linear in the group $G$ generators, this result proves also that the semi-classical evolution approximation reproduce the exact evolution in the limit $S \to \infty$.

# List of acronyms

1. **EoM:** Equation of Motion;
2. **FCS:** Field Coherent State;
3. **SSCS:** Single-Spin Coherent State;
4. **GCS:** Generalized Coherent State;
5. **HS:** Hilber-Schmidt;
6. **KdV:** Korteweg-de Vries;
7. **KG:** Klein-Gordon;
8. **SG:** Sine-Gordon;
9. **BH:** Burgers-Hopf;
10. **RKKY:** Ruderman-Kittel-Kasuya-Yoshida;
11. **NLS:** Non-Linear Schrödinger.

# Acknowledgements

First and foremost I want to thank my three advisors, Alessandro Cuccoli, Paola Verrucchi e Ruggero Vaia, although Alessandro is the only appearing as the "official" supervisor of my work, all of them gave an equally important contribution for the birth of this work and for my growth as a researcher and as a person, sharing with me their ideas, expertise and knowledge. In particular I want to thank Paola for her incessant optimism and for being the driving force of our group, Ruggero for his strong physical intuition and for his indisputable taste for the simple and clear (as well as rigorous) formalism, and Alessandro for being a rock-solid support when I had doubts and for being my mentor since my Bachelor's thesis.

Sincere thanks to my PhD colleagues with whom I shared fears, difficulties and also a lot of happy moments during the last three years. Special thanks to Lucio for being one of the most helpful people I know, and to Eduardo for being a friend, besides a great office-mate.

Last but not least I want to thank my family for their never-ending love and support throughout my entire life, and Barbara not only for being my best friend and the most valuable colleague, but also for giving me the best moments during the last ten years of our lives.

# Bibliography


[1] J. I. Cirac and P. Zoller. Quantum computations with cold trapped ions. *Phys. Rev. Lett.*, 74:4091–4094, May 1995.

[2] Neil A. Gershenfeld and Isaac L. Chuang. Bulk spin-resonance quantum computation. *Science*, 275(5298):350–356, 1997.

[3] Daniel Loss and David P. DiVincenzo. Quantum computation with quantum dots. *Phys. Rev. A*, 57:120–126, Jan 1998.

[4] E. Knill, R. Laflamme, and G. J. Milburn. A scheme for efficient quantum computation with linear optics. *Nature*, 409(6816):46–52, January 2001.

[5] E. Knill. Quantum computing with realistically noisy devices. *Nature*, 434(7029):39–44, March 2005.

[6] D. B. Tretyakov, I. I. Beterov, V. M. Entin, and I. I. Ryabtsev. Cold atoms in optical lattices as qubits for a quantum computer. *Russian Microelectronics*, 35(2):74–77, 2006.

[7] Jonathan P. Home, David Hanneke, John D. Jost, Jason M. Amini, Dietrich Leibfried, and David J. Wineland. Complete methods set for scalable ion trap quantum information processing. *Science*, 325(5945):1227–1230, 2009.

[8] Lieven M. K. Vandersypen, Matthias Steffen, Gregory Breyta, Costantino S. Yannoni, Mark H. Sherwood, and Isaac L. Chuang. Experimental realization of shor's quantum factoring algorithm using nuclear magnetic resonance. *Nature*, 414(6866):883–887, December 2001.

[9] Alberto Politi, Jonathan C. F. Matthews, and Jeremy L. O'Brien. Shor's quantum factoring algorithm on a photonic chip. *Science*, 325(5945):1221–1221, 2009.

[10] M. W. Johnson, M. H. S. Amin, S. Gildert, T. Lanting, F. Hamze, N. Dickson, R. Harris, A. J. Berkley, J. Johansson, P. Bunyk, E. M. Chapple, C. Enderud, J. P. Hilton, K. Karimi, E. Ladizinsky, N. Ladizinsky, T. Oh, I. Perminov, C. Rich, M. C. Thom, E. Tolkacheva, C. J. S. Truncik, S. Uchaikin, J. Wang, B. Wilson, and G. Rose. Quantum annealing with manufactured spins. *Nature*, 473(7346):194–198, May 2011.

[11] Sergio Boixo, Troels F. Ronnow, Sergei V. Isakov, Zhihui Wang, David Wecker, Daniel A. Lidar, John M. Martinis, and Matthias Troyer. Evidence for quantum annealing with more than one hundred qubits. *Nat Phys*, 10(3):218–224, March 2014.

[12] Philipp-Immanuel Schneider and Alejandro Saenz. Quantum computation with ultracold atoms in a driven optical lattice. *Phys. Rev. A*, 85:050304, May 2012.

[13] D. Kielpinski, V. Meyer, M. A. Rowe, C. A. Sackett, W. M. Itano, C. Monroe, and D. J. Wineland. A decoherence-free quantum memory using trapped ions. *Science*, 291(5506):1013–1015, 2001.

[14] H. Häffner, C.F. Roos, and R. Blatt. Quantum computing with trapped ions. *Physics Reports*, 469(4):155 – 203, 2008.

[15] Antonio S. Coelho, Luca S. Costanzo, Alessandro Zavatta, Catherine Hughes, M. S. Kim, and Marco Bellini. Universal continuous-variable state orthogonalizer and qubit generator. *Phys. Rev. Lett.*, 116:110501, Mar 2016.

[16] Hyunseok Jeong, Alessandro Zavatta, Minsu Kang, Seung-Woo Lee, Luca S. Costanzo, Samuele Grandi, Timothy C. Ralph, and Marco Bellini. Generation of hybrid entanglement of light. *Nat Photon*, 8(7):564–569, July 2014.

[17] Torsten Gaebel, Michael Domhan, Iulian Popa, Christoffer Wittmann, Philipp Neumann, Fedor Jelezko, James R. Rabeau, Nikolas Stavrias, Andrew D. Greentree, Steven Prawer, Jan Meijer, Jason Twamley, Philip R. Hemmer, and Jorg Wrachtrup. Room-temperature coherent coupling of single spins in diamond. *Nat Phys*, 2(6):408–413, June 2006.

[18] M. V. Gurudev Dutt, L. Childress, L. Jiang, E. Togan, J. Maze, F. Jelezko, A. S. Zibrov, P. R. Hemmer, and M. D. Lukin. Quantum register based on individual electronic and nuclear spin qubits in diamond. *Science*, 316(5829):1312–1316, 2007.

[19] J. R. Maze, P. L. Stanwix, J. S. Hodges, S. Hong, J. M. Taylor, P. Cappellaro, L. Jiang, M. V. Gurudev Dutt, E. Togan, A. S. Zibrov, A. Yacoby, R. L. Walsworth, and M. D. Lukin. Nanoscale magnetic sensing with an individual electronic spin in diamond. *Nature*, 455(7213):644–647, October 2008.

[20] G. Balasubramanian, P. Neumann, D. Twitchen, M. Markham, R. Kolesov, N. Mizuochi, J. Isoya, J. Achard, J. Beck, J. Tissler, V. Jacques, P. R. Hemmer, F. Jelezko, and J. Wrachtrup. Ultralong spin coherence time in isotopically engineered diamond. *Nature Materials*, 8:383–387, May 2009.

[21] Bernhard Grotz, Moritz V. Hauf, Markus Dankerl, Boris Naydenov, Sébastien Pezzagna, Jan Meijer, Fedor Jelezko, Jörg Wrachtrup, Martin Stutzmann, Friedemann Reinhard, and Jose A. Garrido. Charge state manipulation of qubits in diamond. *Nature Communications*, 3:729–, March 2012.

[22] Hans-Andreas Engel, L. P. Kouwenhoven, Daniel Loss, and C. M. Marcus. Controlling spin qubits in quantum dots. *Quantum Information Processing*, 3(1-5):115–132, October 2004.

[23] F. H. L. Koppens, C. Buizert, K. J. Tielrooij, I. T. Vink, K. C. Nowack, T. Meunier, L. P. Kouwenhoven, and L. M. K. Vandersypen. Driven coherent oscillations of a single electron spin in a quantum dot. *Nature*, 442(7104):766–771, August 2006.

[24] K A Long and A R Bishop. Nonlinear excitations in classical ferromagnetic chains. *Journal of Physics A: Mathematical and General*, 12(8):1325, 1979.

[25] H C Fogedby. Solitons and magnons in the classical heisenberg chain. *Journal of Physics A: Mathematical and General*, 13(4):1467, 1980.

[26] N. Elstner and H.-J. Mikeska. Solitons in the anisotropic xy chain: semiclassical treatment of quantum effects. *Journal of Physics Condensed Matter*, 1:1487–1494, February 1989.

[27] A.M. Kosevich, B.A. Ivanov, and A.S. Kovalev. Magnetic solitons. *Physics Reports*, 194(3–4):117 – 238, 1990.

[28] Heinz-Jürgen Schmidt, Christian Schröder, and Marshall Luban. Modulated spin waves and robust quasi-solitons in classical heisenberg rings. *Journal of Physics: Condensed Matter*, 23(38):386003, 2011.

[29] Anton Wöllert and Andreas Honecker. Solitary excitations in one-dimensional spin chains. *Phys. Rev. B*, 85:184433, May 2012.

[30] J. K. Kjems and M. Steiner. Evidence for Soliton Modes in the One-Dimensional Ferromagnet $CsNiF_3$. *Physical Review Letters*, 41:1137–1140, October 1978.

[31] J.P. Boucher, L.P. Regnault, J. Rossat-Mignod, J.P. Renard, J. Bouillot, and W.G. Stirling. Solitons in the one-dimensional antiferromagnet tmmc. *Solid State Communications*, 33(2):171 – 174, 1980.

[32] A. P. Ramirez and W. P. Wolf. Specific heat of $csnif_3$: Evidence for spin solitons. *Phys. Rev. Lett.*, 49:227–230, Jul 1982.

[33] F. Borsa, M. G. Pini, A. Rettori, and V. Tognetti. Magnetic specific-heat contributions from linear *vis-à-vis* nonlinear excitations in the one-dimensional antiferromagnet $(ch_3)_4nmncl_3$ (tmmc). *Phys. Rev. B*, 28:5173–5183, Nov 1983.

[34] H.-J. Mikeska and M. Steiner. Solitary excitations in one-dimensional magnets. *Advances in Physics*, 40(3):191–356, 1991.

[35] H J Mikeska and H Frahm. The soliton contribution to the specific heat of csnif 3 : quantum effects and out-of-plane fluctuations. *Journal of Physics C: Solid State Physics*, 19(17):3203, 1986.

[36] Alessandro Cuccoli, Valerio Tognetti, Paola Verrucchi, and Ruggero Vaia. Quantum thermodynamics of easy-plane ferromagnetic chains. *Phys. Rev. B*, 44:903–905, Jul 1991.

[37] Alessandro Cuccoli, Valerio Tognetti, Paola Verrucchi, and Ruggero Vaia. Quantum thermodynamics of the easy-plane ferromagnetic chain. *Phys. Rev. B*, 46:11601–11616, Nov 1992.

[38] Alessandro Cuccoli, Riccardo Giachetti, Valerio Tognetti, Ruggero Vaia, and Paola Verrucchi. The effective potential and effective hamiltonian in quantum statistical mechanics. *Journal of Physics: Condensed Matter*, 7(41):7891, 1995.

[39] Alessandro Cuccoli, Valerio Tognetti, Paola Verrucchi, and Ruggero Vaia. Semiclassical approach to the thermodynamics of spin chains. *Phys. Rev. B*, 62:57–60, Jul 2000.

[40] Alessandro Cuccoli, Davide Nuzzi, Ruggero Vaia, and Paola Verrucchi. Getting through to a qubit by magnetic solitons. *New Journal of Physics*, 17(8):083053, 2015.

[41] Alessandro Cuccoli, Davide Nuzzi, Ruggero Vaia, and Paola Verrucchi. Single-qubit remote manipulation by magnetic solitons. *Journal of Magnetism and Magnetic Materials*, 400:149 – 153, 2016. Proceedings of the 20th International Conference on Magnetism (Barcelona) 5-10 July 2015.

[42] Alessandro Cuccoli, Davide Nuzzi, Ruggero Vaia, and Paola Verrucchi. Using solitons for manipulating qubits. *International Journal of Quantum Information*, 12(02):1461013, 2014.

[43] Alessandro Cuccoli, Davide Nuzzi, Ruggero Vaia, and Paola Verrucchi. Quantum gates controlled by spin chain soliton excitations. *Journal of Applied Physics*, 115(17), 2014.

[44] D. Nuzzi, A. Cuccoli, R. Vaia, and P. Verrucchi. Entanglement generation via semi-classical channels. *To be submitted*, 2017.

[45] Dario Calvani, Alessandro Cuccoli, Nikitas I. Gidopoulos, and Paola Verrucchi. Parametric representation of open quantum systems and cross-over from quantum to classical environment. *Proceedings of the National Academy of Sciences*, 110(17):6748–6753, 2013.

[46] Paweł Horodecki. Measuring quantum entanglement without prior state reconstruction. *Phys. Rev. Lett.*, 90:167901, Apr 2003.

[47] Zhi Zhao, Yu-Ao Chen, An-Ning Zhang, Tao Yang, Hans J. Briegel, and Jian-Wei Pan. Experimental demonstration of five-photon entanglement and open-destination teleportation. *Nature*, 430(6995):54–58, July 2004.

[48] S. P. Walborn, P. H. Souto Ribeiro, L. Davidovich, F. Mintert, and A. Buchleitner. Experimental determination of entanglement with a single measurement. *Nature*, 440(7087):1022–1024, April 2006.

[49] J. D. Jost, J. P. Home, J. M. Amini, D. Hanneke, R. Ozeri, C. Langer, J. J. Bollinger, D. Leibfried, and D. J. Wineland. Entangled mechanical oscillators. *Nature*, 459(7247):683–685, June 2009.

[50] Stephanie Simmons, Richard M. Brown, Helge Riemann, Nikolai V. Abrosimov, Peter Becker, Hans-Joachim Pohl, Mike L. W. Thewalt, Kohei M. Itoh, and John J. L. Morton. Entanglement in a solid-state spin ensemble. *Nature*, 470(7332):69–72, February 2011.

[51] Charles H. Bennett, David P. DiVincenzo, John A. Smolin, and William K. Wootters. Mixed-state entanglement and quantum error correction. *Phys. Rev. A*, 54:3824–3851, Nov 1996.

[52] M.A. Nielsen and I.L. Chuang. *Quantum Computation and Quantum Information*. Cambridge Series on Information and the Natural Sciences. Cambridge University Press, 2000.

[53] Scott Hill and William K. Wootters. Entanglement of a pair of quantum bits. *Phys. Rev. Lett.*, 78:5022–5025, Jun 1997.

[54] William K. Wootters. Entanglement of formation of an arbitrary state of two qubits. *Phys. Rev. Lett.*, 80:2245–2248, Mar 1998.

[55] D. Salgado, J. L. Sánchez-Gómez, and M. Ferrero. Evolution of any finite open quantum system always admits a kraus-type representation, although it is not always completely positive. *Phys. Rev. A*, 70:054102, Nov 2004.

[56] D. M. Tong, L. C. Kwek, C. H. Oh, Jing-Ling Chen, and L. Ma. Operator-sum representation of time-dependent density operators and its applications. *Phys. Rev. A*, 69:054102, May 2004.

[57] W. Forrest Stinespring. Positive functions on c*-algebras. *Proceedings of the American Mathematical Society*, 6(2):211–216, 1955.

[58] Elliott H. Lieb. The classical limit of quantum spin systems. *Communications in Mathematical Physics*, 31(4):327–340, 1973.

[59] R. Gilmore. The classical limit of quantum nonspin systems. *Journal of Mathematical Physics*, 20(5):891–893, 1979.

[60] Barry Simon. The classical limit of quantum partition functions. *Communications in Mathematical Physics*, 71(3):247–276, 1980.

[61] Laurence G. Yaffe. Large $n$ limits as classical mechanics. *Rev. Mod. Phys.*, 54:407–435, Apr 1982.

[62] Roy J. Glauber. Photon correlations. *Phys. Rev. Lett.*, 10:84–86, Feb 1963.

[63] Roy J. Glauber. The quantum theory of optical coherence. *Phys. Rev.*, 130:2529–2539, Jun 1963.

[64] E. C. G. Sudarshan. Equivalence of semiclassical and quantum mechanical descriptions of statistical light beams. *Phys. Rev. Lett.*, 10:277–279, Apr 1963.

[65] John R. Klauder. Continuous representation theory. i. postulates of continuous representation theory. *Journal of Mathematical Physics*, 4(8):1055–1058, 1963.

[66] John R. Klauder. Continuous representation theory. ii. generalized relation between quantum and classical dynamics. *Journal of Mathematical Physics*, 4(8):1058–1073, 1963.

[67] E. Schrödinger. Der stetige übergang von der mikro- zur makromechanik. *Naturwissenschaften*, 14(28):664–666, 1926.

[68] F. T. Arecchi, Eric Courtens, Robert Gilmore, and Harry Thomas. Atomic coherent states in quantum optics. *Phys. Rev. A*, 6:2211–2237, Dec 1972.

[69] J M Radcliffe. Some properties of coherent spin states. *Journal of Physics A: General Physics*, 4(3):313, 1971.

[70] Robert Gilmore. Geometry of symmetrized states. *Annals of Physics*, 74(2):391 – 463, 1972.

[71] R Gilmore. Exact spectrum and wave functions of the hyperbolic scarf potential in terms of finite romanovski polynomials. *Rev. Mex. de Fisica*, 23:143, 1974.

[72] A. M. Perelomov. Coherent states for arbitrary lie group. *Communications in Mathematical Physics*, 26(3):222–236, 1972.

[73] Wei-Min Zhang, Da Hsuan Feng, and Robert Gilmore. Coherent states: Theory and some applications. *Rev. Mod. Phys.*, 62:867–927, Oct 1990.

[74] B. A. Nikolov and D. A. Trifonov. On the dynamics of Generalized Coherent States. 1. Exact and stable evolution. *Commun. JINR E2-81-797*, 1981.

[75] B. A. Nikolov and D. A. Trifonov. On the dynamics of Generalized Coherent States. 2. Classical equation of motion. *Commun. JINR E2-81-798*, 1981.

[76] T. Dauxois and M. Peyrard. *Physics of Solitons*. Cambridge University Press, 2006.

[77] R. Rajaraman. *Solitons and Instantons: An Introduction to Solitons and Instantons in Quantum Field Theory*. North-Holland personal library. North-Holland Publishing Company, 1982.

[78] L. L. Van Zandt. Dna solitons with realistic parameter values. *Phys. Rev. A*, 40:6134–6137, Nov 1989.

[79] L.V. Yakushevich. Nonlinear dna dynamics: A new model. *Physics Letters A*, 136(7):413 – 417, 1989.

[80] Michel Peyrard. *Nonlinear excitations in biomolecules: Les Houches School, May 30 to June 4, 1994*. Centre de physique des Houches. Springer, 1995.

[81] Giuseppe Gaeta. A realistic version of the y model for dna dynamics and selection of soliton speed. *Physics Letters A*, 190(3):301 – 308, 1994.

[82] Thierry Dauxois. Dynamics of breather modes in a nonlinear "helicoidal" model of dna. *Physics Letters A*, 159(8):390 – 395, 1991.

[83] Akira Hasegawa. An historical review of application of optical solitons for high speed communications. *Chaos*, 10(3):475–485, 2000.

[84] Y.S. Kivshar and G. Agrawal. *Optical Solitons: From Fibers to Photonic Crystals*. Elsevier Science, 2003.

[85] L.F. Mollenauer and J.P. Gordon. *Solitons in Optical Fibers: Fundamentals and Applications*. Elsevier Science, 2006.

[86] A. Fernández-Pacheco, D. Petit, R. Mansell, R. Lavrijsen, J. H. Lee, and R. P. Cowburn. Controllable nucleation and propagation of topological magnetic solitons in cofeb/ru ferrimagnetic superlattices. *Phys. Rev. B*, 86:104422, Sep 2012.

[87] Reinoud Lavrijsen, Ji-Hyun Lee, Amalio Fernandez-Pacheco, Dorothee C. M. C. Petit, Rhodri Mansell, and Russell P. Cowburn. Magnetic ratchet for three-dimensional spintronic memory and logic. *Nature*, 493(7434):647–650, January 2013.

[88] Reinoud Lavrijsen, Dorothée C M C Petit, Amalio Fernández-Pacheco, JiHyun Lee, Rhodri Mansell, and Russell P Cowburn. Multi-bit operations in vertical spintronic shift registers. *Nanotechnology*, 25(10):105201, 2014.

[89] G. Finocchio, V. Puliafito, S. Komineas, L. Torres, O. Ozatay, T. Hauet, and B. Azzerboni. Nanoscale spintronic oscillators based on the excitation of confined soliton modes. *Journal of Applied Physics*, 114(16), 2013.

[90] A. Auerbach. *Interacting Electrons and Quantum Magnetism*. Graduate Texts in Contemporary Physics. Springer New York, 1998.

[91] Maria Gloria Pini and Angelo Rettori. Failure of the classical approximation for csnif$_3$. *Phys. Rev. B*, 29:5246–5249, May 1984.

[92] H. J. Jensen, O. G. Mouritsen, H. C. Fogedby, P. Hedegrd, and A. Svane. Analytical and numerical studies of the easy-plane antiferromagnetic chain: Application to $(ch_3)_4nmncl_3$. *Phys. Rev. B*, 32:3240–3250, Sep 1985.

[93] Michael Durnan Johnson and Nancy Faye Wright. Soliton specific heat of spin chains: Limitations of the quantum sine-gordon model. *Phys. Rev. B*, 32:5798–5803, Nov 1985.

[94] J. Tjon and Jon Wright. Solitons in the continuous heisenberg spin chain. *Phys. Rev. B*, 15:3470–3476, Apr 1977.

[95] L.A. Takhtajan. Integration of the continuous heisenberg spin chain through the inverse scattering method. *Physics Letters A*, 64(2):235 – 237, 1977.

[96] M. Krech, Alex Bunker, and D.P. Landau. Fast spin dynamics algorithms for classical spin systems. *Computer Physics Communications*, 111(1):1 – 13, 1998.

[97] Haruo Yoshida. Construction of higher order symplectic integrators. *Physics Letters A*, 150(5):262 – 268, 1990.

[98] Etienne Forest and Ronald D. Ruth. Fourth-order symplectic integration. *Physica D: Nonlinear Phenomena*, 43(1):105 – 117, 1990.

[99] Masuo Suzuki. General theory of higher-order decomposition of exponential operators and symplectic integrators. *Physics Letters A*, 165(5):387 – 395, 1992.

[100] Shan-Ho Tsai, H. K. Lee, and D. P. Landau. Molecular and spin dynamics simulations using modern integration methods. *American Journal of Physics*, 73(7):615–624, 2005.

[101] Till Kamppeter, Franz G. Mertens, Esteban Moro, Angel Sánchez, and A. R. Bishop. Stochastic vortex dynamics in two-dimensional easy-plane ferromagnets: Multiplicative versus additive noise. *Phys. Rev. B*, 59:11349–11357, May 1999.

[102] William Fuller Brown. Thermal fluctuations of a single-domain particle. *Phys. Rev.*, 130:1677–1686, Jun 1963.

[103] D. A. Garanin. Fokker-planck and landau-lifshitz-bloch equations for classical ferromagnets. *Phys. Rev. B*, 55:3050–3057, Feb 1997.

[104] José Luis García-Palacios and Francisco J. Lázaro. Langevin-dynamics study of the dynamical properties of small magnetic particles. *Phys. Rev. B*, 58:14937–14958, Dec 1998.

[105] Matthias Meister and Franz G Mertens. Stochastic motion of solitary excitations on the classical heisenberg chain. *Journal of Physics A: Mathematical and General*, 33(11):2195, 2000.

[106] J Tejada, E M Chudnovsky, E del Barco, J M Hernandez, and T P Spiller. Magnetic qubits as hardware for quantum computers. *Nanotechnology*, 12(2):181, 2001.

[107] Jarryd J. Pla, Kuan Y. Tan, Juan P. Dehollain, Wee H. Lim, John J. L. Morton, Floris A. Zwanenburg, David N. Jamieson, Andrew S. Dzurak, and Andrea Morello. High-fidelity readout and control of a nuclear spin qubit in silicon. *Nature*, 496(7445):334–338, April 2013.

[108] G. de Lange, Z. H. Wang, D. Ristè, V. V. Dobrovitski, and R. Hanson. Universal Dynamical Decoupling of a Single Solid-State Spin from a Spin Bath. *Science*, 330:60–, October 2010.

[109] C. J. Wedge, G. A. Timco, E. T. Spielberg, R. E. George, F. Tuna, S. Rigby, E. J. L. McInnes, R. E. P. Winpenny, S. J. Blundell, and A. Ardavan. Chemical engineering of molecular qubits. *Phys. Rev. Lett.*, 108:107204, Mar 2012.

[110] P. Gambardella, A. Dallmeyer, K. Maiti, M. C. Malagoli, W. Eberhardt, K. Kern, and C. Carbone. Ferromagnetism in one-dimensional monatomic metal chains. *Nature*, 416(6878):301–304, March 2002.

[111] A. Vindigni, A. Rettori, M.G. Pini, C. Carbone, and P. Gambardella. Finite-sized heisenberg chains and magnetism of one-dimensional metal systems. *Applied Physics A*, 82(3):385–394, 2006.

[112] Sougato Bose. Quantum communication through an unmodulated spin chain. *Phys. Rev. Lett.*, 91:207901, Nov 2003.

[113] Sougato Bose. Quantum communication through spin chain dynamics: an introductory overview. *Contemporary Physics*, 48(1):13–30, 2007.

[114] L Banchi, T J G Apollaro, A Cuccoli, R Vaia, and P Verrucchi. Long quantum channels for high-quality entanglement transfer. *New Journal of Physics*, 13(12):123006, 2011.

[115] S. Campbell, T. J. G. Apollaro, C. Di Franco, L. Banchi, A. Cuccoli, R. Vaia, F. Plastina, and M. Paternostro. Propagation of nonclassical correlations across a quantum spin chain. *Phys. Rev. A*, 84:052316, Nov 2011.

[116] T. J. G. Apollaro, L. Banchi, A. Cuccoli, R. Vaia, and P. Verrucchi. 99%-fidelity ballistic quantum-state transfer through long uniform channels. *Phys. Rev. A*, 85:052319, May 2012.

[117] Simone Paganelli, Salvatore Lorenzo, Tony J. G. Apollaro, Francesco Plastina, and Gian Luca Giorgi. Routing quantum information in spin chains. *Phys. Rev. A*, 87:062309, Jun 2013.

[118] S. Sahling, G. Remenyi, C. Paulsen, P. Monceau, V. Saligrama, C. Marin, A. Revcolevschi, L. P. Regnault, S. Raymond, and J. E. Lorenzo. Experimental realization of long-distance entanglement between spins in antiferromagnetic quantum spin chains. *Nat Phys*, 11(3):255–260, March 2015.

[119] A. Fasano, S. Marmi, and B. Pelloni. *Analytical Mechanics: An Introduction*. Oxford Graduate Texts. OUP Oxford, 2006.

[120] Radha Balakrishnan and A. R. Bishop. Nonlinear excitations on a quantum ferromagnetic chain. *Phys. Rev. Lett.*, 55:537–540, Jul 1985.

[121] R. Balakrishnan, J. A. Holyst, and A. R. Bishops. Soliton dynamics in the uniaxially anisotropic quantum ferromagnetic chain. *Journal of Physics Condensed Matter*, 2:1869–1883, February 1990.